DOCTORAL THESIS

Trace-Metal Hyper-Enrichment in Tremadocian Black Shales of the Baltic Palaeobasin: Mechanisms and Palaeoenvironmental Implications

Mawo Ndiaye

TALLINNA TEHNIKAÜLIKOOL
TALLINN UNIVERSITY OF TECHNOLOGY
TALLINN 2025

TALLINN UNIVERSITY OF TECHNOLOGY
DOCTORAL THESIS
7/2026

Trace-Metal Hyper-Enrichment in Tremadocian Black Shales of the Baltic Palaeobasin: Mechanisms and Palaeoenvironmental Implications

MAWO NDIAYE

TAL TECH PRESS

TALLINN UNIVERSITY OF TECHNOLOGY
School of Science
Department of Geology

This dissertation was accepted for the defence of the degree of Doctor of Philosophy in Earth Sciences 23/12/2025

Supervisor: Dr. Rutt Hints
School of Science
Tallinn University of Technology
Tallinn, Estonia

Opponents: Dr. Niels H. Schovsbo
Geological Survey of Denmark and Greenland
Copenhagen, Denmark

Dr. Kaarel Mänd
Institute of Ecology and Earth Sciences
University of Tartu
Tartu, Estonia

Defence of the thesis: 28/01/2026, Tallinn

Declaration:
Hereby I declare that this doctoral thesis, my original investigation and achievement, submitted for the doctoral degree at Tallinn University of Technology has not been submitted for doctoral or equivalent academic degree.

Mawo Ndiaye

---
signature

European Union
European Regional
Development Fund

Investing
in your future

ISSN 2585-6898 (publication)
ISBN 978-9916-80-447-6 (publication)
ISSN 2585-6901 (PDF)
ISBN 978-9916-80-448-3 (PDF)
DOI https://doi.org/10.23658/taltech.7/2026
Printed by EVG Print

Ndiaye, M. (2025). *Trace-Metal Hyper-Enrichment in Tremadocian Black Shales of the Baltic Palaeobasin: Mechanisms and Palaeoenvironmental Implications* [TalTech Press]. https://doi.org/10.23658/taltech.7/2026

TALLINNA TEHNIKAÜLIKOOL
DOKTORITÖÖ
7/2026

Jälgmetallide hüperrikastumine Balti Paleobassini Tremadoci-ealistes mustades kiltades: mehhanismid ja tekkekeskkond

MAWO NDIAYE

TAL TECH
KIRJASTUS

Contents

List of publications

The list of the author's publications, based on which the thesis has been prepared:

I. **Ndiaye, M**., Pajusaar, S., Liiv, M., Graul, S., Kallaste, T., & Hints, R. (2023a). Fine-clay shuttle as a key mechanism for V hyper-enrichment in shallow-water Tremadocian black shale from Baltica. Chemical Geology, 634, 121583. https://doi.org/10.1016/j.chemgeo.2023.121583

II. **Ndiaye, M**., Liiv, M., Kallaste, T., Graul, S., & Hints, R. (2023b). Nitrogen and organic-carbon isotope record in Tremadocian highly metalliferous black shales from the Baltic. Estonian Journal of Earth Sciences, 72, 78–81. https://doi.org/10.3176/earth.2023.25

III. **Ndiaye, M**., Graul, S., Liiv, M., Kallaste, T., Algeo, T. J., & Hints, R. (2025). Trace-metal hyper-enrichment in Tremadocian black shales of the Baltic Palaeobasin linked to transgression and ultra-slow sedimentation rates. Chemical Geology, 690, 122910. https://doi.org/10.1016/j.chemgeo.2025.122910

Author's contribution to the publications

Contribution to the publications in this thesis are as follows:

I. In Paper I, the author contributed to the article's conceptualization, participated in data collection, data analysis, and interpretation, and had a leading role in writing the manuscript.
II. In Paper II, the author was partly responsible for the article's conceptualization, participated in data collection, data analysis, and interpretation, and had a leading role in writing the manuscript.
III. In Paper III, the author contributed to the article's conceptualization, participated in data collection, data analysis, and interpretation, and had a leading role in writing the manuscript.

Introduction

Metalliferous black shales are organic-rich sedimentary rocks that serve as valuable archives of ancient marine redox conditions and geochemical processes. These ancient mud deposits preserve detailed records of palaeoenvironmental dynamics through the syngenetic enrichment of redox-sensitive trace metals including molybdenum, uranium, and vanadium (Algeo & Maynard, 2004; Scott & Lyons, 2012) along with sulfide and organic accumulation. Formed under oxygen-depleted conditions, black shales could capture variations in water-column and pore water chemistry, nutrient cycling, and climatic influences (Tribovillard et al., 2006). Their elevated concentrations of critical metals often exceeding crustal averages by an order of magnitude make them significant repositories for elements essential to modern industries, including energy storage (V), nuclear power (U), and steel production (Mo and V) (Hatch, 2012). Despite major advances in understanding enrichment mechanisms primarily controlled by redox zonation in sedimentary environments the extremely high anomalous concentrations and mismatching RSE enrichment patterns observed in many black shale deposits remain difficult to explain (Crawford et al., 2021; Xu et al., 2024).

Recent studies indicate that the control on local hyper-enrichment of RSE is likely specific to individual seabasins and hydrographic conditions (Algeo & Herrmann, 2018; Gilleaudeau et al., 2023; Liu & Algeo, 2020). This underscores the need for multi-instrumental high-resolution datasets on redox-sensitive element variability, integrated with compositional and sedimentary records, to (1) contextualize RSE-based palaeoproxies within specific palaeobasins or facies, and (2) develop site- to region-specific metallogenic models.

The Tremadocian period (Early Ordovician, 485–477 Ma) represents a transitional phase in Earth's geochemical and biological evolution, marked by rising atmospheric oxygen levels, high global palaeotemperatures, widespread marine transgression, and the onset of the Great Ordovician Biodiversification Event (Saltzman et al., 2011; Servais & Harper, 2018; Trotter et al., 2008). The Baltic Palaeobasin, located on the Baltica palaeocontinent, submerged much of the craton, forming a shallow epicontinental sea characterized by basin-wide deposition of organic-rich, metalliferous sediments (Graul et al., 2023; Hints et al., 2014b). The Türisalu Formation, a Tremadocian black shale unit in northeastern Estonia, records these conditions in the shallow inner-shelf of the palaeobasin and exhibits local hyper-enrichment in Mo (> 200 ppm), U (> 100 ppm), and V (> 1000 ppm) in some cases significantly exceeding values from basinal settings (Bian et al., 2021; Schovsbo, 2002) as well as highly heterogeneous enrichment patterns (Hints et al., 2014a; Vind et al., 2023; Vind & Bauert, 2020; Voolma et al., 2013). Resolving this discrepancy could clarify palaeoenvironmental factors that shaped shallow sea conditions during this pivotal period of biotic diversification and refine genetic models for metalliferous black shale hyper-enrichment in inner-shelf settings of Baltica. The insights gained would extend beyond the specific stratigraphic and geographic scope considered here.

Research gap

Despite extensive research on black shale metallogeny, significant gaps remain in understanding element-specific syngenetic enrichment pathways and environmental controls, particularly in shallow-water depositional settings in deep time (Coveney et al., 1991; Schovsbo, 2002).

The general models suggest that RSE enrichment can occur in settings with water-column anoxia in restricted water bodies, under high bioproductivity conditions such as upwelling systems in oceans, or in cases of ocean-scale anoxia (Algeo & Lyons, 2006; Jenkyns, 2010; Scholz et al., 2011). The balance between organic matter (OM) input, degradation and burial rate acts as the primary driver for redox transitions in seawater and pore water and the related selective capture of RSE depending on the redox state. For example, Mo enrichment is linked to hydrogen sulfide availability while the onset of V enrichment, in contrast, is associated with suboxic conditions (Algeo & Maynard, 2008; Algeo & Tribovillard, 2009; Rimmer, 2004; Tribovillard et al., 2006). RSE and OM in ancient organic rich sediments show general positive covariance (Algeo & Lyons, 2006). Still, in highly metalliferous beds differential RSE enrichment has been recorded, pointing to additional variables being critical for preferential hyper-enrichment of particular redox-sensitive elements beside redox zonation. These might include altered seawater composition including hydrothermal fluid influx, preferential scavenging of metals from seawater, and changes in reduction pathways (Scholz et al., 2013; Stylo et al., 2015).

Furthermore, the enrichment of Mo, U, and V in shallow marine organic-rich shales remains poorly constrained compared to deep water analogues. As existing enrichment models are based largely on modern restricted basins or oxygen-depleted deep-water analogues, they may not translate well to inner-shelf settings of the ancient epicontinental seas such as the Baltic Palaeobasin. Like distal deep-water settings the latter apparently experienced very low net sediment accumulation rates and terrigenous input, considered to be crucial prerequisites for RSE enrichment, but likely presented more variable hydrodynamic and sedimentary conditions due to a shallow water column and the influence of sea level changes on sediment accumulation (Artyushkov et al., 2000; Hints et al., 2014b). These settings could also record transient palaeoenvironmental signals such as primary productivity or salinity variations. The covariance between RSE enrichment and local sedimentary changes remains poorly explored in palaeoenvironmental studies of organic-rich assemblages, yet it may be crucial for interpreting anomalous local hyper-enrichment of RSE. For instance, V enrichment has been reported to covary with clay phases in organic-rich mudstones, suggesting a link between sedimentary dynamics and the capture of redox-sensitive elements (Lu et al., 2021).

Previous studies have documented both spatially and stratigraphically variable enrichment levels of redox-sensitive elements within the Türisalu Formation, with concentrations often significantly exceeding those observed in modern anoxic muds, as well as differential accumulation patterns of Mo, U, and V (Pukkonen & Rammo, 1992; Voolma et al., 2013).

These observations raise key questions:

- Which palaeoenvironmental conditions prompted the extreme but differential enrichment of specific RSE?
- To what extent do these patterns reflect local syngenetic environmental conditions versus broader regional or global controls?

Resolving these questions is essential for refining metallogenic models for metalliferous black shales and developing robust redox frameworks for Early Palaeozoic epicontinental seas.

Objectives

This study addresses these gaps by investigating a Tremadocian black shale succession using an integrated geochemical, isotopic, and sedimentological approach. The overall aim of this thesis was to develop a site-specific metallogenic model for Eastern Estonia.

The studies include the following specific objectives:

1. To identify major variability patterns and trends of V, Mo and U based on the high-resolution geological dataset in selected core sections across black shales and adjacent lithologies.
2. To interpret the recorded variability in the context of geochemical-lithological-sedimentary trends in the inner-shelf of Baltica.
3. To complement the element distribution patterns with isotopic system records, including $\delta^{98}Mo$, $\delta^{238}U$, $\delta^{15}N$ and $\delta^{13}C_{org}$ using selected samples, to evaluate RSE uptake and partitioning mechanisms.
4. To work toward an integrated view on the relevant local versus global palaeoenvironmental enablers and modifiers behind RSE hyper-enrichment.

Scope

The thesis focuses on the Türisalu Formation, specifically in NE Estonia, comprising the youngest and shallowest-water portions of the extensive Middle Cambrian-Tremadocian black shales of the Baltic Palaeobasin. The thin black shales from the study area are known to contain U, Mo and V enrichment and show well defined lithological variability (Hints et al., 2014b). The low thermal maturity of these rocks, together with the absence of known hydrothermal systems in the Baltic Palaeobasin during the Tremadocian, makes these complexes excellent targets for studying syngenetic and early diagenetic metal uptake in organic-rich sediments in a broader geological context.

The study is based primarily on a whole-rock, high-resolution geochemical dataset (> 300 samples) from two drill cores within the Toolse and Aseri shelly phosphorite deposit areas. The geochemical work is supported by mineralogical, lithological, and microanalytical investigations. Although other stratigraphic intervals and regions of the Baltic Palaeobasin were not examined, the results are interpreted in the context of published datasets across the palaeobasin and of comparable modern and ancient anoxic complexes to generalize findings.

This thesis is organized into the following chapters:

- Literature review
- Geology of the study area
- Materials and methods
- Results
- Discussion
- Prospects for future research
- Conclusions.

Abbreviations

Chlo	Chlorite
$\delta^{13}C_{org}$	Delta-13-carbon
$\delta^{15}N$	Delta-15-nitrogen
$\delta^{98}Mo$	Delta-98-molybdenum
$\delta^{238}U$	Delta-238-uranium
DOM	Dissolved organic matter
Ill/Sm	Illite-smectite
Ill	Illite
MC-ICP-MS	Multi-collector inductively coupled plasma mass spectrometry
OM	Organic matter
Qz	Quartz
RSE	Redox-sensitive elements
SEM	Scanning electron microscopy
SSA	Specific surface area
SRMs	Standard reference materials
TEM	Transmission electron microscopy
TN	Total nitrogen
TOC	Total organic carbon
µM	Micromolar
XRF	X-ray fluorescence spectrometry
XRD	X-ray diffraction

1 Literature review

1.1 Black shales and trace metal enrichment

Black shales are organic-rich, fine-grained sedimentary rocks spanning from the Archean to the Cenozoic. These deposits are globally distributed and vary widely in geochemical composition, enriched metal assemblages, and economic significance (Arthur & Sageman, 1994). Nevertheless, enrichment of redox-sensitive and chalcophile elements indicates that redox changes in the original muds and overlying waters were the primary controls on metal accumulation in all these deposits.

Prominent metalliferous examples include the Lower Cambrian black shales from South China (Lehmann et al., 2022), Devonian-Mississippian Bakken Formation of North America (Scott et al., 2017), the Jurassic Posidonia Shale of Germany (Röhl et al., 2001), the Permian Phosphoria Formation of the western United States (Hein et al., 2004), and Cambrian-Tremadocian Alum Shale Formation from Scandinavia (Andersson et al., 1985). Extremely metal-rich Lower Cambrian Ni, Mo, platinum group elements, and V-rich black shales of South China on the Yangtze Platform probably evolved via the combined effect of highly productive water column, hydrothermal fluid flux and very low clastic input to the palaeosea (Lehmann et al., 2022). The Bakken Formation is attributed to a shallow water restricted intracratonic basin and exhibits high Mo, Zn and V concentrations linked to high levels of dissolved H_2S in bottom waters and short transit time of organic matter through water column (Scott et al., 2017). The Posidonia Shale, deposited in an epicontinental sea, shows cyclic Mo and U enrichment tied to orbital forcing, nutrient upwelling, and episodic anoxia (Brumsack, 2006). The Phosphoria Formation is notable for V hyper-enrichment, attributed to high primary productivity, suboxic conditions and phosphatic mineral associations (Hein et al., 2004). Local extreme U enrichment in Cambrian-aged beds and V enrichment in Tremadocian-aged beds of the Alum Shale Formation have been attributed to extremely slow burial rates, anoxia and strongly sulfidic conditions in the lower water column, as well as a dynamic sedimentary environment (Bian et al., 2021, 2022; Schovsbo, 2002).

Trace metal enrichment in black shales results primarily from redox gradients in sedimentary environment but is also linked to complex interplay between organic matter burial, sedimentation dynamics, basin hydrography, and diagenetic processes. Under suboxic (O_2 ~1–10 μM, $H_2S \approx 0$ μM) to euxinic conditions ($O_2 \approx 0$ μM, $H_2S >$ ~1–2 μM), RSE such as V, U, and Mo are reduced from soluble oxyanions to insoluble forms, sequestered via complexes with organic ligands or sulfides, or adsorbed onto clay and oxide surfaces (Algeo & Maynard, 2008). Organic matter plays a complex role: it consumes oxygen during decomposition, promoting reducing conditions, and metal ions can interact with OM through different mechanisms including redox mediation, complexation, adsorption and coprecipitation (Tribovillard et al., 2006). Basin restriction, combined with water column stratification as observed in the modern Black Sea amplifies metal concentrations by enabling the long-term trapping of dissolved metals in stagnant, anoxic waters below the chemocline (Calvert & Pedersen, 1993). Early post-sedimentary processes such as organic matter degradation, dissolution of metastable phases, and the precipitation of pyrite or phosphate can redistribute trapped metals and complicate interpretations of past redox conditions (Tribovillard et al., 2006).

Depositional setting could potentially exert a profound impact enrichment mechanisms. Deep-water fine-grained deposits might exhibit nearly permanent uniform anoxia and high metal contents, while shallow-water deposits in epicontinental seas

might experience more fluctuating redox conditions and more variable clastic input leading to more heterogeneous uptake of RSE (Algeo & Herrmann, 2018; Arthur & Sageman, 1994). Also, the short timescale for the delivery of labile 'fresh' organic matter to the sea bottom in shallow water settings might determine specific conditions for RSE enrichment in sediments (Scott et al., 2017).

These differences underscore the importance of site-specific studies in shallow-water systems to refine black shale metallogeny models and validate RSE-based palaeoenvironmental reconstructions in such settings (Algeo & Herrmann, 2018; Algeo & Maynard, 2004; Tribovillard et al., 2006).

1.2 Geochemistry of Mo, U, and V

Molybdenum, uranium, and vanadium are multivalent elements widely used as palaeoredox proxies because their solubility changes markedly between oxic and anoxic conditions being highly soluble in oxidized forms but far less soluble in reduced forms. However, the reduction of each of these elements can take place under notably different redox potentials. Their capture in oxygen-depleted sediments is therefore closely linked to the sequential consumption of electron acceptors during microbial degradation of organic matter, beginning with the most energetically favourable oxic pathways and progressing toward less favourable ones (O_2, NO_3^-, MnO_2, $Fe(OH)_3$, $SO_4^{2-}$and CO_2).

Vanadium reduction takes place, via two steps, across suboxic to sulfidic gradients, starting with reduction from soluble V(V) (HVO_4^{2-}) to particle reactive V(IV) (VO^{2+}) and, in rare cases, V(III) under strongly reducing euxinic conditions. Due to two step reduction scheme, V enrichment is less dependent on H_2S availability compared to Mo, possibly relying strongly on sorption onto clay minerals, Fe-oxides, or organic matter, particularly in aluminosilicate-rich sediments (Bian et al., 2022; Tribovillard et al., 2006). This affinity for mineral phases often results in V correlating with clay proxies like Al or Ti, as observed for example in the Phosphoria Formation (Breit & Wanty, 1991).

Uranium accumulation starts under more reducing, ferruginous conditions after the available Fe(III) is consumed and is largely restricted to sediment beds. U(VI), present as uranyl carbonate in seawater, diffuses across the sediment-water interface and is reduced to insoluble U(IV), which may precipitate as uraninite (UO_2), coffinite, or form organometallic complexes (Morford & Emerson, 1999). Recent studies suggest that both abiotic and biotic U reduction pathways may operate in sediments, with the latter potentially leading to the formation of less stable monomeric forms of U(IV) (Bhattacharyya et al., 2017). The redox transition may lead to U concentrations far exceeding crustal levels (3–5 ppm) in anoxic shales (Rudnick & Gao, 2003). However, enrichment is controlled by the diffusion rates of dissolved U in sediments, the typically slow kinetics of U reduction as well as uptake limitations due to nucleation barriers of stable U(IV) phases (Bargar et al., 2013; Klinkhammer & Palmer, 1991; Loreggian et al., 2020; Pan et al., 2020). Isotopic $\delta^{238}U$ (expresses ratio between the heavy isotope ^{238}U and the lighter ^{235}U) fractionation during reduction and uptake in anoxic sediments typically ranges from –0.2 to +0.6 ‰ relative to seawater (+0.3 ‰) (Andersen et al., 2014; Weyer et al., 2008). Under oxidizing conditions, uranium is prone to post-depositional remobilization, which can alter enrichment patterns, as documented in weathered black shales (Klinkhammer & Palmer, 1991). These complexities highlight the need for combined elemental and isotopic analyses to accurately reconstruct U enrichment and cycling (Andersen et al., 2017; Cole et al., 2020).

Molybdenum is a highly effective tracer of euxinic conditions. In oxygenated waters, Mo exists as the stable molybdate ion (MoO_4^{2-}), but in euxinic settings with free H_2S (> 11 μM), it transforms into particle-reactive thiomolybdate species ($MoO_xS_{4-x}^{2-}$), which precipitate with pyrite, organic matter, or other Fe-sulfides (Erickson & Helz, 2000; Helz et al., 1996; Helz & Vorlicek, 2019). This process can yield Mo concentrations several orders of magnitude above crustal averages (1–2 ppm) (Rudnick & Gao, 2003). The 'Fe-Mn shuttle' where Mo is adsorbed and desorbed via oxide precipitation and dissolution can enhance enrichment of Mo in dynamic redox settings (Anbar & Rouxel, 2007). The isotopic fractionation of molybdenum δ^{98}Mo (the ratio of the heavy isotope ^{98}Mo to the lighter isotope ^{95}Mo) can further refine redox interpretations; in closed systems under fully euxinic conditions, authigenic δ^{98}Mo of sediments approaches seawater values (+2.3 ‰), but in dynamic suboxic to weakly euxinic settings, lighter isotopes may be preferentially adsorbed onto Fe-Mn oxides, yielding values as low as –0.5 to +1.0 ‰ in sediments (Arnold et al., 2004; Barling et al., 2001). These elemental and isotopic fractionation patterns make Mo a useful proxy for both local and global redox studies (Kendall et al., 2017).

Still, the element-specific reduction pathways presented here highlight the challenge of disentangling redox, mineralogical, and diagenetic controls in hyper-enriched shales. Integrated approaches combining elemental ratios, isotopic signatures, and mineralogical data are essential to resolve these complexities, particularly in settings with variable depositional conditions (Lyons et al., 2009).

1.3 The Baltic Palaeobasin in the Early Ordovician

The Baltic Palaeobasin, covering much of the Baltica palaeocontinent in the Early Palaeozoic, underwent significant hydrographic and environmental evolution from the Ediacaran to the Ordovician. Initially a stable cratonic margin, it developed into a broad epicontinental sea by the Early Ordovician, driven by thermal subsidence (Nielsen & Schovsbo, 2011). During the Tremadocian (486-477 Ma), a global sea-level rise prompted by a super-greenhouse climate flooded Baltica, shifting deposition from coarse siliciclastics to fine-grained, organic-rich muds in the inner stable shelf of the palaeobasin (Artyushkov et al., 2000; Munnecke et al., 2010; Nielsen & Schovsbo, 2011). The transgression across the low-lying interior of Baltica shifted shorelines, deepened the basin, and reduced clastic input, transforming it into a shallow, sediment-starved epicontinental sea less than 100 m deep across much of its extent (Nielsen & Schovsbo, 2011). Palaeoclimatic models suggest warm surface waters, which enhanced primary productivity and oxygen depletion, as evidenced by conodont thermometry (Trotter et al., 2008).

The conditions for primary organic-rich mud accumulation on the basin's inner-shelf likely differed from those in the deeper-water organic-rich facies of the palaeobasin such as the Alum Shale Formation in Sweden, Denmark, and Norway which probably experienced more stable redox conditions (Schovsbo, 2001). Shallow-water dynamics such as episodic ventilation, storm reworking, and terrestrial runoff introduced higher sedimentary and redox variability, as well as nutrient supply and trapping nearshore (Hints et al., 2014a). The likely absence of major river systems on Baltica, coupled with tectonic quiescence and very slow denudation rates of the Fennoscandian Shield, minimized detrital dilution, and allowed organic matter and authigenic minerals to dominate the sediment budget (Popov et al., 2019).

The evolution of the Baltic Palaeobasin at the onset of the Ordovician coincided with the beginning of the Great Ordovician Biodiversification Event, linking its geochemical

record to broader ecological transformations (Servais & Harper, 2018). This shallow, open to semi-restricted sea developed on a stable continental platform, with limited diagenetic alteration and a well-established biostratigraphic framework, providing a valuable perspective on the chemistry and redox dynamics of Tremadocian oceans and epicontinental seas during this transition.

1.4 Tremadocian black shales in Estonia

Tremadocian shales in the inner-shelf of the Baltic Palaeobasin are characterized by fine siliciclastic mineral matrix (K-feldspar, quartz, illite/mica, and illite-smectite), high total organic carbon (TOC: 5-15 wt%), and abundant pyrite (3-7 wt%) (Hints et al., 2014b; Loog et al., 2001; E. Pukkonen, 1989). The longitudinal black shale belt along the margin of the Fennoscandian Shield, forming the Türisalu Formation in Estonia, exceeds 6 m in thickness in northwestern Estonia and thins eastward and south-eastward. Biostratigraphic evidence indicates that the formation's lower boundary is diachronous, with progressively younger deposits toward the NE, reflecting facies shifts during transgression (Kaljo & Kivimägi, 1970). On a regional scale, the distribution of the inner-shelf black shale belt, which extends into the Leningrad region of Russia, is patchy, with erosional hiatuses and variable preservation resulting from post-depositional uplift and exposure along the Baltic Klint (Popov et al., 2019). The black shales pinch out in central Estonia, underscoring their restricted depositional extent compared to the thicker, more extensive Cambrian–Tremadocian black shales from the middle and outer shelf of the palaeobasin (Nielsen & Schovsbo, 2011; Schulz et al., 2021).

Black shales are genetically related to the underlying shallow-water siliciclastic complexes containing shelly phosphorites and are overlain by organic-poor grey mudstones or glauconitic sandstones in northern Estonia. Figure 1 illustrates the palaeogeographic context, showing Baltica's inundated craton, the Türisalu Formation's isopach trends, and locations of the study sites.

The Türisalu Formation exhibits spatially and stratigraphically heterogeneous trace metal distributions (Hints, et al., 2014b; Pukkonen, 1989; Vind et al., 2023; Voolma et al., 2013). Previous RSE distribution mapping studies suggest that maximum RSE enrichment tends to occur in the lower and middle parts of the formation, while the uppermost zones of the black shales are comparatively depleted in trace elements. Pukkonen (1989) distinguished three geochemical zones western, middle, and eastern in the Türisalu Formation. The eastern zone is marked by the highest Mo, U, and V concentrations within a thin black shale interval interbedded with organic-poor siliciclastic layers.

2 Geology of the study area

The studies focused on the inner-shelf of the palaeobasin, specifically in northeastern Estonia, where two drill cores Aseri PH012B (59.426053°N, 26.755267°E) and Toolse PH016B (59.460274°N, 26.445899°E) were targeted by multianalytical investigations. The Türisalu Formation in these cores represents thin but highly metalliferous black shales, forming the youngest and shallowest part of the Tremadocian black shale complexes in the palaeobasin (Heinsalu et al., 2003).

Stratigraphically, the Türisalu Formation overlies the Kallavere Formation a Furongian unit of phosphate-rich siltstones and sandstones with black shale interbeds and is capped by the organic-poor grey mudstones of the Varangu Formation. Investigations also included materials from these lithologies near the contact with the Türisalu Formation.

In the Aseri and Toolse cores, the Türisalu Formation can be subdivided into three units Units I, II, and III based on lithological and geochemical trends that reflect facies shifts during a transgressive highstand sequence. Unit I consists of finely laminated black shales. Unit II is marked by cyclic interbeds of pyritized biosilica within the black shales, indicating episodic benthic oxygenation, and by glendonite-like carbonate concretions. Unit III, the uppermost part of the formation, grades into thinly laminated, lighter-coloured shales with erosional surfaces, likely marking the onset of regression and reduced organic preservation (Hints, et al., 2014b). The overlying grey mudstones of the Varangu Formation, deposited above the hiatal surface that defines the upper boundary of the Kallavere Formation, record continued fine-clastic sedimentation on the inner shelf. Their low organic content suggests improved ventilation of the lower water column during the later Tremadocian. Beneath the Türisalu Formation, the Kallavere Formation displays rhythmic alternations of fine-grained quartzose siltstone with phosphatic brachiopod detritus and thin black shale interbeds. The black shale laminae commonly contain irregular, intensely pyritized silty layers, reflecting a dynamic regime of terrigenous input in a shallow-marine setting. Overall, the formation records a coastal to subtidal environment associated with gradual deepening during transgression.

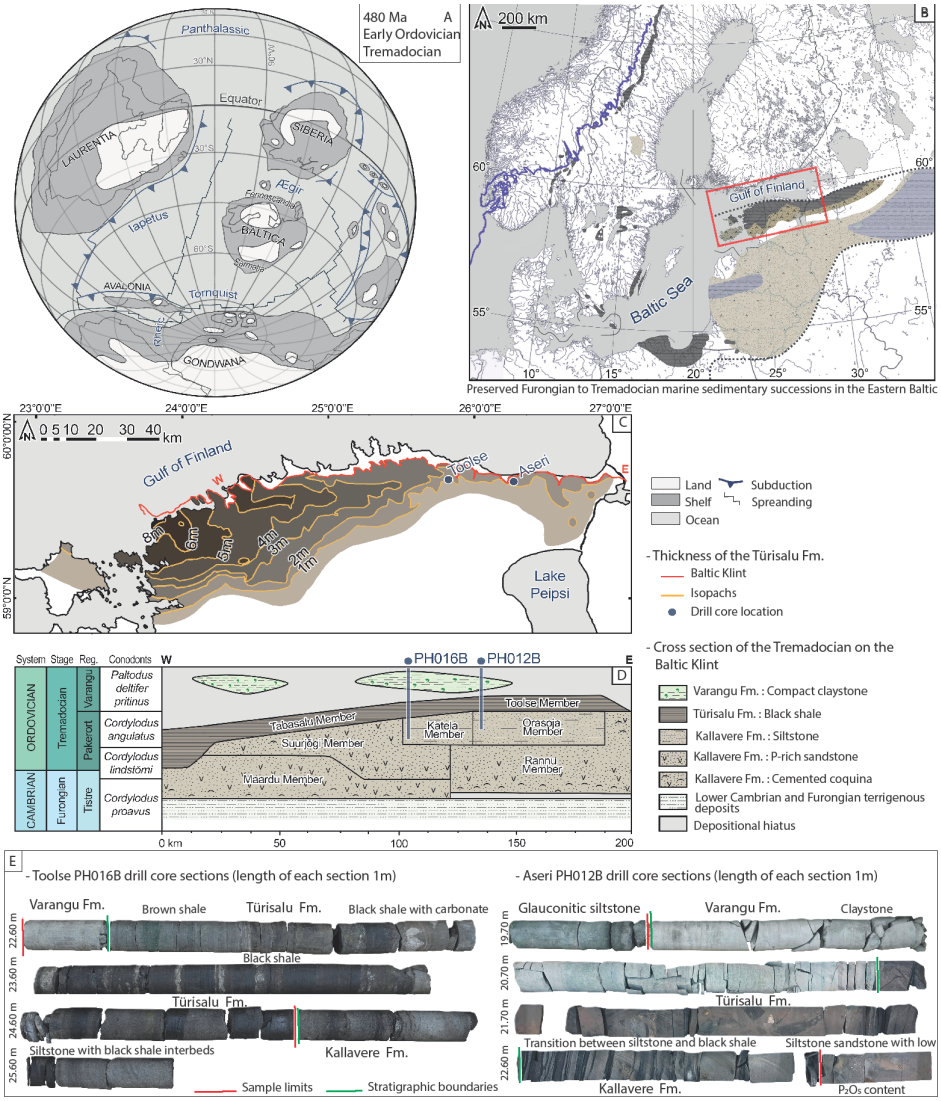

Figure 1 *(A) Position of the main palaeocontinents and Baltica during the Early Ordovician, after Cocks and Torsvik (2002). Extensively overflooded Baltica encompassed two land areas: the Fennoscandian Shield and the Ukrainian Shield. (B) Distribution area of Middle Cambrian to Lower Ordovician black shales and other siliciclastic facies of the Baltic Palaeobasin, after Schovsbo et al. (2018) and Popov et al. (2019). Note that black shales are preserved only in limited areas within the supposed original distribution limits of the organic-rich facies. (C) Location scheme of the Türisalu Formation; isopach lines show formation thickness after Pukkonen (1989). (D) Lithostratigraphy and biostratigraphy of Furongian and Tremadocian deposits on the Baltic Klint section. The blue dot marks the location of cores Aseri PH012B and Toolse PH016B. (E) The drillcore section of Aseri PH012B and Toolse PH016B. Stratigraphically, the oldest siltstone-fine-grained sandstone beds with phosphatic detritus belong to the Kallavere Formation. The upper part of the formation shows interfingeringof siltstone and black shale laminae. The overlying Türisalu Formation contains black shales exhibiting distinct lithological changes (see text for further details). Grey silty claystones of the Varangu Formation cap the Türisalu Formation.*

3 Materials and methods

3.1 Sampling strategy

To capture fine-scale variability in lithology, geochemistry, and isotopic composition within the Tremadocian successions, high-resolution sampling was conducted. Continuous sampling at 1 cm intervals was carried out on the Aseri PH012B (21.36–23.22 m depth) and Toolse PH016B (22.87–24.66 m depth) drill cores, targeting the Kallavere Formation (uppermost Orasoja Member), Türisalu Formation (Units I-III), and Varangu Formation. In total, 187 samples were collected from Aseri PH012B and 186 from Toolse PH016B, yielding 373 samples altogether. The 1 cm resolution was selected to resolve high-frequency palaeoenvironmental signals and ensure a detailed record of lithostratigraphic boundaries, redox shifts, and metal enrichment patterns.

3.2 Elemental analysis of whole-rock samples

For elemental analysis by X-ray fluorescence (XRF), all whole-rock samples (~20 g) were crushed and homogenized in an agate mortar using a tungsten carbide mill. For major element analysis, fused disks were prepared with a Claisse M4 Gas Fusion instrument. A 0.66 g portion of the crushed sample was fused in a platinum crucible using a flux of lithium metaborate:lithium tetraborate:lithium bromide. For trace element analysis, ~8 g of powder was pressed into a pellet using 5% Mowiol solution (one drop per gram of sample). Pressed pellets and fused disks were analysed using a Bruker S4 spectrometer, with internal calibration based on six local in-house black shale reference samples (Pajusaar et al., 2021) and quality control using the GeoPT48/MzBP sample from the IAG proficiency testing series. Loss-on-ignition measurements were conducted on all samples as follows: 1 g of material was placed in a crucible and heated in a Nabertherm furnace at 550 °C and 950 °C for 4 hours. Samples were then cooled to room temperature in desiccators and weighed.

Total organic carbon and total nitrogen were determined by combustion in a FLASH 2000 organic elemental analyser. Depending on loss-on-ignition values, 4–15 mg of dried, powdered sediment (typically about 8 mg) was weighed into a silver container. The material was pre-treated with 10% HCl to remove inorganic carbon, dried on a hotplate at 80 °C for 5 hours, cooled, and wrapped to form granules. Prior to analysis, the silver capsules were packed into tin containers to facilitate combustion. Cystine (Thermo Fisher Scientific) served as the standard, and high-organic carbon-rich sediment (IVA Analysentechnik e.K.) was used as the reference material.

3.3 Mo, U, N and C isotope analysis

The Mo and U isotopic analyses were conducted on selected whole-rock samples from the same sample set. Sixteen samples from the Türisalu Formation were selected at intervals of 5 cm, except for five samples in Units II and III, which were picked at 10 cm intervals. Additionally, selected black shale interbeds from the Kallavere Formation (n = 2) and grey mudstones from the Varangu Formation (n = 2) were included, totalling twenty samples. Approximately 1 g of powdered material was used for isotopic analyses.

Samples for both Mo and U isotopic analyses were prepared using digestion with aqua regia (AR; a 3:1 mixture of concentrated HCl [30%] and HNO_3 at [65%]) combined with hydrofluoric acid (48%) to ensure complete digestion of refractory phases. Digestion was carried out at approximately 120 °C for 4 hours in Teflon beakers. After complete dissolution

was visually confirmed, the digests were evaporated to dryness. For U isotopic analysis specifically, the residue was refluxed overnight with 4 mL of aqua regia to remove excess fluoride, then evaporated again to dryness and re-dissolved in 6 M HNO_3. Subsequently, uranium was separated using pre-packed 2 mL TEVA resin columns. The purified U fraction was then evaporated to dryness and finally re-dissolved in 0.8 M HNO_3. For Mo isotope analyses, samples were digested exclusively with aqua regia under identical conditions due to the absence of Mo in the silicate fraction.

Mo and U isotopic compositions were determined using multi-collector inductively coupled plasma mass spectrometry (MC-ICP-MS) at ALS Scandinavia Laboratories (Luleå, Sweden), employing a Neptune PLUS (Thermo Fisher Scientific) instrument equipped with an OnToolBooster Jet interface pump (Pfeiffer). An external calibration method was utilized, using bracketed isotope standard reference materials to correct for instrumental mass bias. Analyses were carried out following ion-exchange separation using Chelex-100 resin for Mo and TEVA resin for U, both of which achieved analyte recoveries greater than 95%.

For U isotope measurements, sample introduction was via an Aridus II desolvating nebulizer, Jet sample cone, X-skimmer cone, and self-aspirated MicroMist nebulizer, achieving a sample uptake of ~70 µL min^{-1} and providing a $\delta^{238}U$ intensity of approximately 40 V per 80 µg L^{-1} (Pontér et al., 2021). All U isotope data are reported as per mille (‰) variation relative to the interpolated composition of the CRM-112a uranium isotope standard (National Institute of Standards and Technology, USA), analysed immediately before and after each sample. Analytical uncertainty was determined by calculating the standard deviation (SD) from two independent consecutive measurements, typically achieving reproducibility better than ±0.1 ‰ (Pontér et al., 2021). The isotopic composition ($\delta^{238}U$) is expressed using δ notation according to Eq. (1):

$$\delta^{238}\mathrm{U}\ (‰) = \left\{ \frac{\frac{238}{235}\mathrm{U}_{\mathrm{sample}}}{\frac{238}{235}\mathrm{U}_{\mathrm{CRM-112a}}} - 1 \right\} \mathrm{x}\ 1000 \qquad (1)$$

Mo isotope measurements followed the protocol described by Malinovsky et al. (2005). Mo isotopic compositions ($\delta^{98}Mo$) were measured against an in-house standard, then corrected and reported relative to the NIST SRM 3134 standard according to Eq. (2) (Malinovsky et al., 2005). Analytical reproducibility, assessed through replicate analyses of standards and secondary reference materials, demonstrated long-term precision (2σ) of ±0.08 ‰ or better for $\delta^{98}Mo$. Tabulated δ-values for Mo and U certified reference materials were taken from the GeoReM database (Jochum et al., 2005).

$$\delta^{98}\mathrm{Mo}\ (‰) = \left\{ \frac{\frac{98}{95}\mathrm{Mo}_{\mathrm{sample}}}{\frac{98}{95}\mathrm{Mo}_{\mathrm{NIST\ SRM\ 3134}}} - 1 \right\} \mathrm{x}\ 1000 + 0.25 \qquad (2)$$

Selected whole-rock samples (n = 26) were also analysed for $\delta^{13}C_{org}$ and $\delta^{15}N$. For carbon isotopes, approximately 1 g of powdered sample was treated with 10% HCl to remove inorganic carbon, rinsed, and dried. Carbon isotopic ratios were measured using a FlashEA 1112 elemental analyser coupled to a Delta V Advantage isotope ratio mass spectrometer, and results are reported as deviations relative to Vienna Peedee belemnite ratio (Eq. (3)). Precision and calibration were ensured using standards from the IAEA and IVA Analysentechnik.

$$\delta^{13}C = \left\{ \frac{^{13}C/\ ^{13}C_{sample}}{^{13}C/\ ^{13}C_{standard}} - 1 \right\} \text{x } 1000 \quad (3)$$

For nitrogen isotopes, 7–20 mg of sample powder was weighed into Sn capsules. Nitrogen isotopic ratios were measured on the same instrumentation (FlashEA 1112 coupled via a ConFlo IV to a Delta V Advantage). $\delta^{15}N$ values are expressed as the relative deviations of the measured $^{15}N/^{14}N$ ratio and with respect to atmospheric N_2 (Eq. (4)). Calibration and precision were monitored using IAEA-N-1 (+0.43 ‰), IAEA-N-2 (+20.41 ‰) and IVA Analysentechnik Urea Isotopic Working Standard (–0.32 ‰).

$$\delta^{15}N = \left\{ \frac{^{15}N/\ ^{14}N_{sample}}{^{15}N/\ ^{14}N_{standard}} - 1 \right\} \text{x } 1000 \quad (4)$$

3.4 Data analysis

The obtained geochemical dataset was analysed using conventional and multivariate descriptive statistics in OriginPro software. Prior to principal component analysis (PCA), the centred log-ratio transformation was applied to the data to overcome spurious correlations within closed compositional data (Aitchison, 1982). Because the original sample set also contained coarse-grained siliciclastic, carbonate-rich, and mixed lithologies, Al_2O_3 > 9 wt% and CaO > 3 wt% were used as threshold values to sort pure carbonate-poor black shale samples. Enrichment factors (X_{EF}) for trace elements (X) were calculated according to the procedure of Tribovillard et al. (2006). The element concentrations were first normalized to the Al content of the sample and divided by the appropriate trace element-to-Al ratio in the Post-Archean Australian Shale (PAAS) standard (Taylor, 1985) (Eq. 5):

$$X_{EF} = \left\{\frac{X}{Al}\right\}\text{sample} \Big/ \left\{\frac{X}{Al}\right\}\text{PAAS} \quad (5)$$

To define the contribution of $\delta^{98}Mo$ and $\delta^{238}U$ from lithogenic and authigenic sources to the measured total isotopic signatures, the authigenic proportion of isotopic compositions was estimated using the following equations for the whole-rock (bulk), authigenic (auth), and detrital (det) fractions (Eqs. 6 and 7):

$$\delta^{98}Mo_{auth} = \delta^{\frac{98}{95}}Mo_{bulk} - \left(\frac{Al}{Mo}\right)_{bulk} \times \left\{ \frac{\delta^{\frac{98}{95}}Mo_{det} - \delta^{\frac{98}{95}}Mo_{bulk}}{\left(\frac{Al}{Mo}\right)_{det} - \left(\frac{Al}{Mo}\right)_{bulk}} \right\} \quad (6)$$

$$\delta^{238}U_{auth} = \delta^{238}U_{bulk} - \left(\frac{Al}{U}\right)_{bulk} \times \left\{ \frac{\delta^{238}U_{det} - \delta^{238}U_{bulk}}{\left(\frac{Al}{U}\right)_{det} - \left(\frac{Al}{U}\right)_{bulk}} \right\} \quad (7)$$

We assumed that the detrital fraction had the same Mo (1.1 ppm), U (2.7 ppm), and Al (8.15 wt%) contents as well as the same $\delta^{98}Mo$ (+0.3 ‰) and $\delta^{238}U$ (−0.3 ‰) isotopic ratios as the average upper continental crust (Noordmann et al., 2016; Rudnick & Gao, 2003; Tissot & Dauphas, 2015; Voegelin et al., 2014).

4 Results

4.1 High-resolution geochemical record from Aseri and Toolse

The black shales of the Türisalu Formation from Aseri PH012B and Toolse PH016B drill cores, together with samples from the underlying siltstone-black shale complexes of the Kallavere Formation (studied in Aseri PH012B) and overlying grey mudstones of the Varangu Formation, provide a detailed record of V, U and Mo enrichment trends in Tremadocian strata in the innermost shelf settings of the Baltic Palaeobasin along with other major geochemical variables (Figure 2 and 3). The obtained data reveal major geochemical shifts at the boundaries of lithostratigraphic units, as well as pronounced centimetre-scale variability within individual units.

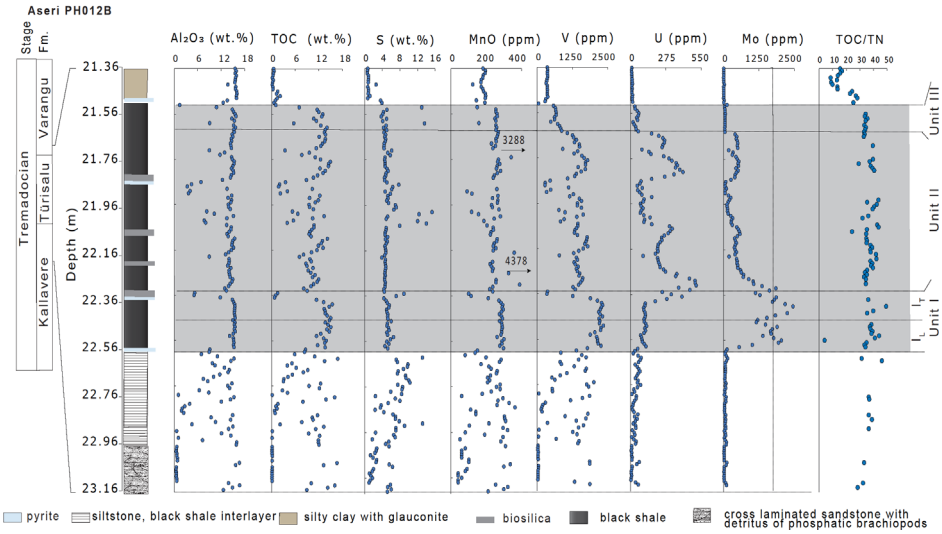

Figure 2 *Stratigraphic distribution trends of selected major and trace elements in the Aseri PH012B drill core. TOC and total organic carbon to total nitrogen (TOC/TN) ratios are also shown.*

Türisalu Formation and the uppermost Kallavere Formation in Aseri PH012B core reveal elevated concentrations of Al_2O_3 (up to 15 wt%), TOC (4-14.5 wt%), and S (4–14 wt%). Maximum RSE enrichment includes up to 2003 ppm V in the Kallavere Formation, up to 2342 ppm in Unit I and up to 1784 ppm in Unit II; U reaches up to 500 ppm in Unit II, and Mo up to 2500 ppm in Unit I. These intervals also exhibit high TOC/TN ratios (40–50 in Units I, II, and the Kallavere Formation), emphasizing high organic matter preservation but with a strong degradation imprint. Conversely, the overlying Unit III of the Türisalu Formations and Varangu Formation show distinct declines in concentrations of V, U, and Mo, coupled with a drop in TOC/TN, S and TOC values in the Varangu Formation.

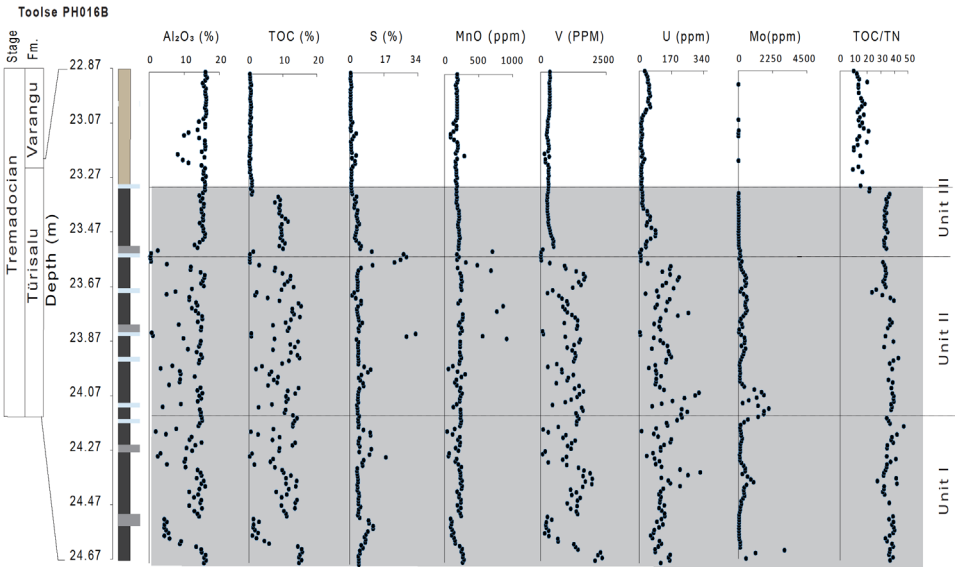

Figure 3 *Stratigraphic distribution of major and trace elements in the Toolse PH016B drill core. TOC and TOC/TN ratios are also shown.*

The black shales of the Türisalu Formation from the Toolse PH016B drill core (Figure 3) show similar geochemical trends. Units I and II exhibit elevated concentrations of Al_2O_3 (up to 18 wt%), TOC (up to 15 wt%), and S (up to 30 wt%). Elevated RSE including V up to 2300 ppm, U up to 340 ppm, and Mo up to 4500 ppm, were recorded in these units, while distinctive drop of RSE enrichment levels appeared in Unit III. The Varangu Formation marks a pronounced shift to more oxic conditions, as reflected by a sharp decline in TOC (~0 wt%), S (< 3 wt%), and redox-sensitive element contents (V < 150 ppm, Mo ~200 ppm, U < 50 ppm).

4.2 Vanadium covariance with major and trace elements

The covariance of V with other measured parameters was examined using conventional and multivariate statistics to clarify underlying genetic relationships in metal-rich units of the Türisalu Formation (Paper I).

Scatter plots illustrating the bivariate relationships of V and Cr with Al_2O_3 and TOC in the Aseri PH012B and Toolse PH016B cores are shown in Figures 4 and 5. Samples from both sites display generally positive correlations among V, Cr, Al_2O_3 and TOC across Units I to III, the Varangu Formation, and the Kallavere Formation. The strength of these relationships varies by unit: V-Al_2O_3 correlations yield R^2 values ranging from 0.26 (n = 12) to 0.85 (n = 72) in Aseri and 0.58 (n = 27) to 0.91 (n = 73) in Toolse, whereas Cr–Al_2O_3 correlations range from 0.71 (n = 24) to 0.94 (n = 12) in Aseri and 0.80 (n = 73) to 0.98 (n = 27) in Toolse. Most correlations exhibit p-values < 0.0001, underscoring the significance of the observed relationships and the dominant influence of fine-grained aluminosilicates (primarily clay minerals) on V and Cr sequestration.

Correlations with TOC are more variable. TOC–V relationships yield R^2 values from 0.01 (Varangu Formation, n = 17) to 0.92 (Unit I, n = 24) in Aseri and from 0.13 (Varangu Formation, n = 44) to 0.84 (Unit I, n = 36) in Toolse. TOC–Cr correlations show similar variability, ranging from 0.01 (Varangu Formation, n = 17) to 0.83 (Kallavere Formation,

n = 62) in Aseri and from 0.15 (Varangu Formation, n = 44) to 0.85 (Unit I, n = 36) in Toolse. The weakest covariances ($R^2 \leq 0.15$) occur consistently in the organic-poor Varangu Formation, indicating minimal organic control on metal accumulation. In contrast, the strongest correlations ($R^2 \geq 0.83$; typically, $p < 0.0001$) occur in Units I and II of the Türisalu Formation and, in Aseri, within the Kallavere Formation, highlighting the substantial role of organic matter in promoting V and Cr enrichment in the most metalliferous intervals.

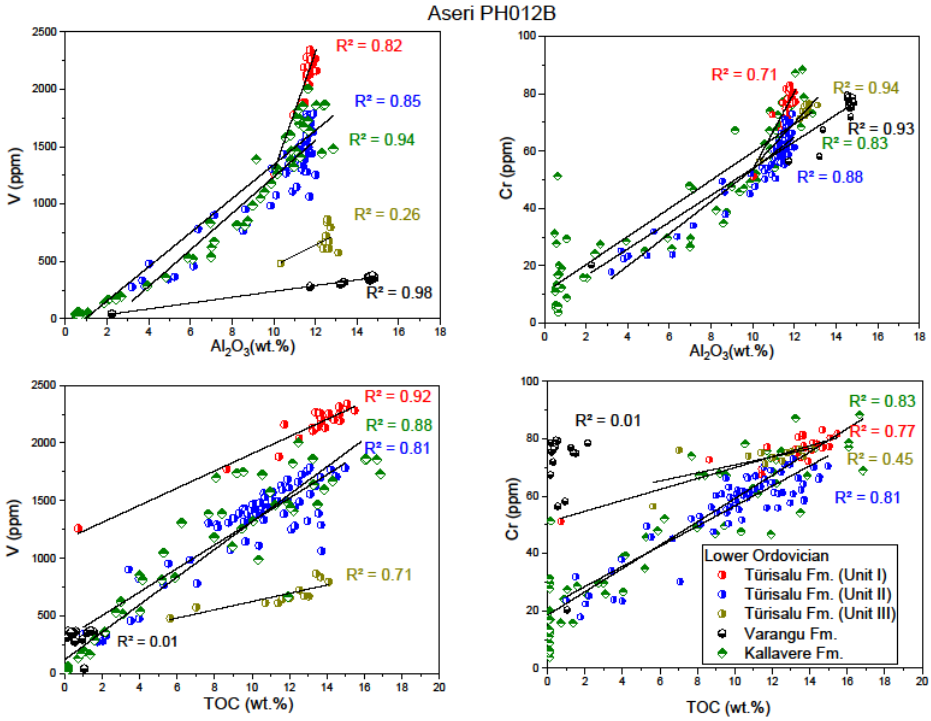

Figure 4 *Correlation of V and Cr concentrations with Al_2O_3 and TOC in the Aseri PH012B drill core. Data points are colour-coded by stratigraphic units: Unit I (black), Unit II (blue), Unit III (olive), Varangu Formation (red), and Kallavere Formation (green). Coefficients of determination (R^2) indicate varying strengths of correlation across units.*

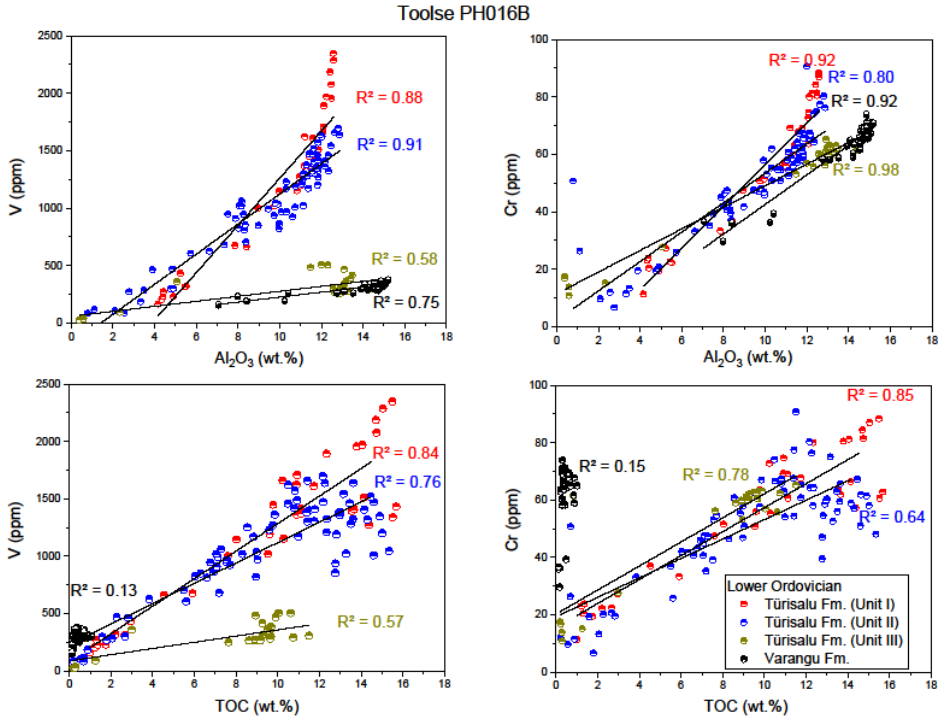

Figure 5 *Correlation of V and Cr concentrations with Al_2O_3 and TOC in the Toolse PH016B drill core. Data points are colour-coded by stratigraphic units: Unit I (black), Unit II (blue), Unit III (olive), and Varangu Formation (red). Coefficients of determination (R^2) indicate variable strengths of linear correlation.*

Principal component analysis biplots (Figure 6) reveal specific element associations for the Toolse PH016B and Aseri PH012B cores. In the Toolse PH016B core, principal component 1 (PC1 62.58%) and principal component 2 (PC2 7.67%) reveal clear clustering of geochemical data. V, Cr and clay-associated elements (Al, Ti, K, Mg), together with TOC, form a tight cluster with positive loadings on PC1, indicating a strong association between aluminosilicates, OM and V enrichment. Sulfur and iron form a separate grouping, reflecting a distinct sulfidic component. Elements associated with coarse-grained sediments, such as Si, Ca, P, and Na, form another discrete cluster corresponding to coarse-grained silicates, phosphates, and carbonate minerals. Similarly, in the Aseri PH012B core, PC1 (39.97%) and PC2 (16.04%) demonstrate comparable element patterns: clay-associated elements (Al, Ti, K, Cr), TOC, and trace metals (Mo, Th, Zr) cluster with aluminosilicates and OM; S and Fe indicate a consistent sulfidic influence; and coarse-grained elements (Si, Ca, P, Na) again form a distinct cluster. Overall, despite lithological differences, both cores exhibit analogous geochemical controls, reflecting consistent depositional and diagenetic processes.

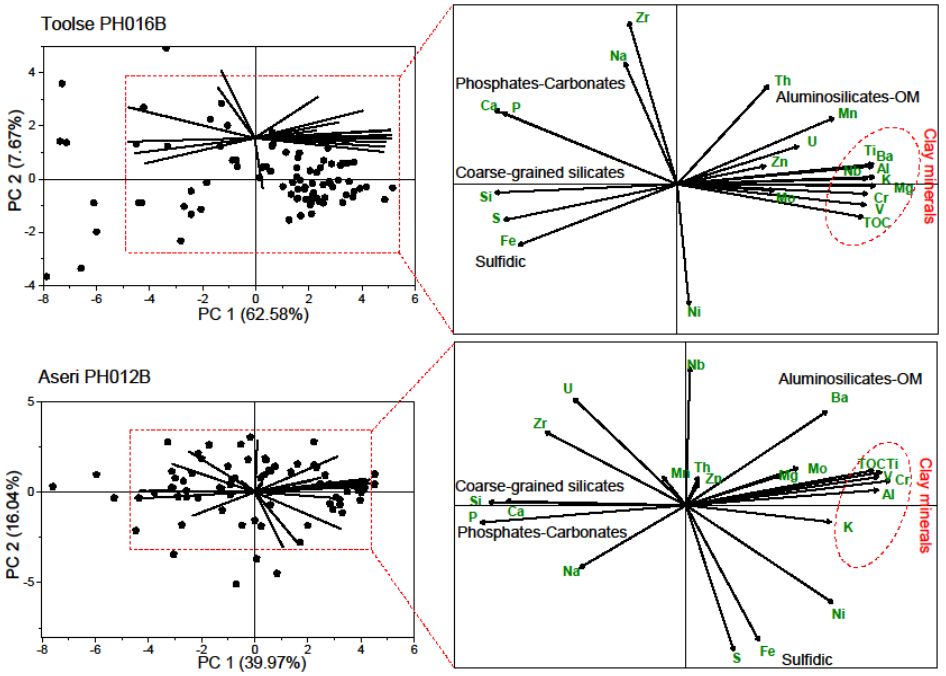

Figure 6 *Principal component analysis results for the Toolse PH016B (top) and Aseri PH012B (bottom) drill cores. The left panels show sample distributions along the PC1 and PC2 axes, explaining 62.58% and 7.67% of variance for Toolse, and 39.97% and 16.04% for Aseri. The right panels display loadings of geochemical elements, highlighting clusters corresponding to clay minerals, organic matter proxies, coarse-grained silicates, phosphates/carbonates, and sulfide-related elements, revealing consistent geochemical patterns across both sites (Paper I).*

4.3 Isotopic trends

The obtained isotope profiles of δ^{98}Mo, δ^{238}U, $\delta^{13}C_{org}$, and δ^{15}N across the upper Kallavere, Türisalu (Units I_L, I_T, II, III), and Varangu formations (Figure 7) exhibit distinct stratigraphic variations. The δ^{98}Mo-δ^{238}U bivariate plot for the Aseri PH012B core (Figure 8) highlights an inverse covariance between Mo and U isotope fractionation-typical for these isotope systems along with a remarkably wide range of values.

In the upper V-rich black shales of the Kallavere Formation, δ^{98}Mo values are notably light (down to −1 ‰). In contrast, δ^{238}U values are distinctly heavy (+0.3 to +0.5 ‰) within the same interval. Up-section, in the Mo- and V-enriched Unit I of the Türisalu Formation, δ^{98}Mo values gradually increase toward less fractionated compositions, reaching near-modern seawater values (+1.5 to +2.0 ‰; modern seawater ≈ +2.3 ‰) in the uppermost Unit I and the lower part of Unit II. Throughout most of Unit I, δ^{238}U remains strongly fractionated (enriched in ^{238}U) but then shows a sharp shift toward less fractionated values relative to modern seawater (down to −0.28 ‰; seawater ≈ −0.39 ‰) in the uppermost subunit IT and basal Unit II, coincident with U hyper-enrichment and a relative decline in Mo content.

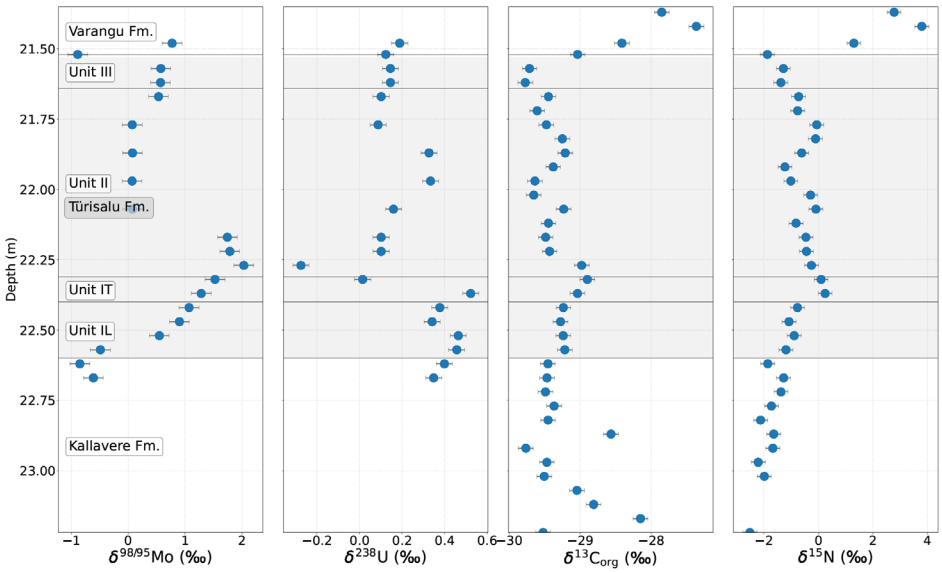

Figure 7 *Stratigraphic variations in Mo (δ^{98}Mo), U (δ^{238}U), organic carbon ($\delta^{13}C_{org}$), and total nitrogen (δ^{15}N) isotope compositions through the upper Kallavere, Türisalu (Units I_L, I_T, II, III), and Varangu formations.*

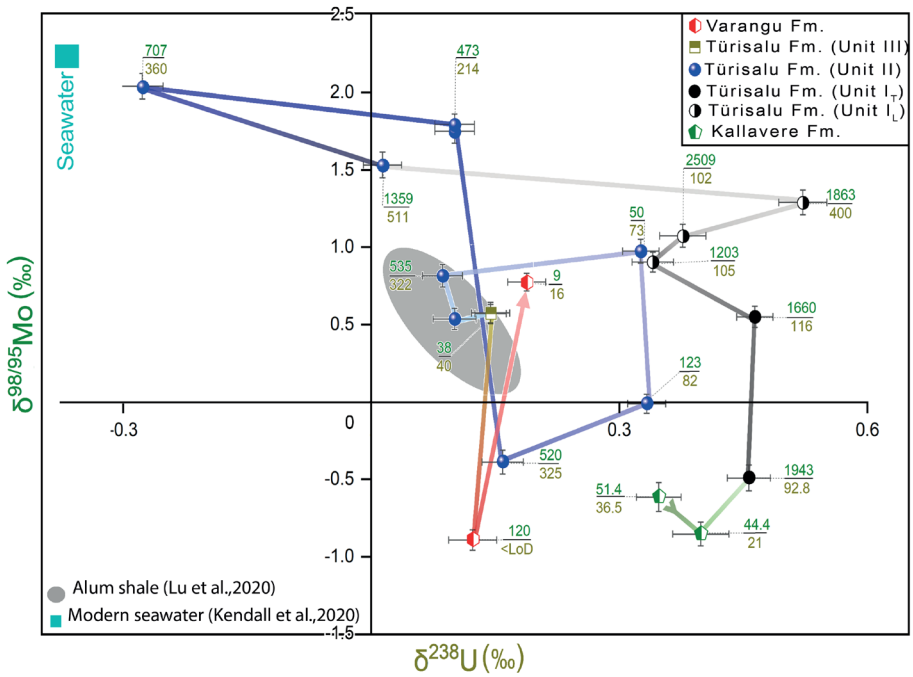

Figure 8 *δ^{98}Mo–δ^{238}U covariation for the Aseri PH012B study core, as well as Mo–U enrichment signatures (Mo (ppm) = green; U (ppm) = greenish beige), highlighting distinct evolutionary trends.*

In the middle and upper part of Unit II more fractionated $\delta^{238}U$ and $\delta^{98}Mo$ values, similar to those reported from different modern and ancient oxygen-deficient settings, appear. Finally, samples from Unit III and the overlying Varangu Formation cluster around intermediate $\delta^{98}Mo$ (~0.5 ‰) and $\delta^{238}U$ (~0.2 ‰) fractionation ranges.

$\delta^{13}C_{org}$ in the studied black shale section from Aseri PH012B remained in a narrow range (mostly between −29.8 to −29.0 ‰) yet shows some stratigraphic variations. $\delta^{15}N$ also exhibits stratigraphic trends, with negative values down to −2.0 ‰ in the lower and upper part of the Türisalu Formation, and values around 0 ‰ in the middle part of the black shale complex (Figure 9). A shift toward positive $\delta^{15}N$ values (> +1.0 ‰) was recorded in the grey shales of the Varangu Formation.

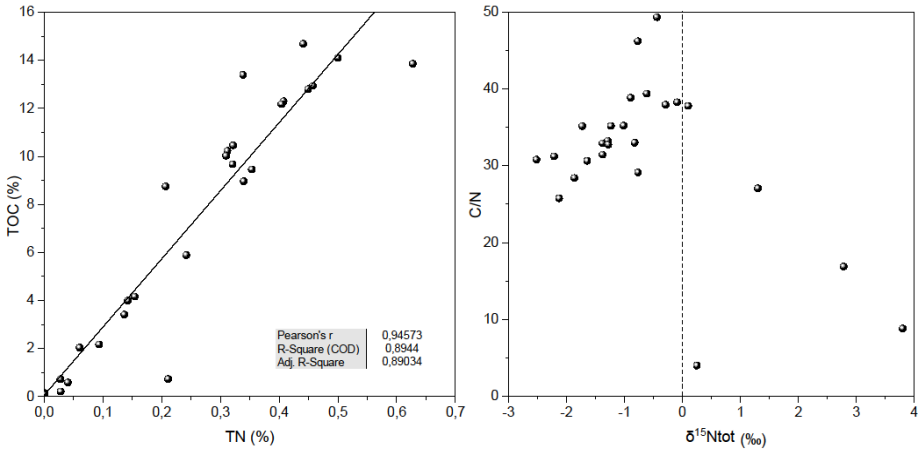

Figure 9 *Scatterplots of C/N ratios versus $\delta^{15}N$ and TOC versus TN for samples from the Aseri PH012B drill core. Abbreviation: Adj. – Adjusted (Paper II).*

5 Discussion

The three studies forming the foundation of this thesis (Paper I, Paper II, Paper III) elucidate the geochemical, isotopic, sedimentological, and biological processes responsible for RSE enrichment in the shallow inner-shelf of the Baltic Palaeobasin. This synthesis integrates their main findings to provide a comprehensive understanding of the palaeoenvironmental factors controlling syngenetic metal hyper-enrichment, with particular attention to redox zoning, water-column stratification, transgressive dynamics and net sedimentation rates, fine-grained clay input, Fe-Mn-P-N-S cycling, and anoxic mineralisation processes governing metal uptake.

5.1 Redox zonation and inventory of RSE metals

Paper III suggests that basin-wide redox stratification-characterised by an oxygen-depleted lower water column maintained through climate-driven density gradients was a key factor controlling the sequential enrichment of V, Mo, and U in the Türisalu Formation. Papers I and II document a stratigraphic metal accumulation trend in Toolse and Aseri sections, with V capture starting under suboxic conditions (Kallavere Formation, Orasoja Member), followed by Mo and U sequestration under dominantly euxinic/anoxic conditions in the Türisalu Formation. This sequence, which follows transgression over a shallow siliciclastic ramp, most likely reflects the expansion of oxygen-deficient subpycnoclinal waters, with a shallow pycnocline and a steep redoxcline that facilitated sharp redox transitions in the water column and at the sediment water interface (Hints et al., 2021; Paper III). Decoupling of Mo and U enrichment above 22.30 m in the Aseri PH012B core, where Mo concentrations decline sharply while U increases, together with $\delta^{238}U$ and $\delta^{98}Mo$ both shifting toward seawater-like values, suggests RSE local drawdown and depletion in the lower seawater column (Liu & Algeo, 2020). The related interval may delineate the boundary between the upper, better-mixed water masses above or near the chemocline and the poorly mixed, subpycnoclinal lower waters, representing a critical physico-chemical interface within the water-column structure.

This differential behaviour of Mo and U underscores their distinct redox sensitivities and uptake mechanisms: Mo requires strongly euxinic conditions for effective scavenging via thiomolybdate species (Helz & Vorlicek, 2019), whereas U can be sequestered through diffusion under a broader range of reducing conditions (Paper III). A basin-wide long-term drawdown of Mo relative to U as would be expected under a stagnant, persistently euxinic stratified lower water column where quantitative scavenging of Mo prevails is however not apparent from the geochemical record. In Unit II, the Mo_{EF}/U_{EF} ratios (2–8; Aseri PH012B core, Figure 10) remain close to modern seawater trends, and most of the $\delta^{98}Mo$ values fall within the range typically attributed to fractionation related to ferruginous or intermittently euxinic conditions (Anbar, 2004), despite the enrichment level of both Mo and U falling to euxinic range. The presence lenses with fossils of benthic sponges in Unit II provides independent evidence for the fluctuating nature of redox conditions in these distal inner-shelf settings. Very high-resolution geochemical studies of Cambrian Tremadocian black shales from the outer shelf of the Baltic Palaeobasin have revealed a cyclic redox pattern interpreted as the result of Milankovitch-cycles climate forcing, with systematic interruption of bottom-water euxinia and short-term oxygenation events (Dahl et al., 2019; Zhao et al., 2025). The centimetre-scale sampling resolution

applied in this study likely averaged out millimetre-scale variations in RSE concentrations, which are evident in these recent high-resolution datasets, therefore preventing detection of short-term fluctuations in redox state.

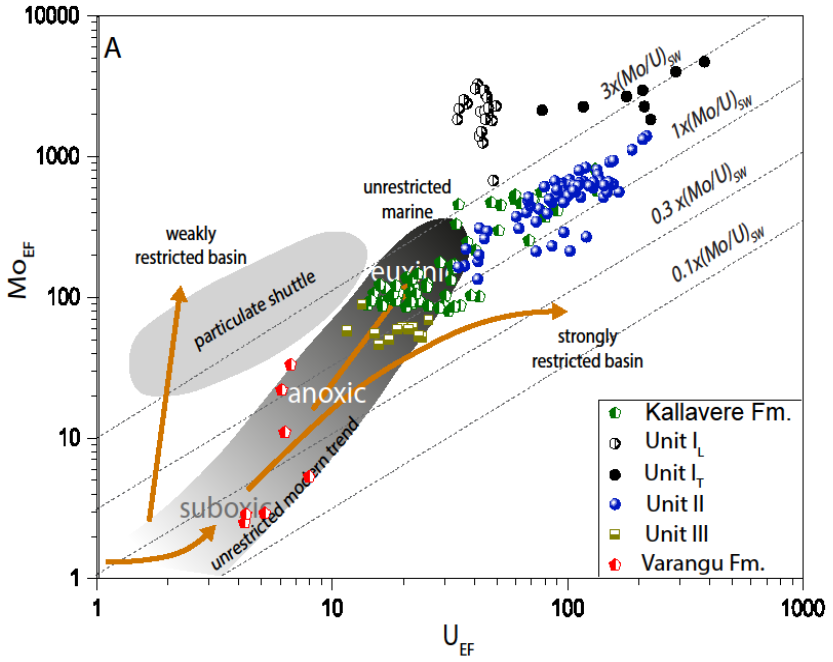

Figure 10 *U_{EF} vs. Mo_{EF} diagram for Aseri PH012B drill core. The diagonal lines represent multiples (0.1, 0.3, 1 and 3) of the Mo/U ratio in present-day seawater; shaded areas and arrows indicate the main geochemical trends associated with different oxygen-deficient redox settings (after Algeo and Tribovillard, 2009). Data from the Kallavere Formation (green diamonds), Unit I_T (black circles), Unit I_L (open black circles), Unit II (blue circles), Unit III (blue squares) and the Varangu Formation (red diamonds) (Paper I).*

At the same time, high TOC and low TN values, resulting in consistently elevated TOC/TN ratios significantly higher than the typical marine phytoplankton (Redfield et al., 1963) in the black shales of the Türisalu Formation and Orasoja Member indicate strongly altered organic matter, preferential loss of nitrogen-rich compounds, and a correspondingly euxinic environment throughout the accumulation of organic-rich muds (Hints et al., 2014a, Paper II). The inconsistency between the stratigraphically variable RSE and isotopic record and that of TOC/TN highlights the difficulty of disentangling palaeoredox conditions of the water column from those of the early diagenetic sediment pore water even in cases of high-resolution sampling. Nevertheless, the data presented here most likely indicate that, against a background of a persistently euxinic sediment column, the redox state of the lower water column fluctuated dynamically during RSE accumulation. Depletion of the RSE inventory in the lower water column likely occurred locally or episodically, suggesting that the renewal rate of dissolved RSE in bottom-water mostly exceeded their removal to the sedimentary sink, consistent with an open or semi-restricted character of the inner-shelf environment.

5.2 Transgression and sedimentation rates

The results presented in Paper III indicate that, beyond the influence of redox gradients, additional environmental factors such as clastic starvation exceptionally low net sedimentation rates, relative sea-level fluctuations, and associated facies shifts played a crucial role in driving RSE hyper-enrichment within the Türisalu Formation (Brumsack, 2006; Rimmer, 2004).

Deposition of the thin interval of organic-rich muds of the Türisalu Formation above the siliciclastic Kallavere Formation marks an upward-deepening trend and a landward facies shift in the study area. At the same time, peak RSE enrichment including U concentrations up to 510 ppm in Unit II (Paper I and III), interpreted in the thesis as the distal inner-shelf transgressive highstand part of the Türisalu Formation significantly exceeds values recorded from deeper basinal Tremadocian settings. The observed coincidence of lithological boundaries, shifts in hyper-enriched RSE associations, and variations in isotopic composition points to a strong covariance with physico-chemical sediment accumulation dynamics and facies-controlled RSE enrichment in the inner-shelf settings of the epicontinental basin.

Peak U hyper-enrichment in Unit II of the Aseri PH012B core occurs together with $\delta^{238}U$ values fluctuating between 0.33 and 0.28 ‰. This pattern is consistent with diffusion of aqueous U(VI) species across the sediment-water interface and their subsequent reduction to U(IV) within sediment porewaters, the main pathway for uranium sequestration. Such uptake is limited by diffusion rates in fine-grained sediment and by slow U-reduction kinetics as was stated earlier, suggesting a direct link between sedimentation rate and authigenic U enrichment (Klinkhammer & Palmer, 1991).

Using a chronostratigraphically constrained U-distribution record from Tremadocian Alum Shale of the outer shelf (Dahl et al., 2019; Schovsbo, 2002) as an analogue, Paper III estimated that average net sediment accumulation rates in Unit II at Aseri were likely less than 1 mm kyr^{-1}, remaining below 1-4 mm kyr^{-1} range suggested for U-rich Cambrian Alum Shale (Zhao et al., 2025). This finding supports the highly condensed nature of the targeted U-enriched interval and aligns with the regional geological characteristics of northeastern Estonia and the Eastern Baltic. Although negligible input of terrestrial weathering products apparently characterized much of the basin (Sturesson et al., 2005) the presence of a pronounced sedimentary hiatus during the middle Tremadocian across the eastern Baltic region (Meidla et al., 2023) suggests that clastic starvation reached an extreme in these parts of Baltica, driven by high sea level, reduced terrestrial runoff, and trapping of siliciclastics in coastal areas (Cattaneo & Steel, 2003). The interplay of transgression and sedimentation dynamics modulated by both water depth and shoreline proximity established the sedimentological framework that governed RSE enrichment.

The ultraslow net sedimentation rates inferred for Unit II from U hyper-enrichment may not apply to the basal or upper parts of the Türisalu Formation, nor to the Kallavere Formation, where lower U concentrations and heavier $\delta^{238}U$ values (Unit I) indicate distinct mechanisms for U uptake. Nevertheless, as emphasized in Paper III, the strongly sulfidic character and diverse pyrite varieties in the studied black shales including black shale interbeds within the Kallavere Formation support formation under slow burial rates and prolonged seawater contact.

5.3 Fine clay dynamics and Fe-Mn redox cycling

Redox stratification in the water column and extreme clastic starvation alone fail to explain the complexity of the observed hyper-enrichment patterns. Findings from Papers I and III suggest that scavenging of RSE by the fine clay fraction and Fe-Mn (oxyhydr)oxides played a pivotal role in the sequestration of V and Mo, linking the flux of primary sediment particles to the sea bottom with the accumulation of metals in the primary muds.

Paper I proposes that fine clay particles with a high specific surface area (SSA) scavenged V-dissolved organic matter (DOM) complexes from suboxic seawater. This interpretation is supported by strong or very strong positive correlations between V, Cr, Al, and Ti, a marked increase in V content with that of Al_2O_3 (from 1200 to 2300 ppm as Al_2O_3 rises from 10.5 to 12 wt%), and clustering of V with clay-related elements in the PCA results (Figure 6). The uptake pathway likely began with the reduction of dissolved V(V) to V(IV) in the suboxic water column, mediated by abundant DOM. The reduced, more particle-reactive V(IV) species complexed with organic ligands and were subsequently adsorbed onto fine clay particles, which acted as a 'shuttle' transferring V from the water column to the sediments. The V hyper-enrichment appears in the most clay-rich black shale horizons (with Al content used as a proxy for clay abundance) within the Kallavere Formation and Unit I of the Türisalu Formation. However, because these intervals are also strongly sulfidic, further reduction of scavenged V(IV) to V(III) by dissolved H_2S or Fe(II) near the sediment–water interface or in the lower water column is consistent with the overall geochemical context (Bian et al., 2022; Breit & Wanty, 1991; Gustafsson, 2019).

Paper III identifies Fe-Mn redox cycling as a key mechanism driving Mo hyper-enrichment (Dellwig et al., 2010; Goldberg et al., 2012), particularly during the early stages of transgression. This conclusion is based on a rather light δ^{98}Mo signal characteristic for Mo fractioning during surface complexation with Mn oxides in oxic water in the lowermost Mo hyper-enriched part of the Türisalu Formation and agrees with the decoupling of Mo_{EF} and U_{EF} (Figure 10) enrichment trends in these intervals. The enhanced formation of Fe-Mn (oxyhydr)oxides near the chemocline in the water column, could have been facilitated by diapycnal mixing or local wind-forcing (Paper III). The Fe-Mn (oxyhydr)oxide particles or coatings scavenged dissolved molybdate species and transported them toward the sea bottom. The progressive upward shift toward heavier δ^{98}Mo signatures, reflecting reduced isotopic fractionation in the Mo-hyper-enriched Unit I, is consistent with the subsequent release of scavenged Mo into H_2S-rich seawater or pore waters and its effective conversion to thiomolybdates under a progressively deepening water column (Archer & Vance, 2008), ensuring long-term Mo retention through binding to sulfides or sulfurized organic matter (Paper III).

5.4 Primary production and OM degradation–preservation

Besides presence of surface-reactivity mineral matter, abundance of labile and dissolved organic matter in sedimentary systems apparently modulated the previously described scavenging mechanisms through set of local feedback loops related to primary production and degradation of OM in the inner-shelf of the palaeobasin (Paper II). The roles of organic matter in syngenetic metal sequestration in black shales evidenced by the typical positive covariance between RSE and OM reported in empirical studies (Tribovillard et al., 2006) remain poorly constrained at the mechanistic level, largely because integrated mechanistic models of complex OM degradation systems have only

recently begun to emerge (Shang, 2023). Commonly stated enhanced bioproductivity versus enhanced preservation dilemma in black shale genesis (Shang, 2023) is likewise fundamental to the problem of RSE hyper-enrichment in studied settings. Paper II, which examines nitrogen and organic carbon isotope records from the Aseri, indicates that both enhanced primary productivity and organic matter burial facilitated by a shallow water column were important factors in the formation of the organic-rich metalliferous black shales.

According to previous studies the OM in the Türisalu Formation is thermally immature, purely marine Type-II kerogen (H/C ≈ 1.24, O/C ≈ 0.16), and was likely produced by cyanobacteria and green sulphur bacteria (Lille, 2003). Low $\delta^{15}N$ values (−2.5 to +0.2 ‰) in the black shales from the Aseri PH012B drill core indicate minimal nitrogen-isotope fractionation relative to atmosphere-like values (Zerkle et al., 2008). The high molar C/N ratios (average 37 for Türisalu, ∼29 for Kallavere) reflect substantial nitrogen loss compared with average marine biomass values (C/N ≈ 106:16 (Martiny et al., 2014)).

The low, unfractionated $\delta^{15}N$ values of the Türisalu Formation suggest a nitrogen-limited environment characterized by a deficit of fixed inorganic nitrogen in seawater. They further indicate that biological N_2 fixation by diazotrophic phytoplankton was likely the principal nitrogen source for primary producers (Zerkle et al., 2008). Biological nitrogen fixation has been shown to produce $\delta^{15}N$ values in cyanobacterial biomass ranging from −1 to 0 ‰, while the $\delta^{15}N$ of dissolved N_2 in seawater is approximately +0.6 ‰. Preservation of an unfractionated $\delta^{15}N$ signal in the black shale agrees with efficient quantitative denitrification in a shallow, oxygen-depleted water column and in sediment, governing the release and loss of N from marine pool via dinitrogen gas (Sigman & Casciotti, 2001). In modern oceans biological N_2 fixation typically appears in nutrient-stressed oligotrophic photic zone. Nevertheless, P and Fe are thought to be key chemical factors limiting N_2 fixation, with their excess supply able to promote diazotroph growth or trigger microbial blooms (Wen et al., 2022). The ample flux of P and Fe to the inner-shelf of the Baltic palaeobasin, at least during accumulation of transgressive mud beds in the Orasoja Member and Unit I of the Türisalu Formation, is evidenced by the characteristic facies transition from shallow water shelly phosphorites to black shales and abundance of iron sulfides, respectively. These geological observations point to the high bioproduction combined with high OM recycling-mineralisation rates in the inner-shelf of palaeobasin.

Scott et al. (2017), who investigated V hyper-enrichment in the Late Devonian Bakken Formation, suggested that a key factor controlling trace metal hyper-enrichment in Palaeozoic black shales of North America was the short transit time of organic matter through the water column; that is, shallow water depths (100-150 m) were critical in allowing the rapid development of euxinic conditions in bottom waters or sediments. In the inner-shelf of the Baltic Palaeobasin, the average water depth was likely around 40 m (Scotese, 2023) and was likely shallower than that during the initial transgressive stages of organic-rich mud accumulation. The very high TOC contents in the black shales of the Orasoja Member and Unit I of the Türisalu Formation suggest that the short transit time of organic matter could have promoted high OM flux to the seafloor and facilitated its subsequent preservation. Given the hyper-enrichment of V and Mo in these intervals, one may infer a rapid onset of H_2S buildup in seawater or porewaters near the sediment water interface. Paper I proposed that efficient sulfate reduction created conditions conducive to V(IV) reduction to V(III), with organosulfur compounds complexing with V (Gomez-Saez et al., 2016), thus aiding long-term sequestration of V. Moreover, the Mo hyper-enrichment and the accompanying shift in $\delta^{98}Mo$ values from Fe-Mn redox

cycling-dominated capture to more quantitative Mo scavenging in the Orasoja Member and Unit I may indicate the expansion of highly sulfidic zone from sediment column into the lower water column, driven by local degradation of OM, as water depth increased (Shang, 2023; Zhang et al., 2014).

At the same time, the stable and low-amplitude $\delta^{13}C_{org}$ record (-29.8 to -29.0 ‰; n = 35) from the Türisalu and Kallavere formations is consistent with the absence of major global carbon-cycle perturbations during the Tremadocian and aligns with values reported from deeper basinal settings (Harris et al., 2001; Tyson, 2001; Van Breugel et al., 2005). The limited variability in the carbon isotope record, contrasted with the pronounced heterogeneity in RSE enrichment, suggests that metal accumulation was governed primarily by local to regional controls.

5.5 Palaeoenvironmental model for Mo, U and V sequestration

The geochemical data from the three case studies, together with earlier work on Baltica, provide the basis for a site-specific palaeoenvironmental framework explaining RSE hyper-enrichment in organic-rich muds deposited on the inner shelf of the Baltic Palaeobasin during the Tremadocian.

The first-order preconditions for the accumulation of metalliferous, organic-rich complexes were likely governed by global to regional factors. The geochemical record indicates open to semi-restricted marine conditions against the backdrop of globally high sea level and a low-relief Baltica landscape during deposition of the primary muds. The composition of seawater the source of the enriched metals appears to have remained largely unmodified, with dissolved U/Mo ratios and isotopic signatures comparable to those of modern oceans. Basin-wide redox stratification was probably maintained by shallow thermohaline layering within a flat-bottomed basin, driven by elevated global temperatures and possibly enhanced mid-latitude precipitation during the Tremadocian. Periodic disruptions of this stratification, including brief bottom-water oxygenation events, were likely cosmogenically induced, as suggested by outer-shelf geochemical variance records. Nutrient supply particularly phosphorus was sustained by upwelling from the Iapetus margin, with dissolved P becoming trapped below the pycnocline without a permanent sedimentary sink in anoxic sediments. These conditions established the framework for sequential, basin-wide enrichment of V, U, and Mo governed by redox zonation.

At the site-specific scale, facies-dependent factors such as sea level rise, diminished clastic input to the distal inner-shelf areas, and ultra-slow sedimentation rates under highstand conditions prolonged interaction between seawater and surface sediments promoting diffusive U uptake from subpycnoclinal waters (Paper III). In coastward organic-rich facies, V and Mo hyper-enrichment proceeded via two-step pathways: (1) scavenging of dissolved metals by surface-reactive particulate matter under oxic-suboxic conditions, followed by (2) reductive transition into low-solubility compounds and sequestration in euxinic muds. Fine-grained clays acted as transport agents for V-organic complexes from suboxic waters to the sea bottom, while Fe-Mn redox cycling between the oxic water column and euxinic muds enhanced Mo capture (Paper I, III). These processes were supported by abundant marine OM derived from a nitrogen-limited, high-productivity ecosystem (Paper II) and short OM transit times that allowed abundant degradable fractions to reach the seafloor. Nutrient inputs (P and Fe) from deeper basinal and terrigenous sources, combined with local C-P recycling loops, likely maintained sharp but spatially variable oxic to euxinic redox transition in shallow inner-shelf settings despite

more active hydrodynamic mixing compared to the distal inner-shelf. Degradation of labile OM by sulfate-reducing bacteria led to H_2S build-up in pore and bottom waters, fostering Fe-sulfide formation and Mo hyper-enrichment. Increasing δ^{98}Mo values with inferred water depth suggest that rising sea level and sustained bottom euxinia enhanced quantitative Mo scavenging from seawater, reflecting a coupled control by Fe-Mn (oxyhydr)oxides and Mo reduction–thiolation processes during hyper-enrichment.

6 Prospects for future research

Although the thesis offers new insights into key aspects of metal enrichment in inner-shelf black shales of Baltica further work is needed to clarify the organic-mineral carriers of RSE and to develop a more coherent view of how syngenetic RSE uptake varied across the epicontinental basin.

New, preliminary data from oxidised grain-size fraction (most OM removed using H_2O_2) from the Türisalu Formation (Table 1), confirm that V in the black shale remains strongly associated with clay minerals, with peak concentrations reaching up to 4832 ppm in the < 0.2 µm fraction (Figure. 11A). The inverse relationship between V concentration and grain size, together with the strong V-Al correlation (Figure. 11B), underscores the dominant role of clay phases for V uptake, and may indicate later diagenetic substitution of V(III) into clay mineral lattices (Peacor et al., 2000). The clay mineral assemblage in the finest fractions (< 0.2 µm) of the black shale comprises illite-smectite (Ill/Sm), illite, and chlorite, with Ill/Sm representing the most likely primary host of V (Figure. 11 C), owing to its high SSA (600–800 $m^2\ g^{-1}$ for smectite components) and high cation exchange capacity. The variability of V concentrations among oxidised grain-size fractions with comparable Al levels suggests that SSA controlled by grain size and the proportion of Ill/Sm versus illite (SSA 70–100 $m^2\ g^{-1}$) was a key variable governing V uptake and retention. Particle-size distribution data from laser diffraction analysis confirm the dominance of ultrafine particles (~0.1 µm) in the < 0.2 µm fraction, emphasizing their high surface area and reactivity. These preliminary results are consistent with the syngenetic adsorption of V(IV)-DOM complexes onto clay surfaces, driven by the electrochemical properties of Ill/Sm, representing a key step in the initial enrichment process. This might have been followed by reduction of V(IV) to V(III) and its subsequent incorporation into Ill/Sm during low-temperature diagenesis, associated with the progressive illitization of primary smectite (Lindgreen et al., 2000).

Table 1 *Chemical composition of sample from the Türisalu Formation, Pakri peninsula, before and after oxidation of OM with H_2O_2.*

	Major elements (wt%)										Trace elements (ppm)	
	SiO_2	TiO_2	Al_2O_3	Fe_2O_3	MnO	MgO	Na_2O	K_2O	P_2O_5	S	V	Zn
Original sample	46.73	0.69	12.12	6.76	0.02	1.08	0.13	7.08	0.15	2.54	981	36
Solid residue	60.46	0.93	16.19	1.25	0.01	1.24	0.04	9.82	0.05	0.05	1106	46
Residual solution	0.01	0.00	0.05	11.17	0.01	0.04	0.00	0.00	0.28	20.16	323	23

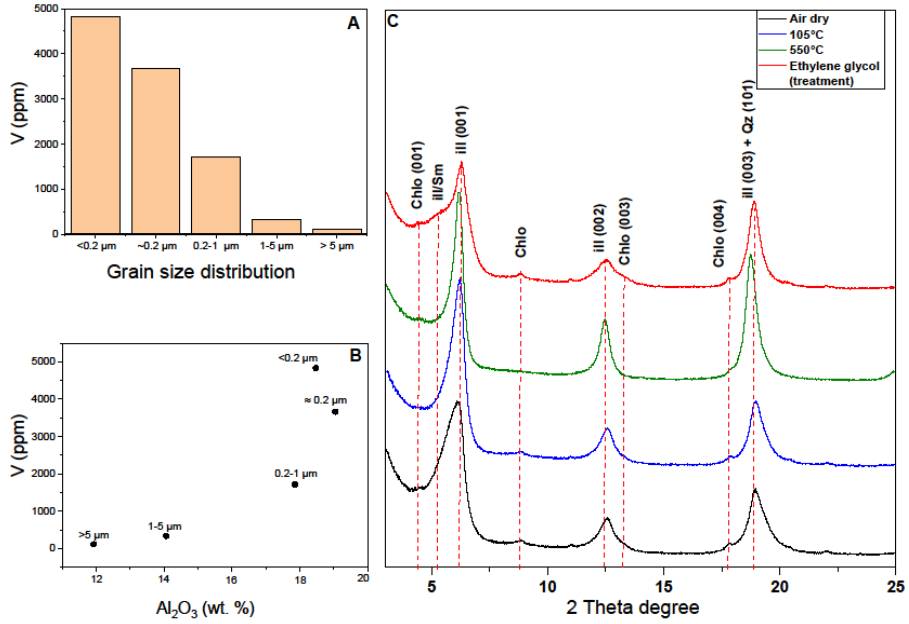

Figure 11 *(A) V concentrations in the fine fractions of black shales from the Türisalu Formation, Pakri peninsula, based on XRF analysis. (B) Al_2O_3 versus V distribution in different grain-size fractions (<0.2 µm, ~0.2 µm, 0.2-0.5 µm, 0.5-1 µm, 1-5 µm). (C) XRD patterns of the oriented slides of the ~0.2 µm fraction under various treatment conditions. Abbreviations: Ill/Sm = mixed-layered illite-smectite, Ill = illite, Chlo = chlorite, Qz = quartz.*

The H_2O_2 treatment nevertheless reveals a complex nature of partitioning of V in the studied black shale. While a significant portion remained bound to the clay-rich residue (1106 ppm; Table 1), a smaller proportion (323 ppm) of V was mobilised into solution, indicating that some V is associated with easily oxidisable OM, probably as V(IV) in organic-metal complexes like V-porphyrins (Paper I). The above-described findings, however, require further verification using milder oxidants and by applying rigorous laboratory protocols.

Unpublished microanalytical studies carried out in GFZ Helmholtz-Zentrum using scanning and transmission electron microscopy (SEM, TEM) reveal two distinct OM varieties in samples from Toolse area: amorphous kerogen and a more granular variety, possibly representing solid bitumen or migrated hydrocarbons. V appears to be preferentially associated with the latter OM type. At finer scale, synchrotron-based X-ray absorption spectroscopy and micro-XRF mapping should be employed to resolve the molecular speciation and coordination environment of metals in both clay and sulfide matrices, distinguishing syngenetic versus diagenetic metal carriers. These micro-analytical approaches could be complemented by focused ion beam-SEM or TEM to directly image submicron mineral-metal associations and assess metal partitioning at clay-organic interfaces. Integrating these data with S and Fe isotope systems would further enable discrimination between biogenic and abiotic pathways of metal fixation.

On the regional scale, a multi-core isotopic transect across the Baltic Palaeobasin, extending from nearshore (Türisalu-type) to offshore (Alum Shale-type) settings, would offer a robust basis for assessing basin-scale redox heterogeneity and metal cycling under Tremadocian greenhouse conditions.

7 Conclusions

The thesis presents the first integrated, high-resolution elemental and isotopic record of Tremadocian V-Mo-U-rich shallow-water black shales from the innermost Baltica shelf, including the first systematic U- and Mo-isotope fractionation data from these settings.

Taken together, Papers I-III show that hyper-enrichment of redox-sensitive elements in the Tremadocian Türisalu Formation reflects a combination of site-specific sedimentological, geochemical, and biological factors, supported by global drivers such as elevated palaeotemperatures and high sea level. The distinct, non-overlapping enrichment patterns of U, Mo, and V record the interplay of local depositional controls with the water masses of a stratified basin characterized by an oxygen-depleted lower water column.

U enrichment peaked during the extremely slow sedimentation associated with transgression, enabled by the prolonged operation of diffusion-reduction pathways beneath anoxic bottom waters on the distal inner shelf. Closer to shore, V sequestration was promoted by clay-mediated uptake linked to dissolved organic matter and abundant fine-grained clays under suboxic conditions. The influx of smectite-rich clay, with high surface area and cation-exchange capacity, exerted strong mineralogical control on V distribution. Mo enrichment reflects the combined influence of Fe-Mn redox cycling and euxinia in porewaters and bottom waters. The wide fractionation ranges of δ^{98}Mo and δ^{238}U support these interpretations and reveal facies-dependent shifts in dominant uptake mechanisms during transgression.

Stable-isotope data (δ^{15}N, $\delta^{13}C_{org}$), together with TOC and TN, indicate enhanced diazotroph-dominated primary production on the inner shelf and substantial nitrogen loss during anoxic degradation of organic matter. Elevated P and Fe fluxes maintained high productivity in the innermost shelf, while very short transit times through the shallow water column ensured high delivery of labile organic matter to the seafloor. This promoted intense sulfate reduction and H_2S production in bottom sediments and near-bottom waters, generating strong local controls and spatial heterogeneity in euxinia and therefore in Mo sequestration. The lack of evidence for hydrothermal activity supports an exclusively sedimentary origin for metal enrichment. These findings can help distinguish sedimentary from syngenetic-hydrothermal signatures in metalliferous black shales elsewhere and strengthen genetic models for resource exploration.

The high-resolution sampling strategy and multi-proxy approach integrating trace-metal geochemistry, Mo-U-N-C isotopes, and sedimentological observations demonstrate the power of such datasets for resolving the complex controls on shallow-water metalliferous black shale formation. The results also highlight the need for context-sensitive use of RSE-based redox proxies in shallow-marine settings and show how combined isotope and trace-element data can clarify enrichment mechanisms and their links to facies evolution. The evidence for a nitrogen-limited, diazotroph-dominated ecosystem on the Tremadocian Baltica shelf also provides new insight into nutrient cycling during a period of major environmental change in the Early Palaeozoic.

Future work should refine models of metal speciation and apply advanced analytical tools to better resolve organic-matter metal interactions. Such integrated studies will deepen understanding of palaeoenvironmental dynamics, improve predictions of metal distribution in metalliferous black shales, and help assess the metal recovery potential of the Cambrian–Tremadocian black shale complexes on Baltica.

List of figures

List of tables

References

Aitchison, J. (1982). The Statistical Analysis of Compositional Data. *Journal of the Royal Statistical Society Series B: Statistical Methodology*, *44*(2), 139–160. https://doi.org/10.1111/j.2517-6161.1982.tb01195.x

Algeo, T. J., & Herrmann, A. D. (2018). An ancient estuarine-circulation nutrient trap: The Late Pennsylvanian Midcontinent Sea of North America. *Geology*, *46*(2), 143–146. https://doi.org/10.1130/G39804.1

Algeo, T. J., & Lyons, T. W. (2006). Mo–total organic carbon covariation in modern anoxic marine environments: Implications for analysis of paleoredox and paleohydrographic conditions. *Paleoceanography*, *21*(1). https://doi.org/10.1029/2004PA001112

Algeo, T. J., & Maynard, J. B. (2004). Trace-element behavior and redox facies in core shales of Upper Pennsylvanian Kansas-type cyclothems. *Chemical Geology*, *206*(3–4), 289–318. https://doi.org/10.1016/J.CHEMGEO.2003.12.009

Algeo, T. J., & Maynard, J. B. (2008). Trace-metal covariation as a guide to water-mass conditions in ancient anoxic marine environments. *Geosphere*, *4*(5), 872. https://doi.org/10.1130/GES00174.1

Algeo, T. J., & Tribovillard, N. (2009). Environmental analysis of paleoceanographic systems based on molybdenum-uranium covariation. *Chemical Geology*, *268*(3–4), 211–225. https://doi.org/10.1016/j.chemgeo.2009.09.001

Anbar, A. D. (2004). Molybdenum stable isotopes: Observations, interpretations and directions. *Reviews in Mineralogy and Geochemistry*, *55*, 429–454. https://doi.org/10.2138/GSRMG.55.1.429

Anbar, A. D., & Rouxel, O. (2007). Metal Stable Isotopes in Paleoceanography. *Annual Review of Earth and Planetary Sciences*, *35*(1), 717–746. https://doi.org/10.1146/annurev.earth.34.031405.125029

Andersen, M. B., Romaniello, S., Vance, D., Little, S. H., Herdman, R., & Lyons, T. W. (2014). A modern framework for the interpretation of 238U/235U in studies of ancient ocean redox. *Earth and Planetary Science Letters*, *400*, 184–194. https://doi.org/10.1016/j.epsl.2014.05.051

Andersen, M. B., Stirling, C. H., & Weyer, S. (2017). Uranium isotope fractionation. *Non-Traditional Stable Isotopes*, *82*, 799–850. https://doi.org/10.2138/RMG.2017.82.19

Andersson, A., Dahlman, B., Gee, D. G., & Snäll, S. (1985). The Scandinavian Alum Shales. *Sveriges Geologiska Undersökning, Serie Ca*, *56*, 52.

Archer, C., & Vance, D. (2008). The isotopic signature of the global riverine molybdenum flux and anoxia in the ancient oceans. *Nature Geoscience*, *1*(9), 597–600. https://doi.org/10.1038/ngeo282

Arnold, G. L., Anbar, A. D., Barling, J., & Lyons, T. W. (2004). Molybdenum Isotope Evidence for Widespread Anoxia in Mid-Proterozoic Oceans. *Science*, *304*(5667), 87–90. https://doi.org/10.1126/science.1091785

Arthur, M. A., & Sageman, B. B. (1994). MARINE BLACK SHALES: Depositional Mechanisms and Environments of Ancient Deposits. *Annual Review of Earth and Planetary Sciences*, *22*(1), 499–551. https://doi.org/10.1146/annurev.ea.22.050194.002435

Artyushkov, E. A., Lindström, M., & Popov, L. E. (2000). Relative sea-level changes in Baltoscandia in the Cumbrian and early Ordovician: the predominance of tectonic factors and the absence of large scale eustatic fluctuations. *Tectonophysics*, *320*(3–4), 375–407. https://doi.org/10.1016/S0040-1951(00)00038-X

Bargar, J. R., Williams, K. H., Campbell, K. M., Long, P. E., Stubbs, J. E., Suvorova, E. I., Lezama-Pacheco, J. S., Alessi, D. S., Stylo, M., Webb, S. M., Davis, J. A., Giammar, D. E., Blue, L. Y., & Bernier-Latmani, R. (2013). Uranium redox transition pathways in acetate-amended sediments. *Proceedings of the National Academy of Sciences*, *110*(12), 4506–4511. https://doi.org/10.1073/pnas.1219198110

Barling, J., Arnold, G. L., & Anbar, A. D. (2001). Natural mass-dependent variations in the isotopic composition of molybdenum. *Earth and Planetary Science Letters*, *193*(3–4), 447–457. https://doi.org/10.1016/S0012-821X(01)00514-3

Bhattacharyya, A., Campbell, K. M., Kelly, S. D., Roebbert, Y., Weyer, S., Bernier-Latmani, R., & Borch, T. (2017). Biogenic non-crystalline U(IV) revealed as major component in uranium ore deposits. *Nature Communications*, *8*(1), 15538. https://doi.org/10.1038/ncomms15538

Bian, L., Chappaz, A., Schovsbo, N. H., & Sanei, H. (2022). A new vanadium species in black shales: Updated burial pathways and implications. *Geochimica et Cosmochimica Acta*, *338*, 1–10. https://doi.org/10.1016/j.gca.2022.09.035

Bian, L., Schovsbo, N. H., Chappaz, A., Zheng, X., Nielsen, A. T., Ulrich, T., Wang, X., Dai, S., Galloway, J. M., Małachowska, A., Xu, X., & Sanei, H. (2021). Molybdenum-uranium-vanadium geochemistry in the lower Paleozoic Alum Shale of Scandinavia: Implications for vanadium exploration. *International Journal of Coal Geology*, *239*, 103730. https://doi.org/10.1016/j.coal.2021.103730

Breit, G. N., & Wanty, R. B. (1991). Vanadium accumulation in carbonaceous rocks: A review of geochemical controls during deposition and diagenesis. *Chemical Geology*, *91*(2), 83–97. https://doi.org/10.1016/0009-2541(91)90083-4

Brumsack, H.-J. (2006). The trace metal content of recent organic carbon-rich sediments: Implications for Cretaceous black shale formation. *Palaeogeography, Palaeoclimatology, Palaeoecology*, *232*(2–4), 344–361. https://doi.org/10.1016/j.palaeo.2005.05.011

Calvert, S. E., & Pedersen, T. F. (1993). Geochemistry of Recent oxic and anoxic marine sediments: Implications for the geological record. *Marine Geology*, *113*(1–2), 67–88. https://doi.org/10.1016/0025-3227(93)90150-T

Cattaneo, A., & Steel, R. J. (2003). Transgressive deposits: a review of their variability. *Earth-Science Reviews*, *62*(3–4), 187–228. https://doi.org/10.1016/S0012-8252(02)00134-4

Cocks, L.R.M., Torsvik, T.H., 2002. Earth geography from 500 to 400 Ma: a faunal and palaeomagnetic Journal of the Geological Society of London, 159, 631–644. https://doi.org/10.11 44/0016-764901-118

Cole, D. B., Planavsky, N. J., Longley, M., Böning, P., Wilkes, D., Wang, X., Swanner, E. D., Wittkop, C., Loydell, D. K., Busigny, V., Knudsen, A. C., & Sperling, E. A. (2020). Uranium Isotope Fractionation in Non-sulfidic Anoxic Settings and the Global Uranium Isotope Mass Balance. *Global Biogeochemical Cycles*, *34*(8). https://doi.org/10.1029/2020GB006649

Coveney, Jr. , R. M., Watney, W. L., & Maples, C. G. (1991). Contrasting depositional models for Pennsylvanian black shale discerned from molybdenum abundances. *Geology*, *19*(2), 147. https://doi.org/10.1130/0091-7613(1991)019<0147:CDMFPB>2.3.CO;2

Crawford, I., Layton-Matthews, D., Peter, J. M., Gadd, M. G., Voinot, A., Leybourne, M. I., & Pufahl, P. (2021). Application of molybdenum and thallium isotopes as indicators of paleoredox conditions and genesis of hyper-enriched black shale deposits, Peel River, Yukon, Canada. *The Canadian Mineralogist*, *59*(5), 1085–1110. https://doi.org/10.3749/canmin.2000099

Dahl, T. W., Siggaard-Andersen, M.-L., Schovsbo, N. H., Persson, D. O., Husted, S., Hougård, I. W., Dickson, A. J., Kjær, K., & Nielsen, A. T. (2019). Brief oxygenation events in locally anoxic oceans during the Cambrian solves the animal breathing paradox. *Scientific Reports*, *9*(1), 11669. https://doi.org/10.1038/s41598-019-48123-2

Dellwig, O., Leipe, T., März, C., Glockzin, M., Pollehne, F., Schnetger, B., Yakushev, E. V., Böttcher, M. E., & Brumsack, H. J. (2010). A new particulate Mn-Fe-P-shuttle at the redoxcline of anoxic basins. *Geochimica et Cosmochimica Acta*, *74*(24), 7100–7115. https://doi.org/10.1016/j.gca.2010.09.017

Erickson, B. E., & Helz, G. R. (2000). Molybdenum(VI) speciation in sulfidic waters: Stability and lability of thiomolybdates. *Geochimica et Cosmochimica Acta*, *64*(7), 1149–1158. https://doi.org/10.1016/S0016-7037(99)00423-8

Gilleaudeau, G. J., Wei, W., Remírez, M. N., Song, Y., Lyons, T. W., Bates, S., Anbar, A. D., & Algeo, T. J. (2023). Geochemical and Hydrographic Evolution of the Late Devonian Appalachian Seaway: Linking Sedimentation, Redox, and Salinity Across Time and Space. *Geochemistry, Geophysics, Geosystems*, *24*(8). https://doi.org/10.1029/2023GC010973

Goldberg, T., Archer, C., Vance, D., Thamdrup, B., McAnena, A., & Poulton, S. W. (2012). Controls on Mo isotope fractionations in a Mn-rich anoxic marine sediment, Gullmar Fjord, Sweden. *Chemical Geology*, *296–297*, 73–82. https://doi.org/10.1016/j.chemgeo.2011.12.020

Gomez-Saez, G. V., Niggemann, J., Dittmar, T., Pohlabeln, A. M., Lang, S. Q., Noowong, A., Pichler, T., Wörmer, L., & Bühring, S. I. (2016). Molecular evidence for abiotic sulfurization of dissolved organic matter in marine shallow hydrothermal systems. *Geochimica et Cosmochimica Acta*, *190*, 35–52. https://doi.org/10.1016/j.gca.2016.06.027

Graul, S., Kallaste, T., Pajusaar, S., Urston, K., Gregor, A., Moilanen, M., Ndiaye, M., & Hints, R. (2023). REE + Y distribution in Tremadocian shelly phosphorites (Toolse, Estonia): Multi-stages enrichment in shallow marine sediments during early diagenesis. *Journal of Geochemical Exploration*, *254*, 107311. https://doi.org/10.1016/j.gexplo.2023.107311

Gustafsson, J. P. (2019). Vanadium geochemistry in the biogeosphere –speciation, solid-solution interactions, and ecotoxicity. *Applied Geochemistry*, *102*, 1–25. https://doi.org/10.1016/j.apgeochem.2018.12.027

Harris, D., Horwáth, W. R., & van Kessel, C. (2001). Acid fumigation of soils to remove carbonates prior to total organic carbon or CARBON-13 isotopic analysis. *Soil Science Society of America Journal*, *65*(6), 1853–1856. https://doi.org/10.2136/SSSAJ2001.1853

Hatch, G. P. (2012). Dynamics in the Global Market for Rare Earths. *Elements*, *8*(5), 341–346. https://doi.org/10.2113/gselements.8.5.341

Hein, J. R., Perkins, R. B., & McIntyre, B. R. (2004). *Chapter 2 Evolution of thought concerning the origin of the phosphoria formation, western us phosphate field* (pp. 19–42). https://doi.org/10.1016/S1874-2734(04)80004-4

Heinsalu, H., Kaljo, D., Kurvits, T., & Viira, V. (2003). The stratotype of the Orasoja Member (Tremadocian, Northeast Estonia): lithology, mineralogy, and biostratigraphy. *Proceedings of the Estonian Academy of Sciences. Geology*, *52*(3), 135–154. https://doi.org/10.3176/geol.2003.3.02

Helz, G. R., Miller, C. V., Charnock, J. M., Mosselmans, J. F. W., Pattrick, R. A. D., Garner, C. D., & Vaughan, D. J. (1996). Mechanism of molybdenum removal from the sea and its concentration in black shales: EXAFS evidence. *Geochimica et Cosmochimica Acta*, *60*(19), 3631–3642. https://doi.org/10.1016/0016-7037(96)00195-0

Helz, G. R., & Vorlicek, T. P. (2019). Precipitation of molybdenum from euxinic waters and the role of organic matter. *Chemical Geology*, *509*, 178–193. https://doi.org/10.1016/j.chemgeo.2019.02.001

Hints, R., Hade, S., Soesoo, A., & Voolma, M. (2014a). Depositional framework of the East Baltic Tremadocian black shale revisited. *GFF*, *136*(3), 464–482. https://doi.org/10.1080/11035897.2013.866978

Hints, R., Pajusaar, S., Urtson, K., Liiv, M., & Kallaste, T. (2021). Metal enrichment in lithologically complex black shales: a case study from the Tremadocian of NE Estonia. *Estonian Journal of Earth Sciences*, *70*(1), 36. https://doi.org/10.3176/earth.2021.04

Hints, R., Soesoo, A., Voolma, M., Tarros, S., Kallaste, T., & Hade, S. (2014b). Centimetre-scale variability of redox-sensitive elements in Tremadocian black shales from the eastern Baltic Palaeobasin. *Estonian Journal of Earth Sciences*, *63*(4), 233–239. https://doi.org/10.3176/earth.2014.24.

Jenkyns, H. C. (2010). Geochemistry of oceanic anoxic events. *Geochemistry, Geophysics, Geosystems*, *11*(3). https://doi.org/10.1029/2009GC002788

Jochum, K. P., Nohl, U., Herwig, K., Lammel, E., Stoll, B., & Hofmann, A. W. (2005). GeoReM: A New Geochemical Database for Reference Materials and Isotopic Standards. *Geostandards and Geoanalytical Research*, *29*(3), 333–338. https://doi.org/10.1111/j.1751-908X.2005.tb00904.x

Kaljo, D., & Kivimägi, E. (1970). On the distribution of graptolites in the dictyonema shale of Estonia and on the uncontemporaneity of its different facies. *Proceedings of the Academy of Sciences of the Estonian SSR. Chemistry and Geology*, *19*(4), 334–341.

Kendall, B., Dahl, T. W., & Anbar, A. D. (2017). Good Golly, Why Moly? The stable isotope geochemistry of molybdenum. *Non-Traditional Stable Isotopes*, *82*, 683–732. https://doi.org/10.2138/RMG.2017.82.16

Klinkhammer, G. P., & Palmer, M. R. (1991). Uranium in the oceans: Where it goes and why. *Geochimica et Cosmochimica Acta*, *55*(7), 1799–1806. https://doi.org/10.1016/0016-7037(91)90024-Y

Lehmann, B., Pašava, J., Šebek, O., Andronikov, A., Frei, R., Xu, L., & Mao, J. (2022). Early Cambrian highly metalliferous black shale in South China: Cu and Zn isotopes and a short review of other non-traditional stable isotopes. *Mineralium Deposita*, *57*(7), 1167–1187. https://doi.org/10.1007/s00126-022-01097-0

Lille, Ü. (2003). CURRENT KNOWLEDGE ON THE ORIGIN AND STRUCTURE OF ESTONIAN KUKERSITE KEROGEN. *Oil Shale*, *20*(3), 253. https://doi.org/10.3176/oil.2003.3.03

Lindgreen, H., Drits, V. A., Sakharov, B. A., Salyn, A. L., Wrang, P., & Dainyak, L. G. (2000). Illite-smectite structural changes during metamorphism in black Cambrian Alum shales from the Baltic area. *American Mineralogist*, *85*(9), 1223–1238. https://doi.org/10.2138/am-2000-8-916

Liu, J., & Algeo, T. J. (2020). Beyond redox: Control of trace-metal enrichment in anoxic marine facies by watermass chemistry and sedimentation rate. *Geochimica et Cosmochimica Acta*, *287*, 296–317. https://doi.org/10.1016/j.gca.2020.02.037

Loog, A., Kurvits, T., Aruväli, J., & Petersell, V. (2001). GRAIN SIZE ANALYSIS AND MINERALOGY OF THE TREMADOCIAN DICTYONEMA SHALE IN ESTONIA. *Oil Shale*, *18*(4), 281. https://doi.org/10.3176/oil.2001.4.02

Loreggian, L., Novotny, A., Bretagne, S. L., Bartova, B., Wang, Y., & Bernier-Latmani, R. (2020). Effect of Aging on the Stability of Microbially Reduced Uranium in Natural Sediment. *Environmental Science & Technology*, *54*(1), 613–620. https://doi.org/10.1021/acs.est.8b07023

Lu, Z., Hu, R., Han, T., Wen, H., Mo, B., & Algeo, T. J. (2021). Control of V accumulation in organic-rich shales by clay-organic nanocomposites. *Chemical Geology*, *567*, 120100. https://doi.org/10.1016/j.chemgeo.2021.120100

Lyons, T. W., Anbar, A. D., Severmann, S., Scott, C., & Gill, B. C. (2009). Tracking Euxinia in the Ancient Ocean: A Multiproxy Perspective and Proterozoic Case Study. *Annual Review of Earth and Planetary Sciences*, *37*(1), 507–534. https://doi.org/10.1146/annurev.earth.36.031207.124233

Malinovsky, D., Rodushkin, I., Baxter, D. C., Ingri, J., & Öhlander, B. (2005). Molybdenum isotope ratio measurements on geological samples by MC-ICPMS. *International Journal of Mass Spectrometry*, *245*(1–3). https://doi.org/10.1016/j.ijms.2005.07.007

Martiny, A. C., Vrugt, J. A., & Lomas, M. W. (2014). Concentrations and ratios of particulate organic carbon, nitrogen, and phosphorus in the global ocean. *Scientific Data*, *1*(1), 140048. https://doi.org/10.1038/sdata.2014.48

Meidla, T., Ainsaar, L., Hints, O., & Radzevičius, S. (2023). Ordovician of the Eastern Baltic palaeobasin and the Tornquist Sea margin of Baltica. *Geological Society, London, Special Publications*, *532*(1), 317–343. https://doi.org/10.1144/SP532-2022-141

Morford, J. L., & Emerson, S. (1999). The geochemistry of redox sensitive trace metals in sediments. *Geochimica et Cosmochimica Acta*, *63*(11–12), 1735–1750. https://doi.org/10.1016/S0016-7037(99)00126-X

Munnecke, A., Calner, M., Harper, D. A. T., & Servais, T. (2010). Ordovician and Silurian sea–water chemistry, sea level, and climate: A synopsis. *Palaeogeography, Palaeoclimatology, Palaeoecology*, *296*(3–4), 389–413. https://doi.org/10.1016/j.palaeo.2010.08.001

Ndiaye, M., Graul, S., Liiv, M., Kallaste, T., Algeo, T. J., & Hints, R. (2025). Trace-metal hyper-enrichment in Tremadocian black shales of the Baltic Palaeobasin linked to transgression and ultra-slow sedimentation rates. *Chemical Geology*, *690*, 122910. https://doi.org/10.1016/j.chemgeo.2025.122910

Ndiaye, M., Liiv, M., Kallaste, T., Graul, S., & Hints, R. (2023). Nitrogen and organic carbon isotope record in Tremadocian highly metalliferous black shales from Baltica. *Estonian Journal of Earth Sciences*, *72*(1), 78–81. https://doi.org/10.3176/earth.2023.25

Ndiaye, M., Pajusaar, S., Liiv, M., Graul, S., Kallaste, T., & Hints, R. (2023). Fine clay shuttle as a key mechanism for V hyper-enrichment in shallow water Tremadocian black shale from Baltica. *Chemical Geology*, *634*, 121583. https://doi.org/10.1016/j.chemgeo.2023.121583

Nielsen, A. T., & Schovsbo, N. H. (2011). The Lower Cambrian of Scandinavia: Depositional environment, sequence stratigraphy and palaeogeography. *Earth-Science Reviews*, *107*(3–4), 207–310. https://doi.org/10.1016/j.earscirev.2010.12.004

Noordmann, J., Weyer, S., Georg, R. B., Jöns, S., & Sharma, M. (2016). 238U/235U isotope ratios of crustal material, rivers and products of hydrothermal alteration: new insights on the oceanic U isotope mass balance. *Isotopes in Environmental and Health Studies*, *52*(1–2), 141–163. https://doi.org/10.1080/10256016.2015.1047449

Pajusaar, S. , Hints, R. , Kallaste, T. , Kiipli, T. , & Urtson, K. (2021). Chemical composition data of Tremadocian black shale reference samples from Estonia. *SARV: Geoscience Data Repository*.

Pan, Z., Bártová, B., LaGrange, T., Butorin, S. M., Hyatt, N. C., Stennett, M. C., Kvashnina, K. O., & Bernier-Latmani, R. (2020). Nanoscale mechanism of UO2 formation through uranium reduction by magnetite. *Nature Communications*, *11*(1), 4001. https://doi.org/10.1038/s41467-020-17795-0

Peacor, D. R., Coveney, R. M., & Zhao, G. (2000). Authigenic Illite and Organic Matter: The Principal Hosts of Vanadium in the Mecca Quarry Shale at Velpen, Indiana. *Clays and Clay Minerals*, *48*(3), 311–316. https://doi.org/10.1346/CCMN.2000.0480301

Pontér, S., Rodushkin, I., Engström, E., Rodushkina, K., Paulukat, C., Peinerud, E., & Widerlund, A. (2021). Early diagenesis of anthropogenic uranium in lakes receiving deep groundwater from the Kiruna mine, northern Sweden. *Science of the Total Environment*, *793*. https://doi.org/10.1016/j.scitotenv.2021.148441

Popov, L. E., Álvaro, J. J., Holmer, L. E., Bauert, H., Ghobadi Pour, M., Dronov, A. V., Lehnert, O., Hints, O., Männik, P., Zhang, Z., & Zhang, Z. (2019). Glendonite occurrences in the Tremadocian of Baltica: first Early Palaeozoic evidence of massive ikaite precipitation at temperate latitudes. *Scientific Reports*, *9*(1), 7205. https://doi.org/10.1038/s41598-019-43707-4

Pukkonen, E. (1989). Major and minor elements in Estonian Graptolite argillite. *Oil Shale*, *6*(1), 11–18.

Pukkonen, E., & Rammo, M. (1992). Distribution of molybdenum and uranium in the Tremadoc graptolitic argillite (Dictyonema shale) of North-Western Estonia. *Bulletin of the Geological Survey of Estonia*, *2*(1), 3–15.

Redfield, A. C., Ketchum, B. H., & Richards, F. A. (1963). The Influence of Organisms on the Composition of the Sea Water. In M. N. Hill (Ed.), *The Sea* (Vol. 2, pp. 26–77). Interscience Publishers.

Rimmer, S. M. (2004). Geochemical paleoredox indicators in Devonian–Mississippian black shales, Central Appalachian Basin (USA). *Chemical Geology*, *206*(3–4), 373–391. https://doi.org/10.1016/j.chemgeo.2003.12.029

Röhl, H.-J., Schmid-Röhl, A., Oschmann, W., Frimmel, A., & Schwark, L. (2001). The Posidonia Shale (Lower Toarcian) of SW-Germany: an oxygen-depleted ecosystem controlled by sea level and palaeoclimate. *Palaeogeography, Palaeoclimatology, Palaeoecology*, *165*(1–2), 27–52. https://doi.org/10.1016/S0031-0182(00)00152-8

Rudnick, R. L., & Gao, S. (2003). Composition of the Continental Crust. In: Rudnick, R.L. (Ed.), The Crust. Treatise on Geochemistry. *Elsevier-Pergamon, Oxford*, *4*.

Saltzman, M. R., Young, S. A., Kump, L. R., Gill, B. C., Lyons, T. W., & Runnegar, B. (2011). Pulse of atmospheric oxygen during the late Cambrian. *Proceedings of the National Academy of Sciences*, *108*(10), 3876–3881. https://doi.org/10.1073/pnas.1011836108

Scholz, F., Hensen, C., Noffke, A., Rohde, A., Liebetrau, V., & Wallmann, K. (2011). Early diagenesis of redox-sensitive trace metals in the Peru upwelling area – response to ENSO-related oxygen fluctuations in the water column. *Geochimica et Cosmochimica Acta*, *75*(22), 7257–7276. https://doi.org/10.1016/j.gca.2011.08.007

Scholz, F., McManus, J., & Sommer, S. (2013). The manganese and iron shuttle in a modern euxinic basin and implications for molybdenum c ycling at euxinic ocean margins. *Chemical Geology*, *355*, 56–68. https://doi.org/10.1016/j.chemgeo.2013.07.006

Schovsbo, N.H., Nielsen, A.T., Harstad, A.O., Bruton, D.L., 2018. Stratigraphy and geochemical composition of the Cambrian Alum Shale Formation in the Porsgrunn core, Skien–Langesund district, southern Norway. Bulletin of the Geological Society of Denmark, 66, 1–20. https://doi.org/10.37570/bgsd-2018-66-01.

Schovsbo, N. H. (2001). Why barren intervals? A taphonomic case study of the Scandinavian Alum Shale and its faunas. *Lethaia*, *34*(4), 271–285. https://doi.org/10.1111/j.1502-3931.2001.tb00056.x

Schovsbo, N. H. (2002). Uranium enrichment shorewards in black shales: A case study from the Scandinavian Alum Shale. *GFF*, *124*(2), 107–115. https://doi.org/10.1080/11035890201242107

Schulz, H.-M., Yang, S., Schovsbo, N. H., Rybacki, E., Ghanizadeh, A., Bernard, S., Mahlstedt, N., Krüger, M., Amann-Hildebrandt, A., Krooss, B. M., Meier, T., & Reinicke, A. (2021). The Furongian to Lower Ordovician Alum Shale Formation in conventional and unconventional petroleum systems in the Baltic Basin – A review. *Earth-Science Reviews*, *218*, 103674. https://doi.org/10.1016/j.earscirev.2021.103674

Scotese, C. R. (2023). Ordovician plate tectonic and palaeogeographical maps. *Geological Society, London, Special Publications*, *532*(1), 91–109. https://doi.org/10.1144/SP532-2022-311

Scott, C., & Lyons, T. W. (2012). Contrasting molybdenum cycling and isotopic properties in euxinic versus non-euxinic sediments and sedimentary rocks: Refining the paleoproxies. *Chemical Geology*, *324–325*, 19–27. https://doi.org/10.1016/j.chemgeo.2012.05.012

Scott, C., Slack, J. F., & Kelley, K. D. (2017). The hyper-enrichment of V and Zn in black shales of the Late Devonian-Early Mississippian Bakken Formation (USA). *Chemical Geology*, *452*, 24–33. https://doi.org/10.1016/j.chemgeo.2017.01.026

Servais, T., & Harper, D. A. T. (2018). The Great Ordovician Biodiversification Event (GOBE): definition, concept and duration. *Lethaia*, *51*(2), 151–164. https://doi.org/10.1111/let.12259

Shang, H. (2023). A generic hierarchical model of organic matter degradation and preservation in aquatic systems. *Communications Earth & Environment*, *4*(1), 16. https://doi.org/10.1038/s43247-022-00667-4

Sigman, D. M., & Casciotti, K. L. (2001). Nitrogen Isotopes in the Ocean. In *Encyclopedia of Ocean Sciences* (pp. 1884–1894). Elsevier. https://doi.org/10.1006/rwos.2001.0172

Sturesson, Ulf., Popov, Leonid., Holmer, L. E., Bassett, M. G., Felitsyn, S., & Belyatsky, B. (2005). Neodymium isotopic composition of Cambrian–Ordovician biogenic apatite in the Baltoscandian Basin: implications for palaeogeographical evolution and patterns of biodiversity. *Geological Magazine*, *142*(4), 419–439. https://doi.org/10.1017/S0016756805000877

Stylo, M., Neubert, N., Wang, Y., Monga, N., Romaniello, S. J., Weyer, S., & Bernier-Latmani, R. (2015). Uranium isotopes fingerprint biotic reduction. *Proceedings of the National Academy of Sciences of the United States of America*, *112*(18), 5619–5624. https://doi.org/10.1073/PNAS.1421841112

Taylor, S. R. M. S. M. (1985). The continental crust: Its composition and evolution. *United States: N. p., Web.*

Tissot, F. L. H., & Dauphas, N. (2015). Uranium isotopic compositions of the crust and ocean: Age corrections, U budget and global extent of modern anoxia. *Geochimica et Cosmochimica Acta*, *167*, 113–143. https://doi.org/10.1016/j.gca.2015.06.034

Tribovillard, N., Algeo, T. J., Lyons, T., & Riboulleau, A. (2006). Trace metals as paleoredox and paleoproductivity proxies: An update. *Chemical Geology*, *232*(1–2). https://doi.org/10.1016/j.chemgeo.2006.02.012

Trotter, J. A., Williams, I. S., Barnes, C. R., Lécuyer, C., & Nicoll, R. S. (2008). Did Cooling Oceans Trigger Ordovician Biodiversification? Evidence from Conodont Thermometry. *Science*, *321*(5888), 550–554. https://doi.org/10.1126/science.1155814

Tyson, R. V. (2001). Sedimentation rate, dilution, preservation and total organic carbon: some results of a modelling study. *Organic Geochemistry*, *32*(2), 333–339. https://doi.org/10.1016/S0146-6380(00)00161-3

Van Breugel, Y., Schouten, S., Paetzel, M., Nordeide, R., & Sinninghe Damsté, J. S. (2005). The impact of recycling of organic carbon on the stable carbon isotopic composition of dissolved inorganic carbon in a stratified marine system (Kyllaren fjord, Norway). *Organic Geochemistry*, *36*(8), 1163–1173. https://doi.org/10.1016/j.orggeochem.2005.03.003

Vind, J., & Bauert, H. (2020). *Geochemical Characterisation of the Tremadocian Black Shale in North-Western Estonia. No. EGF9330*.

Vind, J., Ofili, S., Mänd, K., Soesoo, A., & Kirsimäe, K. (2023). Redox-sensitive trace metal hyper-enrichment in Tremadocian Alum Shale (graptolite argillite) in northwestern Estonia, Baltic Palaeobasin. *Chemical Geology*, *640*, 121746. https://doi.org/10.1016/j.chemgeo.2023.121746

Voegelin, A. R., Pettke, T., Greber, N. D., von Niederhäusern, B., & Nägler, T. F. (2014). Magma differentiation fractionates Mo isotope ratios: Evidence from the Kos Plateau Tuff (Aegean Arc). *Lithos*, *190–191*, 440–448. https://doi.org/10.1016/j.lithos.2013.12.016

Voolma, M., Soesoo, A., Hade, S., Hints, R., & Kallaste, T. (2013). Geochemical heterogeneity of Estonian graptolite argillite. *Oil Shale*, *30*(3), 377. https://doi.org/10.3176/oil.2013.3.02

Wen, Z., Browning, T. J., Cai, Y., Dai, R., Zhang, R., Du, C., Jiang, R., Lin, W., Liu, X., Cao, Z., Hong, H., Dai, M., & Shi, D. (2022). Nutrient regulation of biological nitrogen fixation across the tropical western North Pacific. *Science Advances*, *8*(5). https://doi.org/10.1126/sciadv.abl7564

Weyer, S., Anbar, A. D., Gerdes, A., Gordon, G. W., Algeo, T. J., & Boyle, E. A. (2008). Natural fractionation of 238U/235U. *Geochimica et Cosmochimica Acta*, *72*(2), 345–359. https://doi.org/10.1016/j.gca.2007.11.012

Xu, L., Lehmann, B., Weyer, S., Wen, H., Mao, J., Neubert, N., & Jian, W. (2024). Inverse Mo versus U isotope correlation of Early Cambrian highly metalliferous black shales in South China indicates synsedimentary metal enrichment from a near-modern ocean. *Mineralium Deposita*, *59*(1), 155–167. https://doi.org/10.1007/s00126-023-01201-y

Zerkle, A. L., Junium, C. K., Canfield, D. E., & House, C. H. (2008). Production of δ15N-depleted biomass during cyanobacterial N2-fixation at high Fe concentrations. *Journal of Geophysical Research: Biogeosciences*, *113*(G3). https://doi.org/10.1029/2007JG000651

Zhang, X., Sigman, D. M., Morel, F. M. M., & Kraepiel, A. M. L. (2014). Nitrogen isotope fractionation by alternative nitrogenases and past ocean anoxia. *Proceedings of the National Academy of Sciences*, *111*(13), 4782–4787. https://doi.org/10.1073/pnas.1402976111

Zhao, Z., Hougård, I. W., Zou, C., Dickson, A. J., Dai, S., Jing, Z., Nielsen, A. T., Ju, P., Guo, Z., Basu, A., Schovsbo, N. H., & Dahl, T. W. (2025). Sub-millimeter molybdenum and uranium isotopes track millennial redox events in the Cambrian ocean. *Communications Earth & Environment*, *6*(1), 766. https://doi.org/10.1038/s43247-025-02722-2

Acknowledgements

I am utterly grateful for the grit and perseverance to keep going until I reached this point. This journey was adventurous, challenging, yet filled with many opportunities for me to grow. For this, I have the following people to thank:

My deepest gratitude goes to my supervisor at Tallinn University of Technology, Dr. Rutt Hints. Thank you for providing me with this valuable opportunity to undertake a PhD journey under your supervision and constantly reminding me that I can do this. My sincerest appreciation also goes to my references and mentors, including Prof. Patricia Patrier, for the guidance, expertise, and support you shared throughout my studies, which have been invaluable. Thank you for allowing me to build on foundations from my earlier education and internships.

I am also grateful to Sylvain Grangeon at BRGM, to whom I am greatly indebted for providing me with guidance, constructive criticism, and support during my research intern period. I cannot thank you enough for going through key steps of my work with me, from experimental conceptualization to data analysis.

Many thanks to all the co-authors for their contributions towards the articles in this thesis, including Sophie Graul, Toivo Kallaste, Thomas Algeo, and others—let's keep doing great science!

To my nearby office mates, Sophie Graul and Nthati Monei, sharing an office with both of you has been a wonderful experience. Thank you for your constant support, helpful insights, and the many fruitful discussions that enriched both my work and daily routine. Nthati, your camaraderie and shared experiences brought positivity and made each day truly enjoyable.

To my dear friends, Oumou Mbacke Fall, Tacko Ka, Ndeye Awa Diakhoumpa, Mame Fatou Mbaye, Fatou Diagne, Moustapha Lo, Mamadou Diop, Abdou Karim Ba, Rogers Evarist Swai, Raoul Bodjrenou, Amadou Coumba Ndao, Gora Fall, Fatou Diagne, Akhmadou Moukhtare Lo, Djily Diop, Seydina Diagne, Moustapha Kassé, El Hadji Abdoulaye Sow and Cheikh Alima Touré, thank you for your unwavering support since the beginning. To all my lovely friends and everyone I've encountered throughout this journey, whom I cannot all mention by name here, thank you for cheering for me.

To my wife, thank you for your unwavering support, for being my confidant and rock throughout my PhD journey. Holding hands with you along this path has been one crazy but awesome ride.

Finally, my loving family, thank you for bearing the long distance and always cheering for me. This thesis is dedicated to you all. To my father and mum, your encouragement from the start has meant everything. To my dear sister Coumba Seye, this one is dedicated to you thank you for your support since the beginning.

This work wouldn't be possible without the financial support from relevant funding bodies, including any grants associated with my PhD at Tallinn University of Technology.

Abstract

Trace-Metal Hyper-Enrichment in Tremadocian Black Shales of the Baltic Palaeobasin: Mechanisms and Palaeoenvironmental Implications

Metalliferous black shales, syngenetically enriched in redox-sensitive elements, are increasingly sought after worldwide as unconventional metal resources. This thesis examines the extreme enrichment of Mo, U, and V in thin, shallow-water, thermally immature Tremadocian black shales of the Türisalu Formation in the Baltic Palaeobasin, with emphasis on the mechanisms driving hyper-enrichment, the governing palaeoenvironmental conditions, and implications for resource exploration.

Using high-resolution sampling and integrated geochemical and stable-isotope analyses (δ^{98}Mo, δ^{238}U, δ^{15}N, $\delta^{13}C_{org}$) from selected drill cores (Aseri PH012B and Toolse PH016B), the study identifies the key sedimentary and redox controls responsible for metal accumulation. The three papers document exceptionally high but non-overlapping enrichments of Mo (up to 2700 ppm), U (up to 510 ppm), and V (up to 2300 ppm) across distinct lithological geochemical units. δ^{98}Mo and δ^{238}U values show wide fractionation ranges (–0.89 to 2.03 ‰ and –0.28 to 0.52 ‰, respectively) and clear stratigraphic trends. Total organic carbon (TOC) ranges from 4 to 15 wt%, and average sulfur remains around 5–6 wt%, underscoring the strongly organic-rich and sulfidic character of the deposit. δ^{15}N values are largely unfractionated (–2.5 to 0.2 ‰), while total nitrogen (TN) stays < 0.5 wt% and TOC/TN ratios remain distinctly high (21–44), consistent with substantial N loss during degradation of organic matter.

These findings indicate that differential hyper-enrichment was driven by transgression-related shifts in redox conditions, shaped by redox-stratified shallow water column in the paleobasin and local sedimentary controls. On the distal inner shelf, an extreme reduction in clastic input allowed U to accumulate through diffusion under ultra-slow sedimentation rates (0.6–1 mm kyr^{-1}) during highstand conditions. On the innermost shelf, V hyper-enrichment was promoted by clay-mediated transport to the seafloor under suboxic conditions. Mo hyper-enrichment reflects combined uptake pathways: scavenging and release during Fe-Mn redox cycling, followed by reduction under locally developed euxinia.

TOC, TN, and δ^{15}N values, together with P and Fe enrichment in underlying phosphatic sandstones, indicate high primary productivity dominated by N_2-fixing cyanobacteria and intense anoxic degradation of organic matter. Shallow water depth likely ensured rapid delivery of labile organic matter to the seabed, promoting localized euxinia and enhancing Mo sequestration.

Preliminary analyses of fine-grained, oxidized clay fractions show peak V concentrations in illite-smectite-rich < 0.2 µm material, highlighting the importance of mixed-layer clays for long-term V retention. Future work using advanced analytical methods should target fine-fraction clay-metal associations, basin-scale isotope mapping, and organic-matter-metal interactions.

Lühikokkuvõte

Jälgmetallide hüperrikastumine Balti Paleobassini Tremadoci-ealistes mustades kiltades: mehhanismid ja tekkekeskkond

Metallirikkad mustad kildad, mis on süngeneetiliselt rikastunud redokstundlike elementidega, on maailmas üha enam tähelepanu pälvimas kui ebatraditsioonilised metalliressursid. Käesolev doktoritöö uurib Mo, U ja V äärmuslikku rikastumist madalveelistes ja madala küpsusastmega Tremadoci-ealistes Türisalu kihistu mustades kildades, keskendudes metallide hüperrikastumise mehhanismidele ning neid kontrollinud keskkonnatingimustele Balti Paleobasseini sisešelfil.

Läbilõigete detailproovimise ning integreeritud geokeemiliste ja stabiilsete isotoopide analüüsidega (δ^{98}Mo, δ^{238}U, δ^{15}N, $\delta^{13}C_{org}$) valitud puuraukudest (Aseri PH012B ja Toolse PH016B) tuvastab doktoritöö sette- ja redokskeskkonna võtmetrendid, mis kontrollisid metallide akumulatsiooni. Kolmes teeside aluseks olevas artiklis on dokumenteeritud lokaalselt erakordselt kõrgeid, kuid omavahel mittekattuvaid Mo (kuni 2700 ppm), U (kuni 510 ppm) ja V sisaldusi (kuni 2300 ppm) Türisalu kihistu kogukivimi proovides. Orgaanilise süsiniku sisaldus (TOC) uuritud mustades kiltades jääb vahemikku 4–15 % ja keskmine väävlisisaldus 5–6 %, rõhutades setendite orgaanikarikast ja sulfiidset iseloomu. Isotoopuuringud toovad esile ebatüüpiliselt laia δ^{98}Mo ja δ^{238}U fraktsioneerumisvahemiku (vastavalt –0,89 kuni 2,03 ‰ ja –0,28 kuni 0,52 ‰) ning selged stratigraafilised trendid. δ^{15}N väärtused viitavad minimaalsele fraktsioneerumisele (–2,5 kuni 0,2 ‰), lämmastikusisaldus (TN) püsib < 0,5 % ning kõrged TOC/TN suhted (21–44) osutavad ulatuslikule lämmastiku kaole orgaanilise aine lagunemise käigus.

Tulemused näitavad, et hüperrikastumine oli seotud meretaseme tõusuga kaasnenud keskkonnatingimuste muutustega, mida kujundas ühelt poolt paleobasseini kihistunud veesammas ja teiselt poolt lokaalsed settekeskkonna tegurid. Sisešelfi kaugemas osas võimaldas purdmaterjali äärmiselt väike sissekanne uraani akumulatsiooni difusiooni–reduktsiooni protsessides üliaeglastes setteakumulatsiooni tingimustes (0,6–1 mm tuhande aasta kohta). Madalmaveelisemas, rannikule lähemal asuvas tsoonis soodustas vanaadiumi hüperrikastumist V(IV)–orgaanika komplekside adsorptsioon savimineraalidele suboksilistes tingimustes ning nende edasine transport saviosakestega merepõhja. Molübdeeni hüperrikastumine peegeldab kahte omavahel seotud rikastumismehhanismi: Mo(IV) adsorptsiooni ja desorptsiooni Fe–Mn oksühüdroksiididel ning sellele järgnenud redutseerumist H_2S-rikkas poorivees või merevees.

TOC, TN ja δ^{15}N andmed, mida toetab uuritud settekivimiläbilõigete fosfori- ja rauarikkus, viitavad kõrgele bioproduktsioonile, N_2-fikseerivate tsüanobakterite kriitilisele rollile biomassi tekkes ning orgaanilise aine ulatuslikule degradeerumisele anaeroobsetes tingimustes. Madal veesügavus tagas tõenäoliselt labiilse orgaanilise aine kiire transpordi põhjamudadesse, soodustades lokaalset H_2S-rikastumist põhjalähedastes kihtides ning luues seeläbi eeldused Mo redutseerumiseks ja püsivaks sidumiseks setetes.

Esmased katsed Türisalu kihistu musta kilda oksüdeeritud peenfraktsioonidega näitavad vanaadiumi maksimaalseid sisaldusi kõige peenemas, illiit-smektiidi-rikkas <0,2 µm fraktsioonis, rõhutades segakihiliste savifaaside tähtsust V pikaajalisel sidumisel uuritud setendis. Edasistes uuringutes tuleks keskenduda rikastunud metallide, savimineraalide ja orgaanilise aine vaheliste seoste ning interaktsioonide täpsemale määratlemisele, samuti basseiniülese isotoopandmestiku kaardistamisele Varapaleosoikumi kiltades.

Appendix

Paper I

Ndiaye, M., Pajusaar, S., Liiv, M., Graul, S., Kallaste, T., Hints, R. (2023a). Fine-clay shuttle as a key mechanism for V hyper-enrichment in shallow-water Tremadocian black shale from Baltica. Chemical Geology, 634, 121583. https://doi.org/10.1016/j.chemgeo.2023.121583.

Chemical Geology 634 (2023) 121583

Contents lists available at ScienceDirect

Chemical Geology

journal homepage: www.elsevier.com/locate/chemgeo

Invited review article

Fine clay shuttle as a key mechanism for V hyper-enrichment in shallow water Tremadocian black shale from Baltica

Mawo Ndiaye *, Siim Pajusaar, Merlin Liiv, Sophie Graul, Toivo Kallaste, Rutt Hints *

Department of Geology, Tallinn University of Technology, Ehitajate tee 5, 19086 Tallinn, Estonia

ARTICLE INFO

Editor: Don Porcelli

Keywords:
Vanadium
Black shale
Baltic Palaeobasin
Ordovician
Clay particle
Chromium

ABSTRACT

The essential role of the fine mineral fraction in V hyper-enrichment in black shales has been suggested in previous studies; however, 'the operational details' of such metallogenic systems remain poorly understood. This study addresses the syngenetic enrichment pathways of V in black shales from the Lower Ordovician in the inner shelf of the Baltic Palaeobasin, showing very high content of redox-sensitive elements, including that of V. X-ray fluorescence spectroscopy (XRF) and organic element analysis (CHNS-O), combined with bivariate and multivariate data analyses, were employed to analyse high-resolution geochemical profiles (> 360 samples) of thermally immature black and grey shales, as well as black shale containing siltstones, from two drill cores from NE Estonia. The detected V (up to 2300 ppm), Mo (up to 4500 ppm), and U (up to 500 ppm) enrichment lacked well-defined co-variance, indicating a complex redox environment and element-specific enrichment pathways. While the maximum V and Mo concentrations were confined to the basal part of the black shale–black shale complex, V hyper-enrichment was also observed in the Mo-U-poor black shale interbeds in the siltstones. Co-variance analyses in metalliferous horizons revealed strong positive relationships between V and organic matter, Al, Ti, and K. Cr, characterised by a high affinity for natural sorbents, demonstrated an almost perfect correlation with V (r = ~95), despite its low concentrations. These patterns are hypothesised to reflect V capture via reduced V(IV)-organic complexes adsorbed to fine clay particles after reduction of V(V) in the seawater column rich in dissolved organic matter. These data suggest that the specific surface area of clay particles acted as the primary limiting parameter for V capture, and the particle flux to the shallow sea bottom defined the degree of V hyper-enrichment in the studied settings.

1. Introduction

Vanadium (V) is a transition metal with multiple redox states that exhibits complex behaviour in natural systems (Gustafsson, 2019). It has been listed as a critical raw material in the European Union and United States (Blengini et al., 2020; Schulz et al., 2017) and has significant potential for renewable energy technologies (Lewicka et al., 2021; Peirò, 2017). Vanadiferous black shales and organic-rich fine-grained deposits have been identified as potential resources for this metal (Kelley et al., 2017). Globally distributed in Phanerozoic marine sequences, well-known examples of such black shales include the Tremadocian Alum Shale (Dictyonema Shale) in Scandinavia and Eastern Europe (Bian et al., 2021; Leventhal, 1991; Wilde et al., 1989), Lower Cambrian metalliferous shales in China (Lehmann et al., 2007; Lu et al., 2021; Pi et al., 2013), the Late Devonian – Early Mississippian (Scott et al., 2017), and Carboniferous black shales (Peacor et al., 2000) from the United States. While V is thought to originate from oxygen-depleted seawater in these sequences (with possibly the potential additional influence of hydrothermal fluids) and its uptake into sediments is primarily related to a decrease in the solubility of reduced V species, the development of extreme V enrichment remains poorly understood.

The geochemical cycle of V in marine systems is linked to the redox state of seawater and the availability of ligands and environmental sorbents (Algeo and Maynard, 2004; Breit and Wanty, 1991). Vanadium occurs in three oxidation states (V(V), V(IV), and V(III)) in Earth's surface environment. The mean concentration of V in modern seawater is estimated to be 1.8 μg/L (Schlesinger et al., 2017) but could vary considerably, ranging from 0.15 to 2.0 μg/L (Bruland et al., 2013; Gustafsson, 2019; Wu et al., 2019). Estimates of its oceanic residence time are in the range of 50–100 kyrs, i.e., ten times longer than the turnover time of the global ocean (Algeo and Maynard, 2004; Emerson and Huested, 1991; Wu et al., 2019). In oxygenated seawater, V is

* Corresponding authors.
E-mail address: mawo.ndiaye@taltech.ee (M. Ndiaye).

https://doi.org/10.1016/j.chemgeo.2023.121583
Received 9 February 2023; Received in revised form 3 May 2023; Accepted 31 May 2023
Available online 8 June 2023

present mainly in highly soluble element like V(V) oxyanion species ($H_2VO_4^-$ and HVO_4^{2-}) and exhibits (quasi-)conservative behaviour. Moreover, reduced V is poorly soluble and has high affinity for organic matter (OM) (Wehrli and Stumm, 1989). V(V) can be scavenged from oxic aqueous solutions using Fe—Mn (oxyhydr)oxides and clay minerals (Morford and Emerson, 1999; Wu et al., 2019). The sorptive behaviour increases significantly with the reduction of dissolved V(V) to V(IV) (Szalay and Szilágyi, 1967). The conversion can begin in a suboxic environment. Organic acids are known to act as major reductants of V (V) (Breit and Wanty, 1991) as well as H_2S and Fe(II) species; additionally, microbially mediated reduction has been reported to be viable (Gustafsson, 2019; O'Loughlin et al., 2021). V(IV) species predominantly occur via oxycations such as VO_2^+ and $VO(OH)^+$, which have a tendency to coordinate with oxygen donor atoms and, therefore, tend to be specifically adsorbed to particles such as hydrous oxides or form strong complexes with organic ligands (Wehrli and Stumm, 1989). Notably, the latter process leads to the thermodynamic stability field of the V(IV) species enlarging toward less reducing and neutral conditions and increases their stability in aqueous solutions. Under sulfidic conditions, further reduction of V(IV) may occur through interaction with H_2S, leading to the formation of highly insoluble V(III) species. However, this conversion process tends to be slow and is thus restricted mainly to post-sedimentary diagenetic alteration (Wanty and Goldhaber, 1992). Due to the progressive burial and maturation of OM, V(III) might be incorporated into illite during the illitisation of smectite via the substitution of Al in the octahedral position in their crystal structure (Peacor et al., 2000). The V(VI) preserved in sediments is thought to be taken up mainly by metal-organic complexes, such as vanadylporphyrins, during diagenesis (Filby, 1994).

While syngenetic enrichment of V in organic-rich muds has been conventionally attributed to V affinity for OM, the influence of different factors in V hyper-enrichment is not fully understood. In addition, the triggers of hyper-enrichment may have varied between different palaeoenvironments. Scott et al. (2017) suggested, using the extremely sulfidic Framvaren Fjord as a modern analogy, that V hyper-enrichment (V > 500 ppm) along with Zn hyper-enrichment in Devonian Bakken Formation shales developed due to the reduction of V(IV) to V(III) in the hypersulfidic lower water column. However, studies of other palaeosettings indicate that hypersulfidic conditions might not have been the sole prerequisite for elevated V capture (Han et al., 2018; Kunert et al., 2020; Lu et al., 2021; Wu et al., 2019; Zhang et al., 2019). Han et al. (2018) argued that V sequestration in Lower Cambrian black shales from China was controlled by down-column fluxes of Fe—Mn (oxyhydr)oxide and organic carbon. Studying the same stratigraphic units, Lu et al. (2021) proposed that the formation of clay-organic nanocomposites played a key role in V cycling, indicating the likely critical interplay between organic and fine-grained terrigenous mineral fluxes in V sequestration.

The strong co-variance between the distribution of V and that of aluminosilicates in V-rich Tremadocian black shales from the Baltic Palaeobasin has been recently demonstrated (Bian et al., 2021; Hints et al., 2021). These black shales belong to the vast Cambrian to Lower Ordovician organic-rich sequences of the Baltica extending from the outer shelf settings to the very shallow inner shelf of the palaeobasin and exhibit, on average, high redox-sensitive element (RSE) enrichment (Hints et al., 2021; Nielsen and Schovsbo, 2006; Pukkonen, 1989; Schovsbo, 2002; Voolma et al., 2013).

The present study investigated a high-resolution geochemical dataset from two drill cores taken from the innermost part of the Baltic Palaeobasin in NE Estonia, where thin, highly V-, Mo-, and U-enriched black shales (Türisalu Formation) overlie sandstones with vast shelly phosphorite resources (Kallavere Formation) and are covered by greenish-grey shales (Varangu Formation). The objective was to assess the applicability of the proposed V hyper-enrichment mechanisms, considering the hypothesis that clay-abled capture is a major pathway for V sequestration (Breit and Wanty, 1991; Lu et al., 2021), and to clarify the physicochemical phenomena and interactions that determine the range of V enrichment in particular settings. The results of this study could support the improvement of predictive models for V distribution. >360 samples, including V-hyper-enriched black shales, V-poor black shales, and grey shales, were collected for this study using continuous sampling of cores in 1-cm-thick intervals.

2. Geological background

2.1. Organic-rich facies of the Baltic Palaeobasin

In the epicontinental Baltic Palaeobasin, organic-rich deposits, which accumulated from the Middle Cambrian to the Early Ordovician and were coupled with general transgression in the flat-bottomed palaeobasin, covered an original depositional area of >800,000 km^2 (Schulz et al., 2021). Their patchily preserved remnants can be tracked from the Norwegian-Swedish Caledonides in the north and northwest of Poland in the south. The shallowest water parts of these deposits occur in Estonia and the St. Petersburg area in Russia (Fig. 1A) (Schulz et al., 2021). Very slow accumulation rates (few millimetres per 1000 years) and high bioproduction combined with high consumption of oxidants during the microbial breakdown of OM, facilitated by the upwelling of deep nutrient-rich waters of the Iapetus Ocean at the western margin of Baltica, allowed the accumulation of extensive OM-rich sulfidic facies enriched in RSE (Leventhal, 1991; Nielsen and Schovsbo, 2006; Pedersen, 1989; Pukkonen and Buchardt, 1994; Schovsbo, 2003; Thickpenny, 1984; Wilde et al., 1989). V hyper-enrichment is limited to the Tremadocian part of the sequence, and most vanadiferous deposits have been reported from the Scania area in Sweden and Estonia (Bian et al., 2021), black shales have different chronostratigraphic spans in different parts of the basin and have been historically denoted using various local names and lithostratigraphic units, such as the Alum Shale Formation (Sweden and Norway), Türisalu Formation, 'Dictyonema shale', 'graptolite argillite' (Estonia), Kaporye Formation (Russia) (Schulz et al., 2019), Słowiński Formation, and Piaśnica Formation (Poland) (Schulz et al., 2021) (Fig. 1B).

2.2. Shallow water black shales of the Türisalu Formation

The study area, located on the passive inner shelf of the palaeobasin on the border zone of the Eastern European Platform and Baltic Shield, was a locus for nearshore shallow water sedimentation punctuated by regression episodes for most of the Lower Palaeozoic (Artyushkov et al., 2000; Nielsen and Schovsbo, 2007). The black shale sequences overlay the coastal sandstones of the Kallavere Formation; the latter contains vast shelly phosphorite resources. The black shales are overlain by organic-poor glauconite-containing grey shales of the Varangu Formation.

The Türisalu Formation is a dark brown, generally horizontally laminated black shale (Fig. 1B). It reaches a maximum thickness of >6 m in NW Estonia, from where it decreases east- and southwards, dropping to 0.5–1 m in NE Estonia. Simultaneously, the number of organic-poor silty interlayers ranging from a fraction of a millimetre to several centimetres in thickness increases. Furthermore, authigenic carbonate concretions and biogenic silica-rich interbeds with remnants of sponge spicules tend to be abundant in the black shales of NE Estonia (Kivimägi and Loog, 1972). Sedimentary features suggest that the accumulation of organic-rich mud occurred under intermittently dynamic water columns at water depths of less than a few tens of meters (Hints et al., 2014). Previous investigations have reported that OM preserved in these black shales is predominantly amorphous, immature (average reflectance of vitrinite-like particles ranges from 0 to 0.55 (Schovsbo, 2002), has H/C 1.0–1.5 and O/C 0.10–0.35 in non-weathered samples, compliant with II-type of kerogen (Veski and Palu, 2003), shows a limited $\delta^{13}C_{org}$ range from −29.0‰ to −29.5‰ (Bian et al., 2021; Hints et al., 2021), and is likely primarily produced by cyanobacteria or possibly by green sulfur

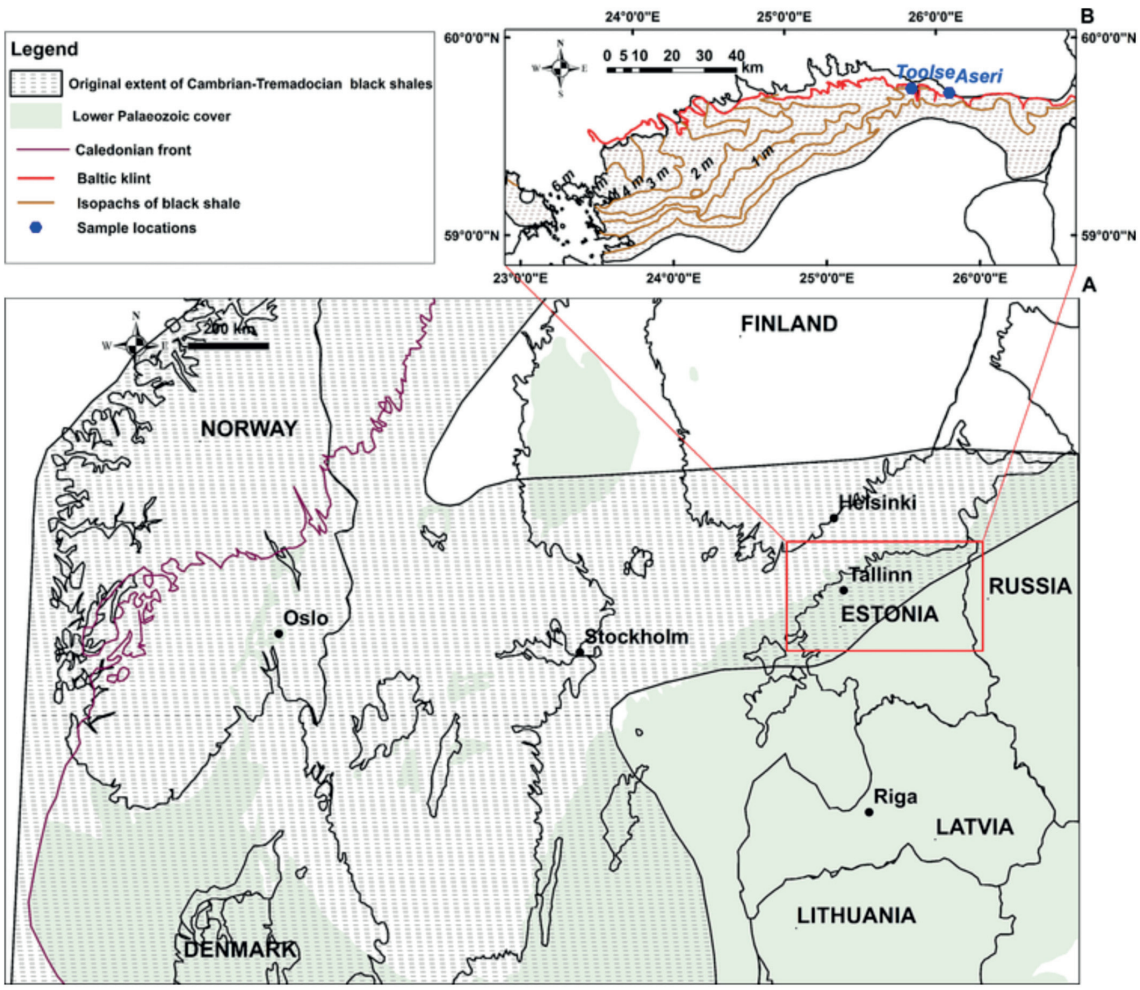

Fig. 1. A. Distribution area of Middle Cambrian to Early Lower Ordovician black shales of the Baltic Palaeobasin (after Schovsbo et al. (2018)). Note that black shales are preserved only in limited areas within the supposed original distribution limits of the organic-rich facies (after Schovsbo et al. (2018)). B. Location schema of the Türisalu Formation; isopach lines show the thickness of the formation (after Pukkonen (1989)). Blue dots mark drillhole locations investigated in the present study: Toolse PH016B and Aseri PH012B. (For interpretation of the references to colour in this figure legend, the reader is referred to the web version of this article.)

bacteria (Lille, 2003).

3. Materials and methods

3.1. Lithological logging and sampling

Samples for the current study were obtained from two new drill cores from NE Estonia Toolse PH016B (59.460274, 26.445899; drill depth from 22.87 to 24.66 m) and Aseri PH012B (59.426053, 26.755267; drill depth from 21.36 to 23.22 m), which were logged prior to sampling. A quarter of the core from the uppermost part of the Kallavere Formation, the Türisalu Formation, and basal part of the Varangu Formation was continuously sampled in 1 cm thick intervals to obtain a V distribution record representative of the observed lithological variability. A similar high-resolution sampling strategy has been lately shown to be efficient for recovering high-frequency palaeoenvironmental signals from black shale sequences (Liu et al., 2019). All samples (~20 g) were crushed and homogenised in an agate mortar using a tungsten carbide mill. Analytical studies were conducted at the Department of Geology, Tallinn University of Technology.

3.2. X-ray fluorescence (XRF)

For major element analysis fused disks were prepared with a Claisse M4 Gas Fusion instrument. 0.66 g of crushed sample was fused using a platinum crucible, and a lithium metaborate: lithium tetraborate: lithium bromide flux. For trace element analysis, ~8 g of powder was pressed into a pellet using 5% Mowiol solution (one drop per gram of sample). Pressed pellets and fused disks were analysed with a Bruker S4 spectrometer by applying internal calibration based on six local in-house reference black shale samples (Pajusaar et al., 2021) and using sample GeoPT48/MzBP from the IAG proficiency testing series for quality control. The laboratory's analytical results from the latest IAG testing round GeoPT52, which used black shales from the Türisalu Formation as the test material, confirmed reliable performance for the specific rock type. For all samples, loss-on-ignition measurements were conducted as

follows: 1 g of material was added to a crucible, placed in a Nabertherm furnace at 550 °C and 950 °C for 4 h, cooled to room temperature in desiccators, and weighed.

3.3. Total organic carbon (TOC)

The samples were analysed for TOC through combustion in a FLASH 2000 organic elemental analyser. Approximately 8 mg of the dried powdered sediment was placed in a silver container. Samples in capsules were pre-treated with 10% HCl to remove inorganic carbon and dried on a hotplate at 80 °C for 5 h. Once dry, the capsules were left to cool and carefully wrapped to form granules. Before analysis, the silver containers were packed into tin containers to facilitate combustion. Cystine was used as the standard (Thermo Fisher Scientific), and high-organic sediment was used as the reference material (IVA Analysentechnik e. K).

3.4. Conventional and multivariate statistical analysis

The obtained dataset was analysed using conventional and multivariate descriptive statistics. Prior to principal component analysis (PCA), the centred log-ratio transformation was applied to the data to overcome spurious correlations within closed-sum compositional data (Aitchison, 1982). PCA was conducted using OriginPro software to reveal multivariate relationships within the dataset. Because the original sample set also contained coarse-grained siliciclastic, carbonate-rich, and mixed lithologies, $Al_2O_3 > 9$ wt% and CaO > 3 wt% were used as threshold values to sort pure carbonate-poor black shale samples.

3.5. Trace element enrichment factors and authigenic fraction

To calculate the enrichment factor (X_{EF}) (Algeo and Maynard, 2004) for a particular trace element (X), trace element concentrations were first normalised to the Al content of the sample and divided into the appropriate trace elements-to-Al ratio in the Post-Archean Australian Shale (PAAS) standard (Taylor and McLennan, 1985) according to the following equation:

$$X_{EF} = (X/Al)_{sample} \Big/ (X/Al)_{PAAS}$$

To define the influence of detrital input on V and Cr co-variance, the authigenic Cr (Cr_{auth}) content of the black shale was calculated according to Lehmann et al. (2016). First, the detrital Cr fraction (Cr_{det}) was calculated based on the Ti and Al content of the samples by normalising the concentrations to the bulk upper continental crust (Rudnick and Gao, 2013):

$$Cr_{det(Ti)} = 0.024 \times Ti_{sample}$$

$$Cr_{det(Al)} = 0.0011 \times Al_{sample}$$

The values of 0.024 and 0.0011 represent the Cr/Ti and Cr/Al ratios in the upper continental crust, respectively.

The Cr_{auth} was then calculated by subtracting the average of the two calculated Cr_{det} values from the measured Cr content of the sample (Cr_{sample}):

$$Cr_{auth} = Cr_{sample} - \left[\left(Cr_{det(Ti)} + Cr_{det(Al)} \right) / 2 \right]$$

4. Results

4.1. Lithological characteristics

The previously applied lithological-geochemical division was adapted for the Türisalu Formation and divided into Zone I (basal), II (middle), and III (upper) (accordingly A, B, and C + D zones after Kivimägi and Loog (1972)). The sampled upper part of the Kallavere Formation below the major black shale sequence presented rhythmic alteration between fine-grained quartzose siltstone beds and black shale interbeds that were a few centimetres thick. This interval also contained irregular and strongly pyritized silty laminae and likely marked a shift toward more immature terrigenous material input to the coastal sea (Heinsalu et al., 2003).

The Türisalu Formation (~1.4 m thick) exhibited considerable lithological variability, including finely laminated, graded, and massive varieties. The cyclic occurrence of biosilica (spiculite) interbeds, commonly associated with syngenetic carbonate concretions, is characteristic of Zone II. Thicker siliciclastic pyritised interbeds occurred in both Zones I and III. The latter was characterised by thinly laminated black shale with alternating lighter and darker laminas, which differed distinctly from the lower part of the formation. The contact of the Türisalu and Varangu Formations was marked by a shift in colour from dark black shales to lighter glauconite containing grey shales but otherwise showed no apparent changes in sedimentological features.

4.2. V enrichment and geochemical profiles

The complete geochemical dataset for the two core sections is provided in the supplementary material 2. The distributions of V and the other selected compounds are illustrated in Fig. 3–4.

The maximum V content recorded in the studied black shales was close to 2350 ppm in both localities, with the highest V enrichment confined to the basal part of the Türisalu Formation (Fig. 2).

In the Toolse drill core, the median concentration of V was 1366 ppm in Zone I, 1168 ppm in Zone II, and dropping to 266 ppm in Zone III. In the Varangu Formation, the median V content is low (314 ppm). For the Aseri drill core, the median V content in Zone I was considerably higher than that in the Toolse core (2196 ppm), which exhibited a more lithologically heterogeneous black shale section.

TOC content reached maximum of ~17 wt% in black shale interbeds from Kallavere Formation.

in the Aseri section, Mo to 4500 ppm in zone I Toolse core, and U to 500 ppm in Zone II Aseri core (Fig. 3–4). The distributions of redox-sensitive trace elements and S showed negligible co-variance, with the latter being preferentially enriched in coarser-grained siliciclastic interbeds. The same intervals also produced high S/TOC ratios (>5), while the typical values in the Türisalu Formation stayed between 0.4 and 1.7. Notably, on average highest S and S/TOC values and most heterogenous distributions of those parameters characterised the siltstone–black shale sequences of the Kallavere Formation. The cyclic variance of Al and Ti contents was positively linked with that of TOC in the metalliferous black shale intervals. The V content normalised to that of Al revealed relatively constant ranges for these beds and a major change in V distribution between Zone II and the metal-poor Zone III in the Türisalu Formation.

4.3. PCA

Only data from Zones I and II excluding those of carbonate-rich samples were used for PCA (Toolse, $n = 92$; Aseri, $n = 73$) (Fig. 5). PC1 accounted for 63% and 40% of the total variance in the Toolse and Aseri datasets, respectively, and showed positive correlations of TOC, V, and Cr. Positive correlations were also observed with Al, K, Ti, and (Ba), which are principal constituents of fine-grained secondary aluminosilicates, such as clay minerals, or tend to associate with the latter in the fine sediment fraction and K-feldspar. The variables showing a strong negative loading on PC1 were Si, Ca, and P, which are typical compounds of coarse-grained clastic fractions (quartz and bioapatite). In the Toolse section, S and Fe (sulfidic association) also exhibited negative loadings on PC1. Mo and U showed moderately strong positive loadings on PC1 in the Toolse core, whereas U provided negative loadings on PC1 in the case of the Aseri dataset. Based on the observed interelement relationship, it can be concluded that V enrichment is intimately linked to the fine grain-size mineral fractions (generally clay minerals) and/or

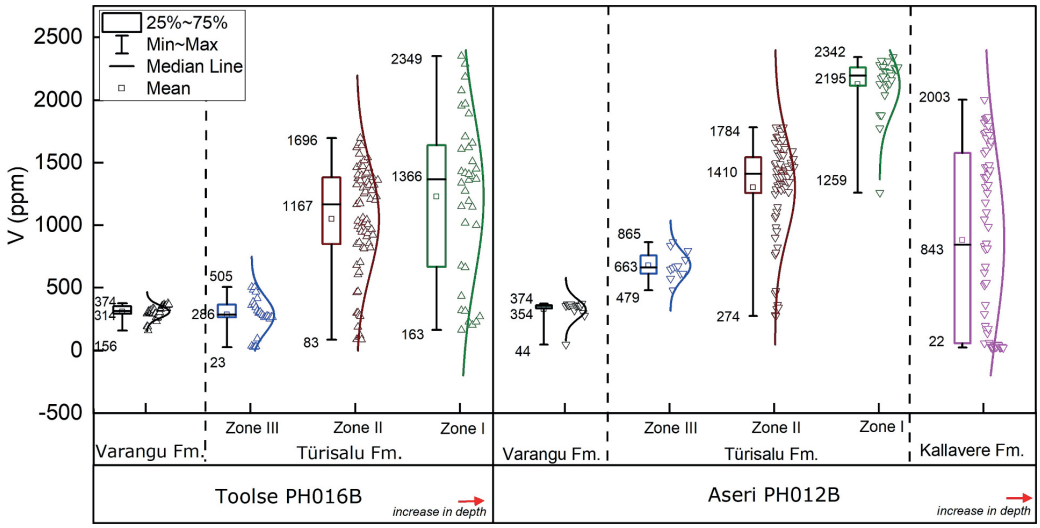

Fig. 2. Box plots show V concentrations in the studied intervals from the Kallavere Formation, Türisalu Formation, and Varangu Formation in Toolse PH16B and Aseri PH012B drill cores.

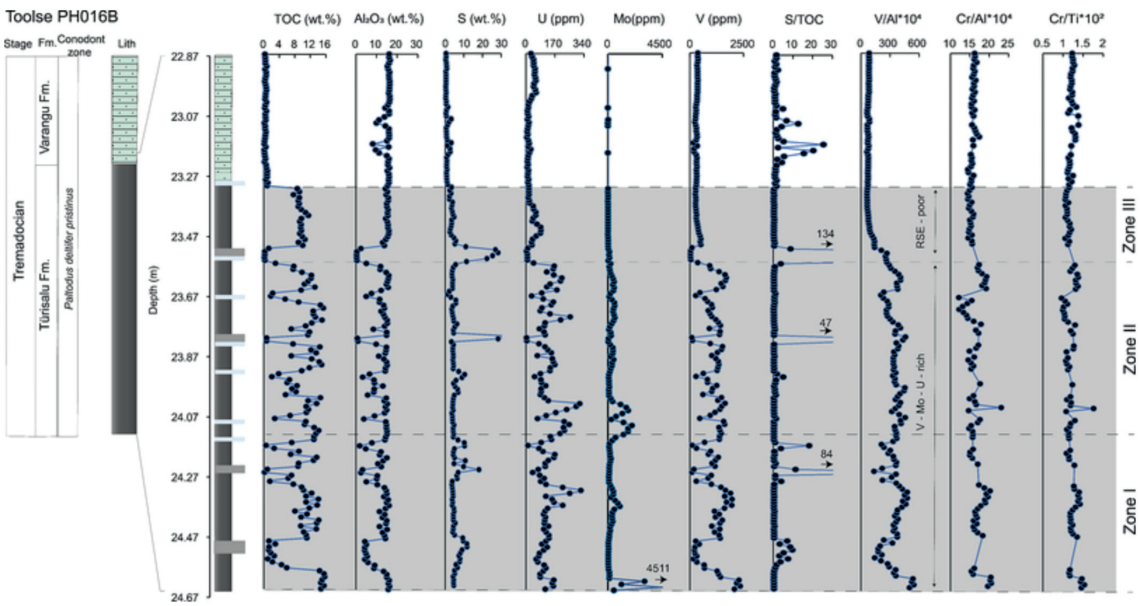

Fig. 3. Vertical distribution trends of selected components in the Toolse PH012B drill core.

OM of the primary mud in the Toolse and Aseri drill cores.

4.4. Bivariate relationships

Pearson correlation coefficients (r) were calculated for the same dataset as used for PCA and showed strong or extremely strong positive correlations between V, Ti, Al, K, TOC, Ba, and Cr (r values from 0.76 to 0.96) in both drill cores (Fig. S1). Whereas the values of the other correlation coefficients slightly decreased in the Aseri drill core compared to the Toolse drill core, the correlation between V and Cr remained consistent (r values 0.96 and 0.95). V and Mo distributions demonstrated a moderate positive correlation in the studied settings (r values 0.55 and 0.63), while no co-variance between U and V was identified in the case of the Aseri drill core (Fig. S1).

The bivariate relationships and coefficients of determination (r^2) for Al_2O_3 vs. V, Al_2O_3 vs. Cr, TOC vs. V, and TOC vs. Cr pairs are illustrated in Fig. 6–7. Generally, high r^2 values characterised all studied couples in Zones I and II of the Türisalu Formation and in the Kallavere Formation in both localities (r^2 varied from 0.64 to 0.94). However, Al demonstrated considerably better predictive power for V and Cr variance

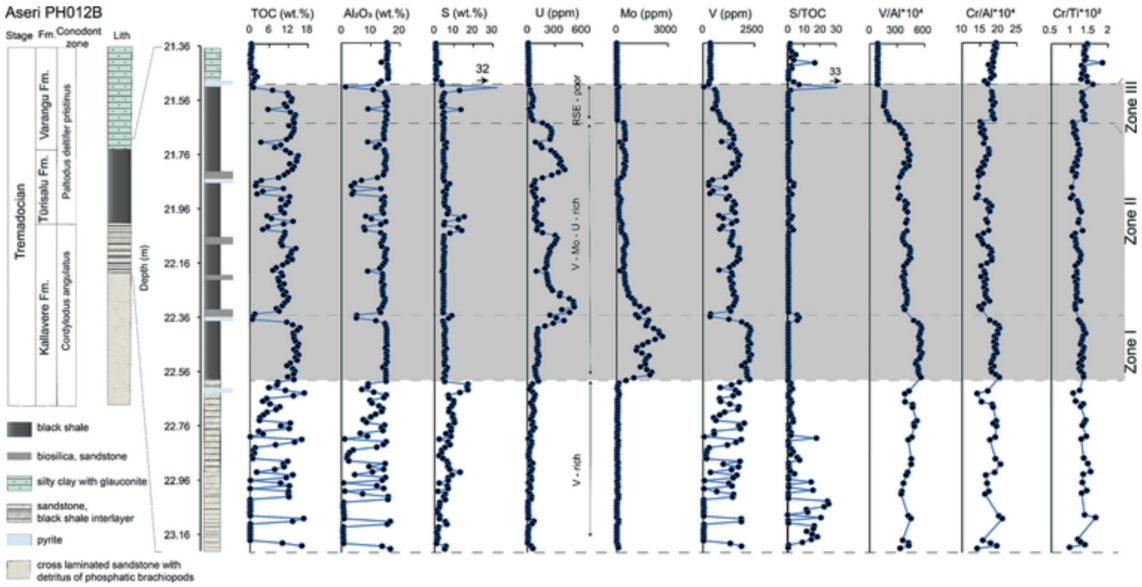

Fig. 4. Vertical distribution trends of selected components in the Aseri PH012B drill core.

compared to that of TOC in the V hyper-enrichment range. Al_2O_3 vs. V and Al_2O_3 vs. Cr produced linear regression lines with significantly different slopes for individual Zones, e.g., within the range of Al_2O_3 content from 10.5 to 12 wt% sharp rise in V content from ~1200 to ~2300 ppm occurred. Notably, a strong similarity in correlation between V vs. Al and Cr vs. Al appeared in V-enriched black shales, despite the Cr content remaining close to the long-term average in the Baltic Palaeobasin (Schovsbo, 2003) and the Varangu Formation.

Fig. 8 presents the relationships between Mo, U, and V contents for the studied settings with hyper-enrichment threshold values based on Bian et al. (2021). The highest average V and Mo hyper-enrichment typified the basal Zone of the Türisalu Formation, and the maximum U enrichment fell into Zone II. Notably, V hyper-enrichment in the organic-rich black shale interbeds of the Kallavere Formation was not accompanied by Mo and V enrichment, while Zone III in the Türisalu Formation and Varangu Formation displayed insignificant Mo, U, and V enrichment with contents close to those in the Varangu Formation.

5. Discussion

5.1. Redox conditions during V enrichment

A decrease in the solubility of RSEs such as V, Mo, and U species in aqueous solutions is the principal pathway for their sequestration into organic-rich marine sediments. However, as RSEs are prone to reduction under various Eh and pH conditions, show affinity for various ligands, and exhibit individual sorption properties, element-specific enrichment patterns characterise natural deposits (Algeo and Liu, 2020). The complexity of deep-time RSE distribution is amplified by changes in the seawater content of RSEs, oxidants, and reductants. These changes are tightly linked to the oxygenation of the Earth's atmosphere and oceans as well as evolutionary changes (Large et al., 2014).

Algeo and Tribovillard (2009) suggested that the Mo—U distribution in ancient deposits can be used for complex palaeoenvironmental analyses of evolving aspects such as the conditions of benthic redox reactions, the role of particulate shuttles, and the evolution of water mass composition. Unlike V, significant uptake of reduced Mo (IV) is known to occur only in a sulfidic environment with $H_2S_{(aq)} > 11$ μM, prompting the conversion of Mo to a reactive particle and its sequestration via a series of thiomolybdates (Algeo and Maynard, 2004; Helz et al., 1996). Thus, Mo enrichment is commonly interpreted as an index for the presence of persistent euxinia (Scott and Lyons, 2012) in settings with a significant influx of Fe—Mn (oxyhydr)oxides into the sea bottom (Goldberg et al., 2009). Conversely, U is prone to reduction under less reducing conditions. However, due to slow reaction kinetics, its capture is limited to the sediment column and shows time-dependent enrichment patterns that adhere to productivity and sedimentation rates (Lau et al., 2020). The calculated Mo_{EF}/U_{EF} (Fig. 9) for V-enriched black shales from the Türisalu Formation and Kallavere Formation fell within the euxinic range and demonstrated normal to very high enrichment compared to modern oxygen-depleted marine environments (Algeo and Maynard, 2004). Furthermore, the values also generally remained higher than those recorded from the middle shelf settings of the palaeobasin, which is in agreement with previous observations (Bian et al., 2021; Schovsbo, 2002). The U and Mo distributions also exhibit significant stratigraphic gradients. Thus, the Mo and U contents show a marked increase combined with an increase in the degree of scatter of Mo_{EF}/U_{EF} ratios in Zones I and II of the Türisalu Formation compared to that of the Kallavere Formation. Notable is the consistent absence of considerable Mo enrichment in the remarkably S-rich Kallavere Formation. Also, distinctly low Mo content appeared in Zone III of the Türisalu Formation. The observed patterns, characterising vertical variability by 1-cm-thick intervals, apparently represent cumulative average concentrations for a long sedimentary period. Dahl et al. (2019) concluded that prevailing anoxic-sulfidic benthic conditions at the middle shelf settings of the Baltic Palaeobasin (Alum Shale Formation) were regularly interrupted by brief oxygenation events spanning 600–3000 years and corresponding to 1–5 mm stratigraphic intervals of black shales. Interestingly, the same intervals were observed to produce peak Mo concentrations. The geochemical signals in the studied samples, such as the absence of strong co-variation between Mo- and TOC, regarded as a distinctive feature of a euxinic benthic environment (Tribovillard et al., 2006), and lack of positive co-variance of Mo with total S content could fit with the Mo uptake controlled by elevated

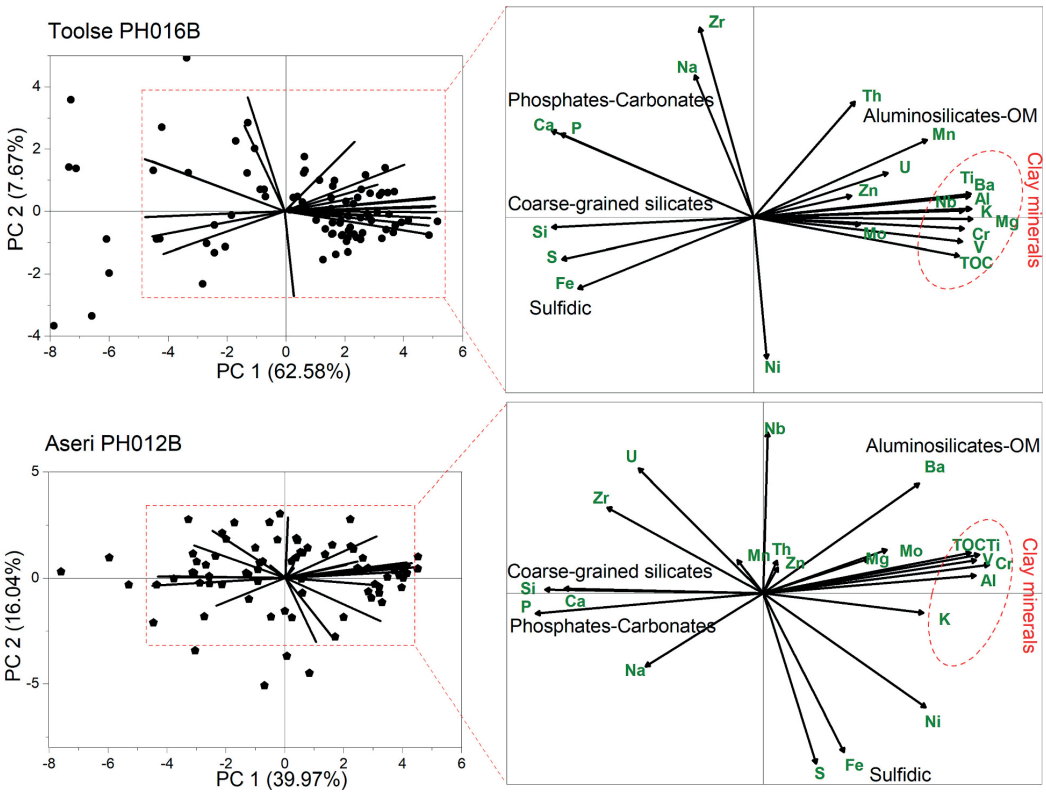

Fig. 5. Principal component analysis (PCA) of geochemical datasets from V-rich black shales from the Türisalu Formation (zone I and II) from Toolse PH16B and Aseri PH012B drill cores. Only samples with $Al_2O_3 > 9$ wt% and CaO < 3 wt% were used for analysis. The first principal component (PC1) accounts for 62.6% and 40.0% of data variability, respectively, and PC2 accounts for 7. 7% and 16.0%, respectively.

microbial sulfate reduction in organic-rich primary sediments and the related diffusive flux of Mo, as opposed to direct scavenging of reduced Mo(IV) in highly sulfidic seawater (Helz and Vorlicek, 2019). However, while peak hyper-enrichment of Mo and V are both confined to the basal transgressive and most organic-rich part of the Türisalu Formation, the high-resolution dataset used in this study could not verify the existence of a direct genetic link between the enrichment of these compounds.

The same holds for the V—U relationship. Compared to Mo, U (VI) reduction to insoluble U(IV) could occur in a benthic environment with less reducing conditions, close to the Fe(III)-Fe(II) transition (Algeo and Maynard, 2008; Sholkovitz et al., 1986). The principal uptake of U in marine muds could have proceeded via diffusion of U(VI) across the sediment–water interface (SWI) and its microbial reduction, as abiotic reduction rates tend to be extremely sluggish in marine sediments (Lau et al., 2020). Zone II in the Türisalu Formation, presenting notable U hyper-enrichment, was also characterised by the rhythmic appearance of interbeds with sponge spicules, suggesting the occurrence of intermittent oxidation events. Both substantial fluctuations in benthic redox conditions and local-scale environmental modifiers (e.g. non-deposition periods and possible redeposition) appear to be relevant for RSA enrichment. Low concentrations of Mo and U in the S-rich Kallavere Formation, on the other hand, may reflect the development of temporal semi-restriction due to morphodynamics of transgressive siliciclastic systems or global scale changes of seawater chemistry triggered by high sea level and extensive anoxic facies accumulation on different palaeocontinents (Landing, 2012; Nielsen and Schovsbo, 2006). Nevertheless, Mo_{EF}/U_{EF} data do not evidence major shifts in the RSE pool of seawater. Alternatively, the influx of excessive Fe (oxyhydr)oxides to nearshore due to fast overflooding of the Baltic Shield areas with mature weathering crusts, efficient uptake of H_2S released by sulfide reduction to metastable iron sulfides and/or transient redox conditions in the water column, could have kept pore water H_2S level below critical threshold values for thiomolybdate formation or aided the release of Mo back to the seawater from sediments (Kowalski et al., 2013). High TS/TOC ratios in considered beds imply that the sedimentation of primary mud took place under normal marine or brackish water columns (Wei and Algeo, 2020). Markedly, very shallow water conditions at the transition from the Türisalu to Kallavere Formation are evidenced by extensive sulfide-cemented hardgrounds with ripple and flow marks in some north Estonian settings. However, post-depositional sulfidation by sulfidic pore water is yet another way to explain the high S content in these sequences (Nemliher and Puura, 1996).

Nevertheless, the average recorded Mo_{EF}-U_{EF} trends for V-hyper-enriched zones follow those of modern euxinic, highly productive open marine settings and thus reflect V uptake from seawater replenished by water exchange with the global ocean.

5.2. *Vanadium co-variance with clays and OM*

The V hyper-enrichment patterns, unlike those of U and Mo, showed very strong co-variance with fine-grained terrigenous input and consistent positive co-variance with TOC. In fine detrital fractions in seawater and sediments, a flake-to-needle-shaped 2:1 clay phase typically dominates. Such particles are mostly weakly negatively charged

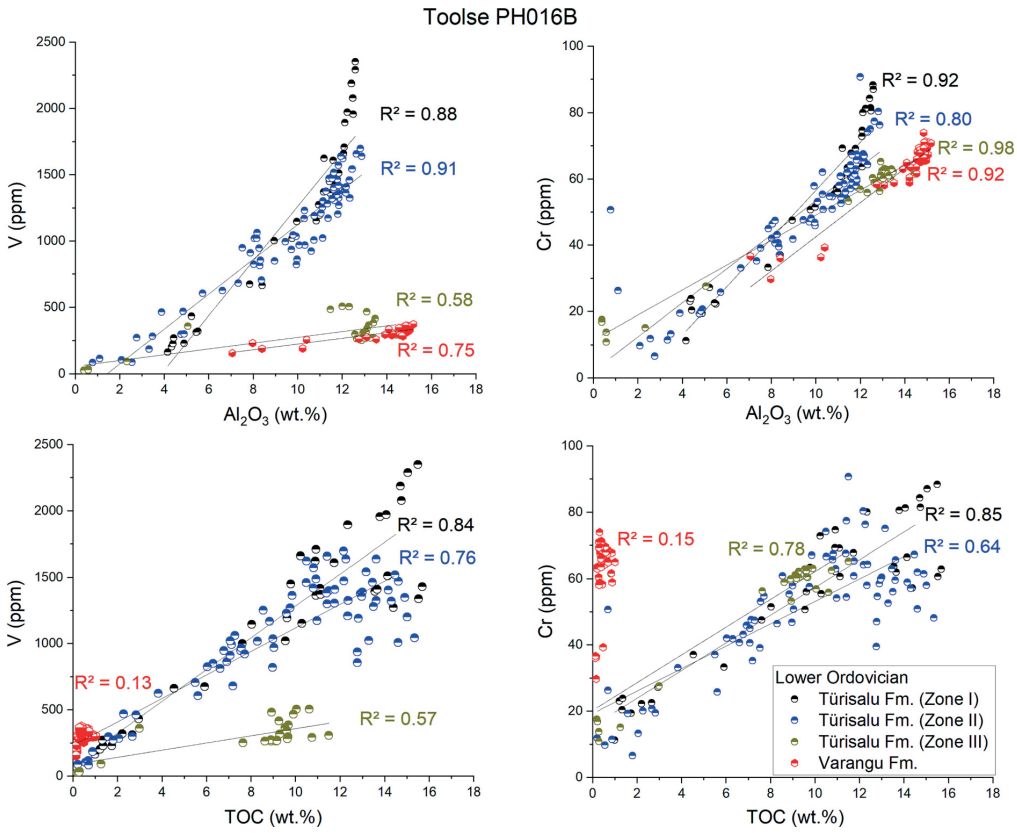

Fig. 6. Scatter plots illustrating co-variance and linear regression lines for Al_2O_3 vs. V, Al_2O_3 vs. Cr, TOC vs. V, and TOC vs. Cr in drill core. For all presented regression lines *p*-value <0.05, regression statistics for the individual sample sets are provided in supplementary materials 1 (Table S1).

and show a high specific surface area (SSA, surface area/volume of phases), which is highest in the case of smectite clays (80–150 mEq/100 g) (Meunier, 2005). The major phyllosilicate phases reported from the Tremadocian black shale complexes of Estonia are illite and illite-smectite (I/S), accompanied by chlorite (Lindgreen et al., 2000). According to Lindgreen et al. (2000), I/S in the beds formed from smectite of volcanic origin, suggesting the input of poorly crystalline clay phases with high surface areas to organic-rich mud. However, primary mineral associations have been overprinted by illitisation and development of diagenetic K-feldspars (Loog et al., 2001).

As Al and Ti are largely immobile during weathering and thus become progressively enriched in terrigenous clay and silt fractions (Taboada et al., 2006), homogenous Al and Ti averages in the studied black and grey shales suggest that there were no principal changes in the character of the terrigenous input during the considered period. Minor rhythmic variability of Al and Ti, which appeared along with lithological lamination cycles in Zones I and II of the Türisalu Formation, possibly reflects variance due to astronomically forced climate cycles (Zhao et al., 2022).

Subtle relationships within the strongly linked V—Cr association could provide more nuanced insights into V sequestration. Chromium, like V, is a redox-sensitive metal; however, unlike V, it occurs only via two stable oxidation states (Cr(III) and Cr(VI)) in natural aqueous environments (Cole et al., 2017). Cr has a very low concentration in modern seawater (average 5 nM, range 0.7–6.8 nM), demonstrating a behaviour between that of conservative and nutrient-type elements (Bonnand et al., 2013; Gueguen et al., 2016; Scheiderich et al., 2020). Cr (VI) forms soluble oxyanions in oxygenated water. It is prone to reduction under denitrifying conditions, that is, under a less oxygen-depleted environment compared to V(V) (Piper, 2001; Rue et al., 1997) with OM and Fe(II) species acting as typical reductants and bio-reduction also common (Chen et al., 1998; Kieber and Helr, 1992; Scheiderich et al., 2020). Reduced Cr(III) is highly particle reactive and therefore effectively scavenged by suspended and sinking particles (Breit and Wanty, 1991; Janssen et al., 2020; Semeniuk et al., 2016). Such particle-reactive behaviour might restrict the release of Cr during weathering and pre-set Cr transport in a particle-bound form. However, complexation with dissolved organic matter (DOM) in seawater can considerably increase the solubility of Cr(III) (Nakayama, 1981) and lead to elevated dissolved reduced Cr pools in coastal waters (Scheiderich et al., 2020).

Deciphering actual authigenic seaborne V enrichment and V—Cr relationships is challenging owing to the uncertainty around the input of those compounds from terrigenous sources (Cole et al., 2017). The potential use of grey shales of the Varangu Formation to evaluate the terrigenous V signal is discredited by their high V content, which is approximately two times higher than that of average shales (150 ppm) (Taylor and McLennan, 1985) and roughly three times higher than that of the continental upper crustal average (97 ppm) (Rudnick and Gao, 2013). Cr content, however, was lower than in average shales (100 ppm) (Taylor and McLennan, 1985) and in the upper continental crust (92 ppm) (Rudnick and Gao, 2013). Accordingly, the Cr/Ti and Cr/Al ratios

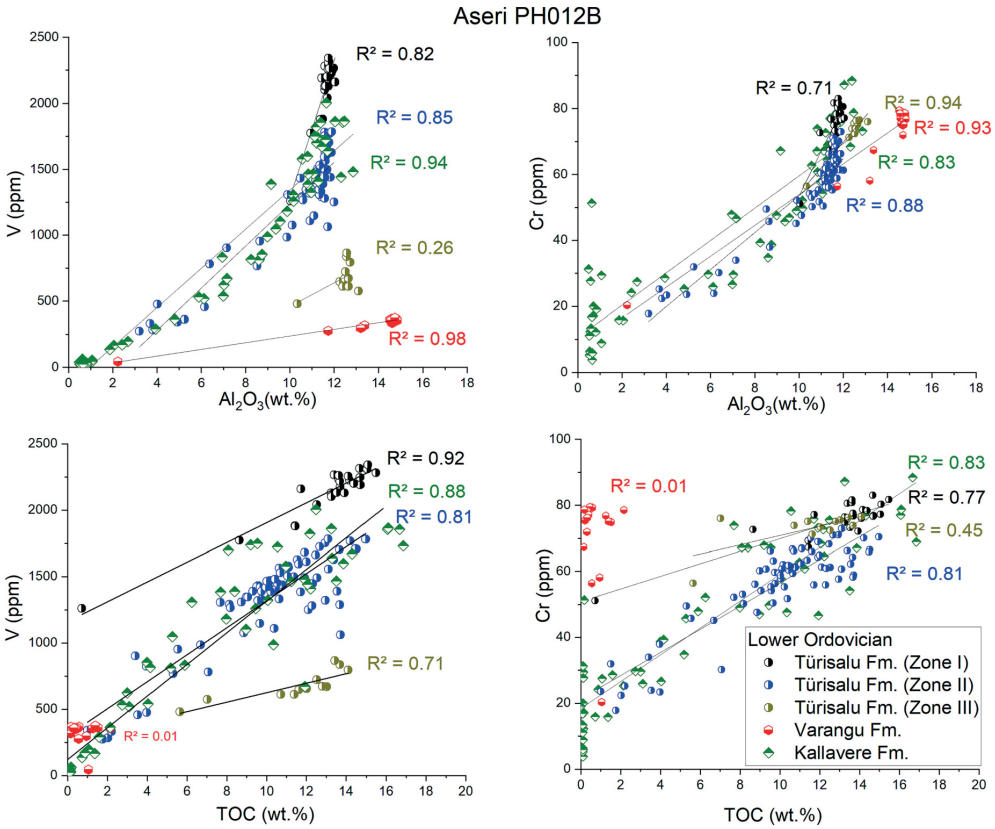

Fig. 7. Scatter plots illustrating co-variance and linear regression lines for Al_2O_3 vs. V, Al_2O_3 vs. Cr, TOC vs. V, and TOC vs. Cr in Aseri PH012B drill core. For all presented regression lines p-value <0.05, regression statistics for the individual sample sets are provided in supplementary materials 1 (Table S2).

for the studied samples were systematically below or close to the bulk upper continental crust. If average Cr/Ti and Cr/Al ratios from Varangu Formation and Zone III Türisalu Formations (respective values 0.012 and 0.0008) were used instead as baseline values, the max Cr_{auth} would be ~ 20 ppm, which is slightly >20% of the Cr_{sample}. This value suggests that most of the Cr originated from terrigenous flux, was transported via adsorbed species, or was bound to the crystal structure of chlorite (Schovsbo, 2003).

Anomalously high V/Cr ratios were recorded in the studied black shales. The V/Cr (> 20) ratios at the same time remained an order of magnitude higher than the V/Cr ratios >2 and > 5 proposed by Jones and Manning (1994) and Hoffman et al. (1998), respectively, for the discrimination of anoxic palaeoenvironments. Such proxy along with many other bivariate element ratios have shown to be largely unreliable for comparison palaeoredox conditions between different basins (Algeo and Liu, 2020). Nevertheless, Cr tends to show a higher concentration compared to average shales in various V-enriched black shales (Dumoulin et al., 2011; Fleurance et al., 2013) denoting simultaneous reduction in oxygen-depleted environment. The absence of Cr enrichment at comparable scales could reflect V sequestration from depleted seawater with respect to Cr. Estimates of Cr residence time in modern oceans vary from 5 to 45 kyr (Campbell and Yeats, 1984; Pöppelmeier et al., 2021; Quinby-Hunt and Turehian, 1983; Reinhard et al., 2013), and very short residence times (on the order of tens of days) have been reported for dissolved Cr(III) in estuarine environments (Emerson et al., 1979).

Still, the tight coupling in Cr and V distribution and, more generally, the presence of the V-Cr-Al-Ti association, provides strong indirect evidence for overlapping mechanisms for their uptake. In muds with progressively higher Al content and thus clay volume, a proportional increase in the finest clay fraction and a substantial increase in clay particle SSA could be expected due to grain-size-dependent screening during transport (Horowitz and Elrick, 1987). This leaves specific clay minerals, primarily smectites, in the finest colloid fraction (< 1 μm). The flux of such particles to the sea bottom largely depends on flocculation, which typically involves the interaction of mineral matter with DOM (Mehta, 2013; Meunier, 2005). In the studied profiles, geochemical relationships are consistent with the V entrapment pathway, where higher enrichment occurred under conditions that favoured precipitation of the fine clay fraction with high SSA. Furthermore, observed V-Al-Ti-Cr co-behaviour was not restricted solely to V-rich black shales but was consistent also in the grey shales of the Varangu Formation, suggesting thus that in both lithologies, adsorption V or its complexes to fine mineral fraction-controlled metal uptake from aqueous solution. This is not surprising as in modern aquatic systems, V uptake to the surface of clays and Fe—Mn (oxyhydr)oxides, likely mainly via V(V) oxyanions, appears to be firmly linked to the SSA of mineral matter. For example, Rawlins et al. (2010) showed that the V distribution in modern fine-grained stream beds can be efficiently used to predict sediment SSA. Thus, the collected dataset is compatible with the hypothesis that the availability of clay minerals as crucial natural sorbents and transport agents of V to the seabed modulates V enrichment patterns.

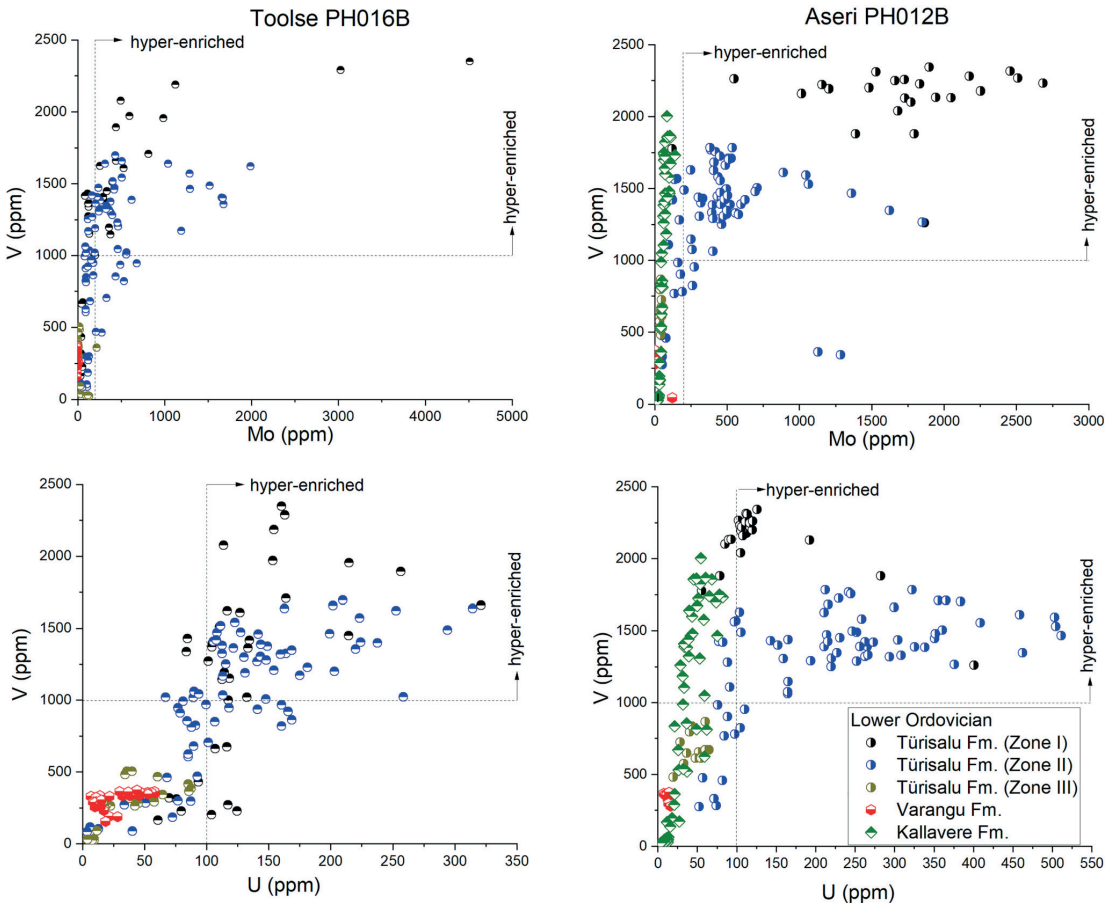

Fig. 8. Scatter plots illustrating co-variance between redox-sensitive elements for Toolse PH16B and Aseri PH012B drill cores. Hyper-enrichment is defined as >200 ppm for Mo, > 100 ppm for U, and > 1000 ppm for V (Bian et al., 2021).

Nevertheless, the reduction of V and effective binding of the formed V species/complexes are essential prerequisites for such uptake (Breit and Wanty, 1991). High primary bioproduction and degradation of OM effectively modulate the Eh and pH of the sedimentary environment, thus controlling V species redox. Different constituents of DOM (e.g. humic-like substances) are the major reductants of V(V). They can also control the behaviour of V(IV) in seawater through complexation (Lu et al., 1998). Marine DOM is produced by photosynthesis of primary producers or released during the partial mineralisation of OM (Dittmar et al., 2021; Jørgensen et al., 2011).

Considering the palaeoenvironmental context and the overall organic-rich nature of the studied black shales, one can assume that the high primary OM concentration in seawater, including the high DOM concentration, maintained by nutrient flux from the upwelling systems of the Iapetus Ocean and high mineralisation rates was supported by steep redox gradients (Bian et al., 2021; Ilyin and Heinsalu, 1990).Evidence of elevated productivity during the accumulation of the Türisalu Formation is supported by the co-occurrence of shelly phosphorites in adjacent inner shelf facies (Heinsalu et al., 2003). Furthermore, the V-rich black shales studied are associated with sponge spiculite beds, which are common in highly productive upwelling settings (Matheson and Frank, 2020). Additionally, nitrogen isotope data from the studied Aseri PH012B drill core indicate the prevalence of N_2-fixing producers during the production of primary biomass for the black shales (Ndiaye et al., 2023). Therefore, it could be hypothesised that DOM acted as the main reductant of V(V) in the upper Fe—Mn reducing water column, whereas V(IV) complexation with organic ligands stabilised the reduced V species over a wide Eh range (Fig. 10). The binding capacity of clay surfaces for such complexes determined V uptake from the marine water mass, while flocculation of mineral-organic colloidal matter led to the formation of larger flocs and the maximum amount of V transported to the sea bottom. The Cr distribution mimicking that of V in hyper-enriched samples agrees with the interpretation that the subsequent possible reduction of V(IV) to V(III) under sulfidic conditions had a minor direct influence on the development of V hyper-enrichment—that is, considerably rapid single-stage enrichment likely dominated V sequestration.

The dominance of V(IV)-DOM complexes in the primary mud may explain the later suppression of V uptake in sediments. Heggie et al. (1986) reported a ten-fold enrichment of V in very shallow pore waters in organic-rich sediments relative to adjacent seawater, which was attributed to the complexation of V with DOM and inhibited the diffusion of V into sediments. Such mechanisms could explain the decoupling of the V signal from that of Mo and U in the studied black shales. While the active sink likely favoured the uptake of Mo and U near the SWI, the continuous release of DOM to porewater possibly prevented V diffusive

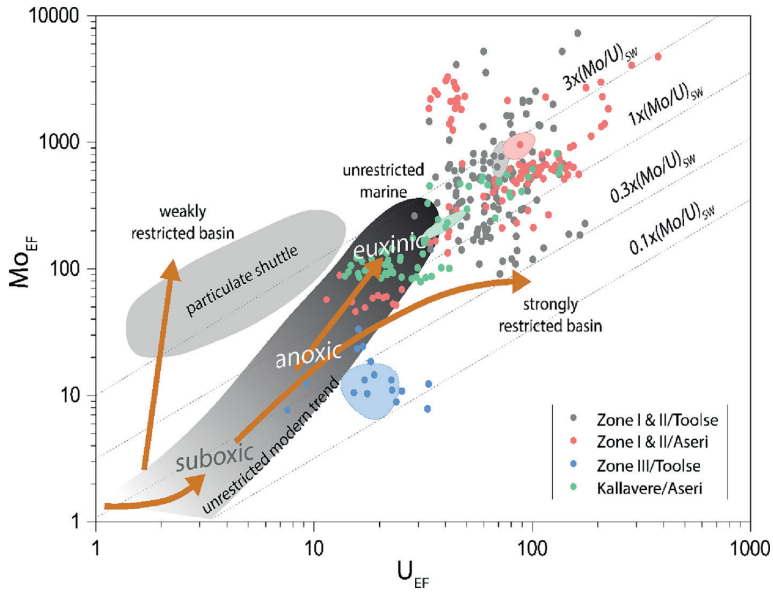

Fig. 9. U_{EF} vs. Mo_{EF} diagram for Toolse PH16B and Aseri PH012B drill core samples. The diagonal lines are multiples (0.1, 0.3, 1, and 3) of the Mo/U ratio of present-day seawater (after Algeo and Tribovillard (2009)). Red, green, blue, and grey areas mark centroid with confident intervals for each data subset. (For interpretation of the references to colour in this figure legend, the reader is referred to the web version of this article.)

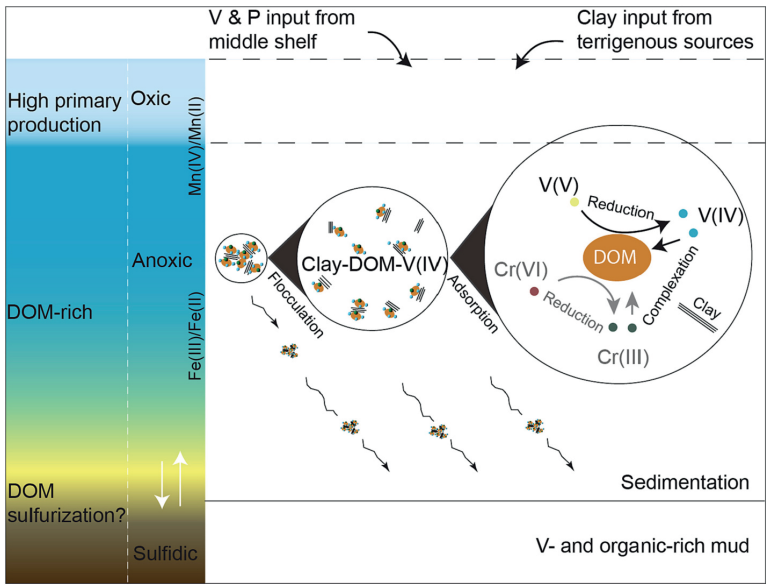

Fig. 10. Proposed model for V hyper-enrichment in shallow-water Tremadocian black shales.

flux to the sediments. The influence of various S species on the syngenetic behaviour of vanadium requires further consideration as V speciation via sulfur-related compounds in Alum Shale from middle shelf settings was recently reported (Bian et al., 2022). In modern euxinic marine environments, DOM sulfurization is a common phenomenon (Gomez-saez et al., 2021). In addition, microbes utilising anoxygenic photosynthesis for their metabolism and associated DOM can host various organosulfur compounds, such as thiols, which may support V (V) reduction and have been shown to complex with both V(IV) and V (V) (Crans et al., 2010).

6. Conclusion

Tremadocian highly metalliferous black shales from the inner shelf

of the Baltic Palaeobasin were evaluated using high-resolution geochemical data to elucidate the potential mechanisms underlying V hyper-enrichment. The presence of V-Mo-U-hyper-enriched, V-hyper-enriched, and Mo-U-poor black shales suggests V capture under a wide redox potential range. Significantly, the observed strong correlation between Cr and V, together with their co-behaviour with Al and Ti, was interpreted to reflect an essential control by the specific surface area of the fine clay fraction and its sedimentary dynamics over V sequestration processes. These results are compatible with the V uptake model in which V(V) is reduced to V(IV) in an oxygen-depleted water column, most likely by DOM, and reduced V complexes with organic ligands, followed by the sorption of V-DOM complexes by clay particles. V hyper-enrichment thus increases with the input of the finest clay fraction to the sea bottom and is possibly transported via OM flocs. From a resource perspective, the dominance of such a V sequestration pathway is expected to lead to the genesis of black shales with persistently high but limited hyper-enrichment ranges.

Declaration of Competing Interest

The authors declare that they have no known competing financial interests or personal relationships that could have appeared to influence the work reported in this paper.

Data availability

Data will be made available on request.

Acknowledgements

We would like to express our gratitude to Thomas Algeo and an anonymous reviewer for providing valuable and constructive feedback that significantly enhanced the quality of the manuscript. This study was supported by the ERDF and Estonian Research Council via project RESTA18.

Appendix A. Supplementary data

Supplementary data to this article can be found online at https://doi.org/10.1016/j.chemgeo.2023.121583.

References

Aitchison, J., 1982. The Statistical Analysis of Compositional Data. J. R. Stat. Soc. Ser. B 44, 139–160. https://doi.org/10.1111/j.2517-6161.1982.tb01195.x.

Algeo, T.J., Liu, J., 2020. A re-assessment of elemental proxies for paleoredox analysis. Chem. Geol. 540, 119549 https://doi.org/10.1016/j.chemgeo.2020.119549.

Algeo, T.J., Maynard, J.B., 2004. Trace-element behavior and redox facies in core shales of Upper Pennsylvanian Kansas-type cyclothems. Chem. Geol. 206, 289–318. https://doi.org/10.1016/j.chemgeo.2003.12.009.

Algeo, T.J., Maynard, J.B., 2008. Trace-metal covariation as a guide to water-mass conditions in ancient anoxic marine environments. Geosphere 4, 872–887. https://doi.org/10.1130/GES00174.1.

Algeo, T.J., Tribovillard, N., 2009. Environmental analysis of paleoceanographic systems based on molybdenum-uranium covariation. Chem. Geol. 268, 211–225. https://doi.org/10.1016/j.chemgeo.2009.09.001.

Artyushkov, E.A., Lindström, M., Popov, L.E., 2000. Relative Sea-level changes in Baltoscandia in the Cambrian and early Ordovician: the predominance of tectonic factors and the absence of large scale eustatic fluctuations. Tectonophysics 320, 375–407. https://doi.org/10.1016/S0040-1951(00)00038-X.

Bian, L., Schovsbo, N.H., Chappaz, A., Zheng, X., Nielsen, A.T., Ulrich, T., Wang, X., Dai, S., Galloway, J.M., Małachowska, A., Xu, X., Sanei, H., 2021. Molybdenum-uranium-vanadium geochemistry in the lower Paleozoic Alum Shale of Scandinavia: Implications for vanadium exploration. Int. J. Coal Geol. 239 https://doi.org/10.1016/j.coal.2021.103730.

Bian, L., Chappaz, A., Schovsbo, N.H., Sanei, H., 2022. A new vanadium species in black shales: Updated burial pathways and implications. Geochim. Cosmochim. Acta 338, 1–10. https://doi.org/10.1016/j.gca.2022.09.035.

Blengini, G.A., Latunussa, C.E.L., Eynard, U., Torres de Matos, C., Wittmer, D., Georgitzikis, K., Pavel, C., Carrara, S., Mancini, L., Unguru, M., Blagoeva, D., Mathieux, F., Pennington, D., 2020. Study on the EU's List of Critical Raw Materials - Final Report (2020). https://doi.org/10.2873/11619.

Bonnand, P., James, R.H., Parkinson, I.J., Connelly, D.P., Fairchild, I.J., 2013. The chromium isotopic composition of seawater and marine carbonates. Earth Planet. Sci. Lett. 382, 10–20. https://doi.org/10.1016/j.epsl.2013.09.001.

Breit, G.N., Wanty, R.B., 1991. Vanadium accumulation in carbonaceous rocks: a review of geochemical controls during deposition and diagenesis. Chem. Geol. 91, 83–97. https://doi.org/10.1016/0009-2541(91)90083-4.

Bruland, K.W., Middag, R., Lohan, M.C., 2013. Controls of trace metals in seawater. In: Treatise on Geochemistry, 2nd ed. Elsevier Ltd. https://doi.org/10.1016/B978-0-08-095975-7.00602-1.

Campbell, J.A., Yeats, P.A., 1984. Dissolved Estuary Chromium in the St. Lawrence, 19, pp. 513–522. https://doi.org/10.1080/10643389891254214.

Chen, J.M., Hao, O.J., Chen, J.M., Hao, O.J., 1998. Microbial chromium (VI) reduction. Crit. Rev. Environ. Sci. Technol. 28, 219–251. https://doi.org/10.1080/10643389891254214.

Cole, D.B., Zhang, S., Planavsky, N.J., 2017. A new estimate of detrital redox-sensitive metal concentrations and variability in fluxes to marine sediments. Geochim. Cosmochim. Acta 215, 337–353. https://doi.org/10.1016/j.gca.2017.08.004.

Crans, D.C., Zhang, B., Gaidamauskas, E., Keramidas, A.D., Willsky, G.R., Roberts, C.R., 2010. Is vanadate reduced by thiols under biological conditions? Changing the redox potential of V (V) / V (IV) by complexation in aqueous solution. Inorg. Chem. 49, 4245–4256. https://doi.org/10.1021/ic100080k.

Dahl, T.W., Siggaard-Andersen, M.L., Schovsbo, N.H., Persson, D.O., Husted, S., Hougård, I.W., Dickson, A.J., Kjær, K., Nielsen, A.T., 2019. Brief oxygenation events in locally anoxic oceans during the Cambrian solves the animal breathing paradox. Sci. Rep. 9, 1–9. https://doi.org/10.1038/s41598-019-48123-2.

Dittmar, T., Lennartz, S.T., Wiese, H.B., Hehemann, J.-H., 2021. Enigmatic persistence of dissolved organic matter in the ocean. Nat. Rev. Earth Environ. 2, 570–583. https://doi.org/10.1038/s43017-021-00183-7.

Dumoulin, J.A., Slack, J.F., Whalen, M.T., Harris, A.G., 2011. Depositional setting and geochemistry of phosphorites and metalliferous black shales in the carboniferous-permian lisburne group, northern Alaska. US Geol. Surv. Prof. Pap. 1–30 https://doi.org/10.3133/pp1776C.

Emerson, S.R., Huested, S.S., 1991. Ocean anoxia and the concentrations of molybdenum and vanadium in seawater. Mar. Chem. 34, 177–196. https://doi.org/10.1016/0304-4203(91)90002-E.

Emerson, S., Cranston, R.E., Liss, P.S., 1979. Redox species in a reducing fjord : equilibrium and kinetic considerations. Oceanogr. Res. Pap. 26, 859–878. https://doi.org/10.1016/0304-4203(91)90002-E.

Filby, R.H., 1994. Origin and nature of trace element species in crude oils, bitumens and kerogens: Implications for correlation and other geochemical studies. Geol. Soc. Spec. Publ. 78, 203–219. https://doi.org/10.1144/GSL.SP.1994.078.01.15.

Fleurance, S., Cuney, M., Malartre, F., Reyx, J., 2013. Origin of the extreme polymetallic enrichment (Cd, Cr, Mo, Ni, U, V, Zn) of the late Cretaceous-early Tertiary Belqa Group, Central Jordan. Palaeogeogr. Palaeoclimatol. Palaeoecol. 369, 201–219. https://doi.org/10.1016/j.palaeo.2012.10.020.

Goldberg, T., Archer, C., Vance, D., Poulton, S.W., 2009. Mo isotope fractionation during adsorption to Fe (oxyhydr) oxides. Geochim. Cosmochim. Acta 73, 6502–6516. https://doi.org/10.1016/j.gca.2009.08.004.

Gomez-saez, G.V., Dittmar, T., Holtappels, M., Pohlabeln, A.M., Lichtschlag, A., Schnetger, B., Boetius, A., Niggemann, J., 2021. Sulfurization of dissolved organic matter in the anoxic water column of the Black Sea. Sci. Adv. 7, 1–11. https://doi.org/10.1126/sciadv.abf6199.

Gueguen, B., Reinhard, C.T., Algeo, T.J., Peterson, L.C., Nielsen, S.G., Wang, X., Rowe, H., Planavsky, N.J., 2016. ScienceDirect the chromium isotope composition of reducing and oxic marine sediments. Geochim. Cosmochim. Acta 184, 1–19. https://doi.org/10.1016/j.gca.2016.04.004.

Gustafsson, J.P., 2019. Vanadium geochemistry in the biogeosphere –speciation, solid-solution interactions, and ecotoxicity. Appl. Geochem. 102, 1–25. https://doi.org/10.1016/j.apgeochem.2018.12.027.

Han, T., Fan, H., Wen, H., 2018. Dwindling vanadium in seawater during the early Cambrian, South China. Chem. Geol. 492, 20–29. https://doi.org/10.1016/j.chemgeo.2018.05.022.

Heggie, D., Kahn, D., Fischer, K., 1986. Trace metals in metalliferous sediments, MANOP site M: interra- cial pore water profiles. Earth Planet. Sci. Lett. 80, 106–116.

Heinsalu, H., Kaljo, D., Kurvits, T., Viira, V., 2003. The stratotype of the Orasoja Member (Tremadocian, Northeast Estonia): lithology, mineralogy, and biostratigraphy. Proc. Est. Acad. Sci. Geol. 52, 135–154. https://doi.org/10.3176/geol.2003.3.02.

Helz, G.R., Vorlicek, T.P., 2019. Precipitation of molybdenum from euxinic waters and the role of organic matter. Chem. Geol. 509, 178–193. https://doi.org/10.1016/j.chemgeo.2019.02.001.

Helz, G.R., Miller, C.V., Charnock, J.M., Mosselmans, J.F.W., Pattrick, R.A.D., Garner, C. D., Vaughan, D.J., 1996. Mechanism of molybdenum removal from the sea and its concentration in black shales : EXAFS evidence. Geochim. Cosmochim. Acta 60 (19), 3631–3642. https://doi.org/10.1016/0016-7037(96)00195-0.

Hints, R., Hade, S., Soesoo, A., Voolma, M., 2014. Depositional framework of the East Baltic Tremadocian black shale revisited. Gff 136, 464–482. https://doi.org/10.1080/11035897.2013.866978.

Hints, R., Pajusaar, S., Urtson, K., Liiv, M., Kallaste, T., 2021. Metal enrichment in lithologically complex black shales: a case study from the tremadocian of NE Estonia. Est. J. Earth Sci. 70, 36–50. https://doi.org/10.3176/EARTH.2021.04.

Hoffman, D.L., Algeo, T.J., JB, M., Joachimski, M.M., Hower, J.C., Jaminski, J., 1998. Regional and Stratigraphic Variation in Bottomwater Anoxia of Offshore Core Shales of Upper Pennsylvanian Cyclothems from the Eastern Midcontinent Shelf (Kansas) U. S.A.

Horowitz, A.J., Elrick, K., 1987. The relation of stream sediment surface area, grain size and composition to trace element chemistry. Appl. Geochem. 2, 437–451. https://doi.org/10.1016/0883-2927(87)90027-8.
Ilyin, A., Heinsalu, H., 1990. Early Ordovician shelly phosphorites of the Baltic Phosphate Basin. Geol. Soc. Lond. Spec. Publ. 52, 253–259. https://doi.org/10.1144/GSL.SP.1990.052.01.18.
Janssen, D.J., Rickli, J., Quay, P.D., White, A.E., Nasemann, P., Jaccard, S.L., 2020. Biological control of chromium redox and stable isotope composition in the surface ocean Key Points. Glob. Biogeochem. Cycles 34. https://doi.org/10.1029/2019GB006397.
Jones, B., Manning, D.A.C., 1994. Comparison of geochemical indices used for the interpretation of palaeoredox conditions in ancient mudstones. Chem. Geol. 111, 111–129. https://doi.org/10.1016/0009-2541(94)90085-X.
Jørgensen, L., Stedmon, C.A., Kragh, T., Markager, S., Middelboe, M., Søndergaard, M., 2011. Global trends in the fl uorescence characteristics and distribution of marine dissolved organic matter. Mar. Chem. 126, 139–148. https://doi.org/10.1016/j.marchem.2011.05.002.
Kelley, K.D., Scott, C., Polyak, D.E., Kimball, B.E., 2017. Vanadium, Professional Paper. Reston, VA. https://doi.org/10.3133/pp1802U.
Kieber, R.J., Helr, G.R., 1992. Indirect photoreduction of aqueous chromium(V I). Environ. Sci. Technol. 26, 307–312. https://doi.org/10.1021/es00026a010.
Kivimägi, E., Loog, A., 1972. The main structural types of graptolitic argillites of the Toolse deposit. Proc. Acad. Sci. Est. SSR. Chem. Geol. 21, 143–147. https://doi.org/10.3176/chem.geol.1972.2.10.
Kowalski, N., Dellwig, O., Beck, M., Gräwe, U., Neubert, N., Nägler, T.F., Badewien, T.H., Brumsack, H.J., van Beusekom, J.E.E., Böttcher, M.E., 2013. Pelagic molybdenum concentration anomalies and the impact of sediment resuspension on the molybdenum budget in two tidal systems of the North Sea. Geochim. Cosmochim. Acta 119, 198–211. https://doi.org/10.1016/j.gca.2013.05.046.
Kunert, A., Clarke, J., Kendall, B., 2020. Molybdenum isotope constraints on the origin of vanadium hyper-enrichments in ediacaran– phanerozoic marine mudrocks. Minerals 10, 1–20. https://doi.org/10.3390/min10121075.
Landing, E., 2012. Time-specific black mudstones and global hyperwarming on the Cambrian-Ordovician slope and shelf of the Laurentia palaeocontinent. Palaeogeogr. Palaeoclimatol. Palaeoecol. 367–368, 256–272. https://doi.org/10.1016/j.palaeo.2011.09.005.
Large, R.R., Halpin, J.A., Danyushevsky, L.V., Maslennikov, V.V., Bull, S.W., Long, J.A., Gregory, D.D., Lounejeva, E., Lyons, T.W., Sack, P.J., Mcgoldrick, P.J., Calver, C.R., 2014. Trace element content of sedimentary pyrite as a new proxy for deep-time ocean – atmosphere evolution. Earth Planet. Sci. Lett. 389, 209–220. https://doi.org/10.1016/j.epsl.2013.12.020.
Lau, K.V., Lyons, T.W., Maher, K., 2020. ScienceDirect Uranium reduction and isotopic fractionation in reducing sediments: insights from reactive transport modeling. Geochim. Cosmochim. Acta 287, 65–92. https://doi.org/10.1016/j.gca.2020.01.021.
Lehmann, B., Nägler, T.F., Holland, H.D., Wille, M., Mao, J., Pan, J., Ma, D., Dulski, P., 2007. Highly metalliferous carbonaceous shale and early Cambrian seawater. Geology 35, 403–406. https://doi.org/10.1130/G23543A.1.
Lehmann, B., Frei, R., Xu, L., Mao, J., 2016. Early cambrian black shale-hosted Mo-Ni and V mineralization on the rifted margin of the Yangtze platform, China: Reconnaissance chromium isotope data and a refined metallogenic model. Econ. Geol. 111, 89–103. https://doi.org/10.2113/econgeo.111.1.89.
Leventhal, J.S., 1991. Comparison of organic geochemistry and metal enrichment in two black shales: Cambrian Alum Shale of Sweden and Devonian Chattanooga Shale of United States. Mineral. Deposita 26, 104–112. https://doi.org/10.1007/BF00195256.
Lewicka, E., Guzik, K., Galos, K., 2021. On the possibilities of critical raw materials production from the EU's primary sources. Resources 10. https://doi.org/10.3390/resources10050050.
Lille, Ü., 2003. Current knowledge on the origin and structure of estonian kukersite kerogen. Oil Shale 20, 253–263. https://doi.org/10.3176/oil.2003.3.03.
Lindgreen, H., Drits, V.A., Sakharov, B.A., Salyn, A.L., Wrang, P., Dainyak, L.G., 2000. Illite-smectite structural changes during metamorphism in black Cambrian Alum shales from the Baltic area, 85, pp. 1223–1238. https://doi.org/10.2138/am-2000-8-916.
Liu, J.S., Algeo, T.J., Jaminski, J., Kuhn, T., Joachimski, M.M., 2019. Evaluation of high-frequency paleoenvironmental variation using an optimized cyclostratigraphic framework: example for C-S-Fe analysis of Devonian-Mississippian black shales (Central Appalachian Basin, U.S.A.). Chem. Geol. 525, 303–320. https://doi.org/10.1016/j.chemgeo.2019.07.019.
Loog, A., Kurvits, T., Aruväli, J., Petersell, V., 2001. Grain size analysis and mineralogy of the Tremadocian Dictyonema shale in Estonia. Oil Shale 18, 281–297. https://doi.org/10.3176/oil.2001.4.02.
Lu, X., Johnson, W.D., Hook, J., 1998. Reaction of Vanadate with Aquatic Humic Substances: an ESR and 51 V NMR Study. Environ. Sci. Technol. 32, 2257–2263. https://doi.org/10.1021/es970930r.
Lu, Z., Hu, R., Han, T., Wen, H., Mo, B., Algeo, T.J., 2021. Control of V accumulation in organic-rich shales by clay-organic nanocomposites. Chem. Geol. 567, 120100 https://doi.org/10.1016/j.chemgeo.2021.120100.
Matheson, E.J., Frank, T.D., 2020. Phosphorites, glass ramps and carbonate factories: the evolution of an epicontinental sea and a late Palaeozoic upwelling system (Phosphoria Rock complex). Sedimentology 67, 3003–3041. https://doi.org/10.1111/sed.12731.
Mehta, A., 2013. Methods of Sediment Classification, in: An Introduction to Hydraulics of Fine Sediment Transport. https://doi.org/10.1142/9789814449496_0003.
Meunier, A., 2005. Clays in sedimentary environments. In: Clays. Springer-Verlag, Berlin/Heidelberg, pp. 295–327. https://doi.org/10.1007/3-540-27141-4_7.
Morford, J.L., Emerson, S., 1999. The geochemistry of redox sensitive trace metals in sediments. Geochim. Cosmochim. Acta 63, 1735–1750. https://doi.org/10.1016/S0016-7037(99)00126-X.
Nakayama, E., 1981. Chemical speciation of chromium in sea water. Anal. Chim. Acta 130, 289–294. https://doi.org/10.1016/S0003-2670(01)93006-5.
Ndiaye, M., Liiv, M., Kallaste, T., Graul, S., Hints, R., 2023. Nitrogen and organic carbon isotope record in Tremadocian highly metalliferous black shales from Baltica. Est. J. Earth Sci 72 (1), 78–81. https://doi.org/10.3176/earth.2023.25.
Nemliher, J., Puura, I., 1996. Upper Cambrian basal conglomerate of the Kallavere Formation on the Pakri peninsula, NW Estonia. Proc. Est. Acad. Sci. Geol. 45, 1–8. https://doi.org/10.3176/geol.1996.1.01.
Nielsen, A.T., Schovsbo, N.H., 2006. Cambrian to basal Ordovician lithostratigraphy in Southern Scandinavia. Bull. Geol. Soc. Denmark 53, 47–92. https://doi.org/10.37570/bgsd-2006-53-04.
Nielsen, A.T., Schovsbo, N.H., 2007. The lithostratigraphic subdivision of the Cambrian successions in Scania. Bull. Geol. Soc. Denmark 53, 47–92.
O'Loughlin, E.J., Boyanov, M.I., Kemner, K.M., 2021. Reduction of vanadium(V) by iron (II)-bearing minerals. Minerals 11, 1–21. https://doi.org/10.3390/min11030316.
Pajusaar, S., Hints, R., Kallaste, T., Kiipli, T., Urtson, K., 2021. Chemical composition data of Tremadocian black shale reference samples from Estonia. SARV Geosci. Data Repos. 1.0 https://doi.org/10.23679/512.
Peacor, D.R., Coveney, R.M., Zhao, G., 2000. Authigenic illite and organic matter: the principal hosts of vanadium in the Mecca Quarry Shale at Velpen, Indiana. Clay Clay Miner. 48, 311–316. https://doi.org/10.1346/CCMN.2000.0480301.
Pedersen, G.K., 1989. The sedimentology of lower Palaeozoic black shales from the shallow wells Skelbro 1 and Billegrav 1, Bornholm, Denmark. Bull. Geol. Soc. Denmark 37, 151–173. https://doi.org/10.37570/bgsd-1988-37-13.
Peirò, T., 2017. Assessment of the Methodology for Establishing the EU List of Critical Raw Materials. Joint Research Centre. https://doi.org/10.2760/73303.
Pi, D.H., Liu, C.Q., Shields-Zhou, G.A., Jiang, S.Y., 2013. Trace and rare earth element geochemistry of black shale and kerogen in the early Cambrian Niutitang Formation in Guizhou province, South China: Constraints for redox environments and origin of metal enrichments. Precambrian Res. 225, 218–229. https://doi.org/10.1016/j.precamres.2011.07.004.
Piper, D.Z., 2001. Marine chemistry of the permian Phosphoria Formation and Basin, Southeast Idaho. Econ. Geol. 96, 599–620. https://doi.org/10.2113/gsecongeo.96.3.599.
Pöppelmeier, F., Janssen, D.J., Jaccard, S.L., Stocker, T.F., 2021. Modeling the marine chromium cycle: new constraints on global-scale processes. Biogeosciences 18, 5447–5463. https://doi.org/10.5194/bg-18-5447-2021.
Pukkonen, E., 1989. Major and minor elements in Estonian graptolite argillite. Oil Shale 6, 11–18. https://doi.org/10.3176/oil.1989.1.02.
Pukkonen, E., Buchardt, B., 1994. The dictyonema shale of Estonia. Geol. Inst. Univ. Copenhagen 1–37.
Quinby-Hunt, M.S., Turehian, K.K., 1983. Distribution of elements in sea water. EOS Trans. Am. Geophys. Union 64, 130. https://doi.org/10.1029/EO064i014p00130.
Rawlins, B.G., Turner, G., Mounteney, I., Wildman, G., 2010. Applied Geochemistry estimating specific surface area of fine stream bed sediments from geochemistry. Appl. Geochem. 25, 1291–1300. https://doi.org/10.1016/j.apgeochem.2010.05.009.
Reinhard, C.T., Planavsky, N.J., Robbins, L.J., Partin, C.A., Gill, B.C., Lalonde, S.V., Bekker, A., Konhauser, K.O., Lyons, T.W., 2013. Proterozoic Ocean redox and biogeochemical stasis. Proc. Natl. Acad. Sci. U. S. A. 110, 5357–5362. https://doi.org/10.1073/pnas.1208622110.
Rudnick, R.L., Gao, S., 2013. Composition of the continental crust. In: Treatise on Geochemistry, Second edition. Elsevier Ltd, pp. 1–51. https://doi.org/10.1016/B978-0-08-095975-7.00301-6.
Rue, E.L., Smith, G.J., Bruland, K.W., 1997. The response of trace element redox couples to suboxic conditions in the water column, 44, pp. 113–134. https://doi.org/10.1016/S0967-0637(96)00088-X.
Scheiderich, K., Amini, M., Holmden, C., Francois, R., 2020. Global variability of chromium isotopes in seawater demonstrated by Pacific, Atlantic, and Arctic Ocean samples. Earth Planet. Sci. Lett. 423, 87–97. https://doi.org/10.1016/j.epsl.2015.04.030.
Schlesinger, W.H., Klein, E.M., Vengosh, A., 2017. Global biogeochemical cycle of vanadium. Proc. Natl. Acad. Sci. U. S. A. 114, E11092–E11100. https://doi.org/10.1073/pnas.1715500114.
Schovsbo, N.H., 2002. Uranium enrichment shorewards in black shales: a case study from the scandinavian alum shale. Mar. Geol. 124, 107–115. https://doi.org/10.1080/11035890201242107.
Schovsbo, N.H., 2003. The geochemistry of lower Palaeozoic sediments deposited on the margins of Baltica. Bull. Geol. Soc. Denmark 50, 11–27. https://doi.org/10.37570/bgsd-2003-50-01.
Schovsbo, N.H., Nielsen, A.T., Harstad, A.O., Bruton, D.L., 2018. Stratigraphy and geochemical composition of the Cambrian alum shale formation in the Porsgrunn core, Skien-Langesund district, Southern Norway. Bull. Geol. Soc. Denmark 66, 1–20. https://doi.org/10.37570/bgsd-2018-66-01.
Schulz, K., Seal, R., Bradley, D., Deyoung, J., 2017. Critical mineral resources of the United States—Economic and environmental geology and prospects for future supply. U. S. Geol. Surv. 797 https://doi.org/10.3133/pp1802.
Schulz, H.M., Yang, S., Panova, E., Bechtel, A., 2019. The role of Pleistocene meltwater-controlled uranium leaching in assessing irradiation-induced alteration of organic matter and petroleum potential in the Tremadocian Koporie Formation (Western

Russia). Geochim. Cosmochim. Acta 245, 133–153. https://doi.org/10.1016/j.gca.2018.10.029.
Schulz, H.M., Yang, S., Schovsbo, N.H., Rybacki, E., Ghanizadeh, A., Bernard, S., Mahlstedt, N., Krüger, M., Amann-Hildebrandt, A., Krooss, B.M., Meier, T., Reinicke, A., 2021. The Furongian to lower Ordovician Alum Shale Formation in conventional and unconventional petroleum systems in the Baltic Basin – a review. Earth-Sci. Rev. 218, 103674 https://doi.org/10.1016/j.earscirev.2021.103674.
Scott, C., Lyons, T.W., 2012. Contrasting molybdenum cycling and isotopic properties in euxinic versus non-euxinic sediments and sedimentary rocks: refining the paleoproxies. Chem. Geol. 324–325, 19–27. https://doi.org/10.1016/j.chemgeo.2012.05.012.
Scott, C., Slack, J.F., Kelley, K.D., 2017. The hyper-enrichment of V and Zn in black shales of the late Devonian-early Mississippian Bakken Formation (USA). Chem. Geol. 452, 24–33. https://doi.org/10.1016/j.chemgeo.2017.01.026.
Semeniuk, D.M., Maldonado, M.T., Jaccard, S.L., 2016. ScienceDirect Chromium uptake and adsorption in marine phytoplankton – implications for the marine chromium cycle. Geochim. Cosmochim. Acta 184, 41–54. https://doi.org/10.1016/j.gca.2016.04.021.
Sholkovitz, E., Cochran, J.K., Carey, A.E., Hole, W., Hole, W., Ma, U.S.A., 1986. The geochemistry of uranium and thorium in coastal marine sediments and sediment pore waters, 50, pp. 663–680. https://doi.org/10.1016/0016-7037(86)90344-3.
Szalay, A., Szilágyi, M., 1967. The association of vanadium with humic acids. Geochim. Cosmochim. Acta 31, 1–6. https://doi.org/10.1016/0016-7037(67)90093-2.
Taboada, T., Martı, A., Garcı, C., Garcı, E., 2006. Particle-size fractionation of titanium and zirconium during weathering and pedogenesis of granitic rocks in NW Spain, 131, pp. 218–236. https://doi.org/10.1016/j.geoderma.2005.03.025.
Taylor, S.R., McLennan, S.M., 1985. The continental crust: its composition and evolution. Blackwell. https://doi.org/10.1017/S0016756800032167.
Thickpenny, A., 1984. The sedimentology of the Swedish Alum Shales. Geol. Soc. 15, 511–525. https://doi.org/10.1144/GSL.SP.1984.015.01.33.
Tribovillard, N., Algeo, T.J., Lyons, T., Riboulleau, A., 2006. Trace metals as paleoredox and paleoproductivity proxies: an update. Chem. Geol. 232, 12–32. https://doi.org/10.1016/j.chemgeo.2006.02.012.
Veski, R., Palu, V., 2003. Investigation of Dictyonema oil shale and its natural and artificial transformation products by a vankrevelenogram. Oil Shale 20, 265–281. https://doi.org/10.3176/oil.2003.3.04.
Voolma, M., Soesoo, A., Hade, S., Hints, R., Kallaste, T., 2013. Geochemical heterogeneity of Estonian graptolite argillite. Oil Shale 30, 377–401. https://doi.org/10.3176/oil.2013.3.02.
Wanty, R.B., Goldhaber, M.B., 1992. Thermodynamics and kinetics of reactions involving vanadium in natural systems: Accumulation of vanadium in sedimentary rocks. Geochim. Cosmochim. Acta 56, 1471–1483. https://doi.org/10.1016/0016-7037(92)90217-7.
Wehrli, B., Stumm, W., 1989. Vanadyl in natural waters: Adsorption and hydrolysis promote oxygenation. Geochim. Cosmochim. Acta 53, 69–77. https://doi.org/10.1016/0016-7037(89)90273-1.
Wei, W., Algeo, T.J., 2020. Elemental proxies for paleosalinity analysis of ancient shales and mudrocks. Geochim. Cosmochim. Acta 287, 341–366. https://doi.org/10.1016/j.gca.2019.06.034.
Wilde, P., Quinby-Hunt, M.S., Berry, W.B.N., Orth, C.J., 1989. Palaeo-oceanography and biogeography in the Tremadoc (Ordovician) Iapetus Ocean and the origin of the chemostratigraphy of Dictyonema flabelliforme black shales. Geol. Mag. 126, 19–27. https://doi.org/10.1017/S0016756800006117.
Wu, F., Owens, J.D., Huang, T., Sarafian, A., Huang, K.F., Sen, I.S., Horner, T.J., Blusztajn, J., Morton, P., Nielsen, S.G., 2019. Vanadium isotope composition of seawater. Geochim. Cosmochim. Acta 244, 403–415. https://doi.org/10.1016/j.gca.2018.10.010.
Zhang, L., Xiao, D., Lu, Shuangfang, Jiang, S., Lu, Shudong, 2019. Effect of sedimentary environment on the formation of organic-rich marine shale: Insights from major/trace elements and shale composition. Int. J. Coal Geol. 204, 34–50. https://doi.org/10.1016/j.coal.2019.01.014.
Zhao, Z., Thibault, N.R., Dahl, T.W., Rasmussen, C.M.Ø., Nielsen, A.T., Schovsbo, N.H., Sørensen, A.L., 2022. Synchronizing rock clocks in the late Cambrian. Nat. Commun. 13 (1990), 1–11. https://doi.org/10.1038/s41467-022-29651-4.

Paper II

Ndiaye, M., Liiv, M., Kallaste, T., Graul, S., Hints, R. (2023b). Nitrogen and organic-carbon isotope record in Tremadocian highly metalliferous black shales from Baltica. Estonian Journal of Earth Sciences 72, 78–81. https://doi.org/10.3176/earth.2023.25

Estonian Journal of Earth Sciences
2023, **72**, 1, 78–81

https://doi.org/10.3176/earth.2023.25

www.eap.ee/earthsciences
Estonian Academy Publishers

SHORT COMMUNICATION

Received 31 March 2023
Accepted 21 April 2023
Available online 14 June 2023

Keywords:
Tremadocian, black shale, nitrogen isotopes, carbon isotopes, Baltica

Corresponding author:
Mawo Ndiaye
mawo.ndiaye@taltech.ee

Citation:
Ndiaye, M., Liiv, M., Kallaste, T., Graul, S. and Hints, R. 2023. Nitrogen and organic carbon isotope record in Tremadocian highly metalliferous black shales from Baltica. *Estonian Journal of Earth Sciences*, **72**(1), 78–81.
https://doi.org/10.3176/earth.2023.25

14TH ISOS
ESTONIA 2023

Nitrogen and organic carbon isotope record in Tremadocian highly metalliferous black shales from Baltica

Mawo Ndiaye, Merlin Liiv, Toivo Kallaste, Sophie Graul and Rutt Hints

Department of Geology, Tallinn University of Technology, Ehitajate 5, 19086 Tallinn, Estonia

ABSTRACT

Tremadocian highly metalliferous black shales and associated grey shales from the Aseri PH012B drill core (NE Estonia) in the innermost part of the Baltic Palaeobasin were targeted to record their nitrogen and organic carbon isotope variance combined with the total organic carbon and total nitrogen record. The obtained molar C/N ratios of black shales from 26 to 52 indicate a considerable loss of N compared to primary biomass. The recorded $\delta^{15}N$ values from −2.5 to 0.2‰ likely evolved due to isotopic fractionation related to N_2 fixation by primary producers, superimposed by later anoxic ammonium oxidation processes within the uppermost sediments. The high net primary productivity, which controlled the accumulation of organic-rich shallow-water complexes, was fuelled by the internal cycling of P in the sea basin and combined with intensive N exchange between marine and atmospheric pools.

Introduction

An interval from the middle Cambrian to the Early Ordovician, represented by vast black shale complexes in the Baltic Palaeobasin, is recognized as a period of major environmental and biodiversity changes. The accumulation of organic-rich sediment throughout the outer and inner shelf of the palaeobasin has been attributed to elevated nutrient input, enhanced bioproduction, and prevailing anoxia in the lower water column, the latter likely disrupted by short-lived oxygenation events (Dahl et al. 2019). However, many fundamental questions remain regarding their genesis. Herein, we present coupled nitrogen ($\delta^{15}N_{tot}$) and carbon ($\delta^{13}C_{org}$) isotope records from the highly V-, U-, and Mo-enriched Tremadocian black shales and related metal-poor black and grey shales (*Cordylodus angulatus–Paltodus deltifer pristinus* biozones) from the inner shelf of the palaeobasin to decipher possible interrelated changes in the nutrient cycle, primary productivity, and redox conditions during their accumulation.

The dynamics of the deep-time biogeochemical cycle of N can be derived from the isotopic composition of the deposits. The cycle is closely tied to the redox state of the ocean and the atmosphere, and the N isotope values that are preserved in organic matter (OM) can reflect the redox state of the water column, as well as metabolic processes and pathways (Algeo et al. 2014). Nitrogen plays a crucial role in the biogeochemical cycling of C and other nutrients in the oceans (Stüeken et al. 2016). It can exist in different forms, including the diatomic molecule (N_2), nitrate (NO_3^-), nitrite (NO_2^-), ammonium (NH_4^+), and dissolved organic nitrogen (DON). Autotrophs in the marine system can fix atmospheric N_2 ($\delta^{15}N = 0‰$) into OM with minimal isotopic fractionation (ε_{org-N2} is ~ −3 to +1‰) (Zerkle et al. 2008; Valley and Cole 2001). The decomposing OM first undergoes ammonification, which also involves little isotopic alteration. Further, under oxic conditions, nitrification converts NH_4^+ to dissolved NO_3^-. The process potentially has a large net isotope fraction effect in settings where incomplete nitrification is favoured (Deutsch et al. 2007). However, it has minor importance in well-oxygenated seawater, where all generated NH_4^+ is effectively oxidized to NO_3^-. Under suboxic conditions, part of the N can escape from the nitrate pool through denitrification, with a potentially large isotopic effect (Valley and Cole 2019). Such an effect is, however, suppressed if quantitative denitrification takes place (Sigman and Fripiat 2001). In the anoxic seawater and sediment column,

N-loss could be further promoted by mineralization of OM through processes such as anoxic ammonium oxidation (anammox) with nitrates or alternative electron acceptors. The N mineralization pathways in anoxic sediments are still poorly understood. Importantly, depletion of bioavailable N-compounds in the water column supports the growth of diazotrophs if other nutrients are available. Interpretations of ancient sedimentary records exhibiting near-zero $\delta^{15}N_{tot}$ values, untypical of modern settings, have conventionally assumed that N_2-fixation should have dominated as the main source of N, thus pointing to the nitrate-poor oxygen-depleted photic zone. For the Tremadocian black shales from the inner part of Baltica a single previously reported $\delta^{15}N$ value of ~ –2‰ is in the aforementioned range (Kiipli and Kiipli 2013).

Our research aimed at better understanding the distribution of $\delta^{15}N_{tot}$, $\delta^{13}C_{org}$, total organic carbon (TOC) and total nitrogen (TN) in those palaeoenvironments. We hypothesized that significant changes in the local nitrogen cycle would coincide with changes in the preservation of OM and the enrichment of redox-sensitive elements (RSE) in the black shales.

Geological setting

The analysed samples come from the Aseri PH012B (59.426053, 26.755267) drill core. During the Tremadocian period, the study area was the innermost shallowest part of the Baltic Palaeobasin. The thin complex of black shales of the Türisalu Formation (~1.1 m) deposited during the transgressive phase above the coastal and shallow-marine bio- and siliciclastic complexes of the Kallavere Formation. The latter is rich in phosphatic brachiopod detritus, but also shows cyclic alteration of black shale interbeds and siltstones in its uppermost part. The Türisalu Formation is overlain by grey shales of the Varangu Formation. The mineral matrix of the organic-rich black shales consists of K-feldspars, quartz, illite/mica, and illite/smectite, while pyrite content varies from 4 to 6%. Also, the presence of thin cyclic biosilica and sulphidic silty interlayers as well as glendonite-like carbonate concretions is characteristic of the study area. The OM of the Türisalu Formation is thermally immature (Schovsbo et al. 2012), purely marine in origin, largely amorphous, and compliant with Type-II kerogen with an average atomic H/C ratio of 1.24 and O/C ratio of 0.16 (Veski and Palu 2003). Lille (2003) suggested that its primary biomass could have been produced by cyanobacteria and possibly by green sulphur bacteria. Very high enrichment of RSE, with maximum content of V ~ 2300 ppm, U ~ 500 ppm, and Mo ~ 2700 ppm, has been documented in the basal and middle part of the Türisalu Formation in the Aseri PH012B section using the same sample set (Ndiaye et al. in press).

Materials and methods

To determine TOC and TN content, 186 samples of the Türisalu Formation and adjacent strata were analysed using combustion in a FLASH 2000 organic elemental analyser. Each sample was approximately 1 cm thick, and 4–15 mg of powdered sediment was used depending on loss-on-ignition values. The samples were pretreated with 10% HCl, dried, and then wrapped into granules before being packed into Sn containers for combustion. Cystine was used as the standard, and organic carbon-rich sediment was used as the reference material.

Selected samples (n = 26) were analysed for $\delta^{13}C_{org}$ and $\delta^{15}N_{tot}$. Approximately 1 g of sample powder was treated with 10% HCl, rinsed, and dried. The C isotopic ratios were measured using a FlashEA 1112 and a Delta V Advantage isotope ratio mass spectrometer. The results were expressed as relative deviations from V-PDB. Standards from the IAEA and IVA Analysentechnik were used for precision and calibration.

For $\delta^{15}N_{tot}$ analysis, 7 to 20 mg of sample powder was weighed into Sn capsules. The N isotopic ratios of the samples were measured using a FlashEA 1112, coupled via a ConFlo IV to a Delta V Advantage isotope ratio mass spectrometer. The $\delta^{15}N_{tot}$ values are expressed as the relative deviations from the measured $^{15}N/^{14}N$ ratio and with respect to atmospheric N_2. Sample precision and data calibration were performed using IAEA standards IAEA-N-1 (+0.43‰) and IAEA-N-2 (+20.41‰) and IVA Analysentechnik Urea Isotopic Working Standard (–0.32‰).

Results and discussion

The TOC content was consistently high in the black shale samples from Kallavere and Türisalu formations, ranging between 8 and 15% (n = 108) and low <1% (n = 16) in the Varangu Formation (Fig. 1). TN values varied accordingly from 0 to 0.66% and <0.07%, presenting strong positive covariance with TOC distribution ($R^2 = 0.89$, n = 26; Fig. 2). This suggests that most of the N resides in OM (note, however, that same samples also present consistent covariance between TOC, TN, and clay fraction indices). The average C/N atomic ratios from black shale of the Türisalu Formation, black shale interbeds from the Kallavere Formation, and grey shales from the Varangu Formation were ~37 (n = 108), ~29 (n = 60), and ~15 (n = 16), respectively. The $\delta^{13}C_{org}$ values of the black shales generally showed low variability ranging between –29.8 and –29.0‰ (n = 35), matching the values reported from Tremadocian complexes from the deeper part of the basin (Terfelt et al. 2014). Heavier $\delta^{13}C_{org}$ values (as high as –27.3‰) were detected in the organic-poor samples of the Varangu Formation and in a few intervals of coarse-grained black shales, with $\delta^{13}C_{org}$ increasing in phase with TOC, TN, and decreasing in C/N. The black shale samples characteristically showed $\delta^{15}N_{tot}$ ~0‰, with an average value for the Türisalu Formation –0.7‰ (n = 24) and for the Kallavere Formation –1.8‰ (n = 8). The $\delta^{15}N_{tot}$ signal range from the uppermost metal-poor part of the Türisalu Formation was similar to that observed for the Kallavere Formation. The total $\delta^{15}N_{tot}$ variance from –2.5 to 0.2‰ is in the same range with typical organic-rich black shales, including those from the Baltic Palaeobasin (Kiipli and Kiipli 2013; Hammer and Svensen 2017). A distinctly different

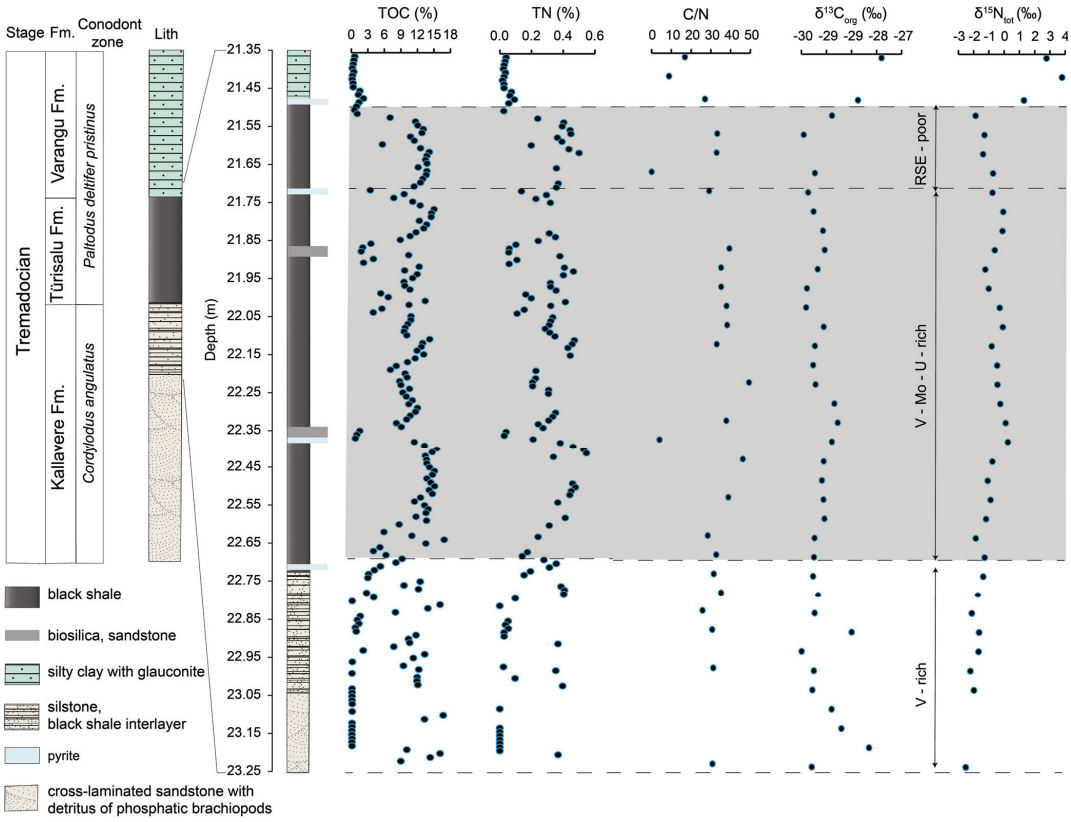

Fig. 1. Distribution of TOC, TN, molar C/N ratios, $\delta^{13}C_{org}$, and $\delta^{15}N_{tot}$ in the Aseri PH012B drill core. Abbreviations: Fm. – Formation, Lith – Lithology. Biozone boundaries after Heinsalu et al. (2003).

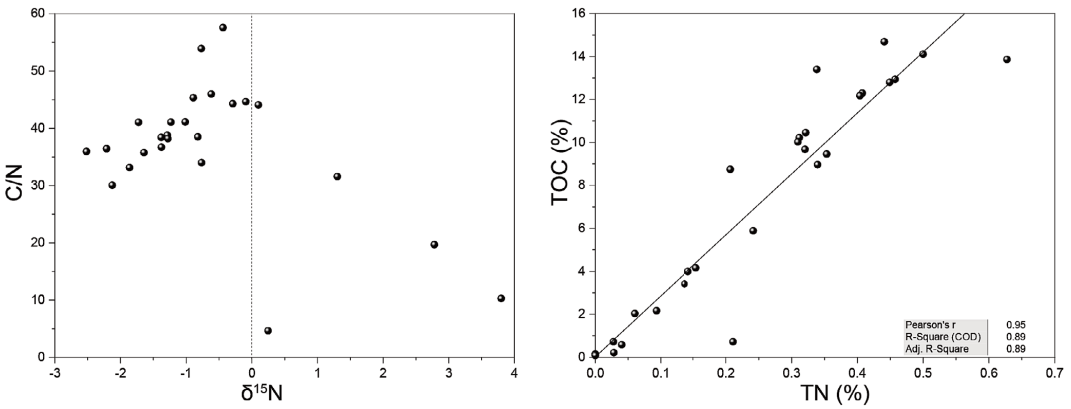

Fig. 2. Scatterplots of C/N ratios versus $\delta^{15}N$ and TOC versus TN for samples from the Aseri PH012B drill core. Abbreviation: Adj. – Adjusted.

$\delta^{15}N_{tot}$ range, between 1 and 4‰, was found in three samples from the Varangu Formation. No clear covariance was detected between TOC and $\delta^{13}C_{org}$ and between TOC and $\delta^{15}N_{tot}$. The distribution of $\delta^{15}N_{tot}$ versus C/N demonstrates that the loss of N from the black shale organic matter (assuming that primary biomass had a Redfield-like stoichiometry C:N ≈ 16:106) is accompanied by a shift of $\delta^{15}N_{tot}$ signal towards atmosphere-like unfractionated values.

We suggest, based on the observed variance, that N_2 fixation functioned as the dominant source of N for phytoplankton, helping to maintain a very high net primary production. The low negative $\delta^{15}N_{tot}$ values of the primary biomass (ranging from ~–2.5 to –1‰) can be explained by

efficient biomass transfer to the sea bottom due to a shallow oxygen-depleted water column in which quantitative denitrification processes dominated. The following release of N near the sediment-water interface via OM mineralization by conventional or sulphate-reducing anammox, combined with decreased net sediment rates, controlled the modification of the sediment N isotope composition and led to a small positive shift (~1‰) in $\delta^{15}N_{tot}$ (Hammer and Svensen 2017). Alternatively, the lower $\delta^{15}N_{tot}$ values in the Kallavere Formation and the RSE-poor part of the Türisalu Formation could be explained simply by a switch to alternative nitrogenase-using species due to Mo-limitation (Zhang et al. 2014) or a switch to another ^{15}N-depleted source of N. Nevertheless, the co-occurring decrease in the C/N ratios and $\delta^{15}N_{tot}$ suggests that the loss of N was most likely the reason behind the observed isotopic variance. The beginning of the accumulation of grey mud in the Varangu Formation marked the principal rearrangement in the nutrient cycle and redox architecture in the considered shallow shelf areas, establishing new equilibria in which NO_3^- assimilation became the major source of N for primary producers in a better oxygenated water column.

Conclusions

The relatively low $\delta^{15}N$ values of –2.5 to 0.2‰, combined with high C/N, suggest that bioproduction during the deposition of organic-rich muds was likely nitrogen-limited. N_2-fixation, as well as N_2-outgassing through denitrification and anoxic mineralization of OM in sediments, played a significant role in the biochemical cycling of nitrogen. The mineralization of OM in anoxic sediments slightly shifted the $\delta^{15}N_{tot}$ of the remaining OM towards heavier isotopic compositions. The principal transition in the local cycle of N in the considered inner shelf settings of Baltica occurred with the start of sediment accumulation in the Varangu Formation with a likely switch from diazotrophic-dependent to nitrate-based primary production, as evidenced by a shift towards positive $\delta^{15}N_{tot}$ values.

Acknowledgements

This study was supported by the ERDF and the Estonian Research Council via project RESTA18. The publication costs of this article were partially covered by the Estonian Academy of Sciences.

References

Algeo, T. J., Meyers, P. A., Robinson, R. S., Rowe, H. and Jiang, G. Q. 2014. Icehouse-greenhouse variations in marine denitrification. *Biogeosciences*, **11**(4), 1273–1295. https://doi.org/10.5194/bg-11-1273-2014

Dahl, T. W., Siggaard-Andersen, M. L., Schovsbo, N. H., Persson, D. O., Husted, S., Hougård, I. W. et al. 2019. Brief oxygenation events in locally anoxic oceans during the Cambrian solves the animal breathing paradox. *Scientific Reports*, **9**, 11669. https://doi.org/10.1038/s41598-019-48123-2

Deutsch, C., Sarmiento, J. L., Sigman, D. M., Gruber, N. and Dunne, J. P. 2007. Spatial coupling of nitrogen inputs and losses in the ocean. *Nature*, **445**(7124), 163–167. https://doi.org/10.1038/nature05392

Hammer, Ø. and Svensen, H. H. 2017. Biostratigraphy and carbon and nitrogen geochemistry of the SPICE event in Cambrian low-grade metamorphic black shale, Southern Norway. *Palaeogeography, Palaeoclimatology, Palaeoecology*, **468**, 216–227. https://doi.org/10.1016/j.palaeo.2016.12.016

Heinsalu, H., Kaljo, D., Kurvits, T. and Viira, V. 2003. The stratotype of the Orasoja Member (Tremadocian, Northeast Estonia): lithology, mineralogy, and biostratigraphy. *Proceedings of the Estonian Academy of Sciences. Geology*, **52**(3), 135–154. https://doi.org/10.3176/geol.2003.3.02

Kiipli, E. and Kiipli, T. 2013. Nitrogen isotopes in kukersite and black shale implying Ordovician–Silurian seawater redox conditions. *Oil Shale*, **30**(1), 60–75. https://doi.org/10.3176/oil.2013.1.06

Lille, Ü. 2003. Current knowledge on the origin and structure of Estonian kukersite kerogen. *Oil Shale*, **20**(3), 253–263. https://www.kirj.ee/public/oilshale/3_lille_2003_3.pdf

Ndiaye, M., Pajusaar, S., Liiv, M., Graul, S., Kallaste, T. and Hints, R. (in press). Fine clay shuttle as a key mechanism for V hyper-enrichment in shallow water Tremadocian black shale from Baltica. *Chemical Geology.* https://doi.org/10.1016/j.chemgeo.2023.121583

Schovsbo, N. H., Moron, J. M., Nielsen, A. T., Nicolas, G., Petersen, H. I. and Stouge, S. 2012. Thermal maturity of lower palaeozoic shales in north-west Europe – Calibration of proxies. In *74th EAGE Conference and Exhibition incorporating EUROPEC 2012, Copenhagen, Denmark, 4–7 June 2012*. European Association of Geoscientists and Engineers.

Sigman, D. M. and Fripiat, F. 2019. Nitrogen isotopes in the ocean. In *Encyclopedia of Ocean Sciences* (Cochran, J., Bokuniewicz, H. and Yager, P., eds). 3rd ed. Elsevier, Oxford, 263–278. https://doi.org/10.1016/B978-0-12-409548-9.11605-7

Stüeken, E. E., Kipp, M. A., Koehler, M. C. and Buick, R. 2016. The evolution of Earth's biogeochemical nitrogen cycle. *Earth-Science Reviews*, **160**, 220–239. https://doi.org/10.1016/j.earscirev.2016.07.007

Terfelt, F., Eriksson, M. E. and Schmitz, B. 2014. The Cambrian–Ordovician transition in dysoxic facies in Baltica – diverse faunas and carbon isotope anomalies. *Palaeogeography, Palaeoclimatology, Palaeoecology*, **394**, 59–73. https://doi.org/10.1016/j.palaeo.2013.11.021

Valley, J. W. and Cole, D. R. (eds). 2001. Stable isotope geochemistry. *Reviews in Mineralogy and Geochemistry*, **43**. https://doi.org/10.1017/cbo9780511809323.008

Veski, R. and Palu, V. 2003. Investigation of Dictyonema oil shale and its natural and artificial transformation products by a vankrevelenogram. *Oil Shale*, **20**(3), 265–281. https://doi.org/10.3176/oil.2003.3.04

Zerkle, A. L., Junium, C. K., Canfield, D. E. and House, C. H. 2008. Production of ^{15}N-depleted biomass during cyanobacterial N_2-fixation at high Fe concentrations. *Journal of Geophysical Research: Biogeosciences*, **113**(G3), 1–9. https://doi.org/10.1029/2007JG00 0651

Zhang, X., Sigman, D. M., Morel, F. M. M. and Kraepiel, A. M. L. 2014. Nitrogen isotope fractionation by alternative nitrogenases and past ocean anoxia. *Proceedings of the National Academy of Sciences of the United States of America*, **111**(13), 4782–4787. https://doi.org/10.1073/pnas.1402976111

Paper III

Ndiaye, M., Graul, S., Liiv, M., Kallaste, T., Algeo, T. J., & Hints, R. (2025). Trace-metal hyper-enrichment in Tremadocian black shales of the Baltic Palaeobasin linked to transgression and ultra-slow sedimentation rates. Chemical Geology, 690, 122910. https://doi.org/10.1016/j.chemgeo.2025.122910

Chemical Geology 690 (2025) 122910

Contents lists available at ScienceDirect

Chemical Geology

journal homepage: www.elsevier.com/locate/chemgeo

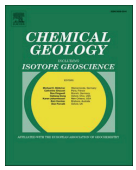

Trace-metal hyper-enrichment in Tremadocian black shales of the Baltic Palaeobasin linked to transgression and ultra-slow sedimentation rates

Mawo Ndiaye [a,*], Sophie Graul [a], Merlin Liiv [a], Toivo Kallaste [a], Thomas J. Algeo [b,c,d], Rutt Hints [a]

[a] Department of Geology, Tallinn University of Technology, Ehitajate tee 5, 19086 Tallinn, Estonia
[b] Department of Geosciences, University of Cincinnati, Cincinnati, OH 45221, USA
[c] State Key Laboratories of Geomicrobiology and Environmental Changes (GMEC) and Geological Processes and Mineral Resources (GPMR), China University of Geosciences, Wuhan 430074, China
[d] State Key Laboratory of Oil and Gas Reservoir Geology and Exploitation, Chengdu University of Technology, Chengdu 610059, China

ARTICLE INFO

Editor: Vasileios Mavromatis

Keywords:
Ordovician
Trace metals
Uranium isotopes
Molybdenum isotopes
Redox
Euxinia

ABSTRACT

Determining the local versus global influence on the metallogeny of redox-sensitive trace-metal-enriched black shales remains challenging despite extensive geochemical research in related topics. A set of local triggers or modifiers of syngenetic metal enrichment, still poorly understood, impedes the ability to adequately predict the potential distribution of metal resources. This study of the Lower Ordovician Türisalu Formation examines the stratigraphic trends of Mo and U isotopes in Mo-U-V hyper-enriched thin transgressive black shales and associated beds from the inner shelf of the Baltic Palaeobasin (Aseri PH012B drillcore, NE Estonia) to reveal underlying connections between isotopic fractionation, palaeoenvironmental changes, and metal enrichment processes. Twenty samples from the basal 28-cm-thick Unit I and overlying 66-cm-thick Unit II were analysed by multi-collector inductively coupled plasma mass spectrometry (MC-ICP-MS) and interpreted within a recently developed high-resolution chemostratigraphic framework. The tested samples yielded variable δ^{98}Mo (from −0.89 to +2.03 ‰) and δ^{238}U values (from −0.27 to +0.52 ‰). Unit I, which is Mo-enriched, yielded the highest δ^{238}U and lowest δ^{98}Mo values, whereas Unit II, which is U-enriched, is marked by sharply lower δ^{238}U values. This black shale succession was deposited under a prolonged sea-level transgression. Variations in δ^{98}Mo and δ^{238}U suggest that the mechanism of Mo and U sequestration changed depending on facies during the transgression. Metal enrichment was influenced by a combination of ultra-slow sedimentation rates (0.6–1.0 mm kyr^{-1}), relative sea-level changes, and shallow redox stratification maintained in part by surface heating under a super-greenhouse climate. Extremely slow sedimentation prolonged seawater-sediment interactions, facilitating diffusion-controlled uptake of U and Mo under euxinic conditions. Landward expansion of the subpycnoclinal oxygen-depleted watermass and related redox shifts from suboxic to euxinic conditions near the seafloor drove the selective hyper-enrichment of Mo, and U. Isotopic trends highlight efficient Mo sequestration in euxinic settings likely aided by recycling of Fe—Mn near redoxcline and U hyper-enrichment under Mo-depleted watermasses.

1. Introduction

1.1. Research aims and context

Beyond well-understood general circumstances, i.e., enrichment enabled by redox gradients in seawater and sediments, the geological contexts of metallogeny in black shales enriched with redox-sensitive metals remain debated. Many recent in-depth studies show significant individualism in black shale metal sequestration environments. In deep time, such variability at first order stems from global-scale changes such as oxygenation of the ocean and atmosphere and biosphere evolution (e.g., Scott et al., 2008). Due to overlapping factors, single isotopic systems might provide contradictory clues for interpreting fractionation pathways and related palaeoenvironmental conditions. However, the coupled U—Mo isotope signals can help to overcome these weaknesses. Such datasets, recently widely exploited for palaeoredox investigations,

* Corresponding author.
E-mail address: mawo.ndiaye@taltech.ee (M. Ndiaye).

https://doi.org/10.1016/j.chemgeo.2025.122910
Received 8 April 2025; Received in revised form 2 June 2025; Accepted 3 June 2025
Available online 4 June 2025

might also help track syngenetic metal enrichment conditions of anomalously metalliferous black shales (Anderson et al., 1989). For example, Xu et al. (2024) utilized U and Mo isotopes to study metal sequestration mechanisms in lower Cambrian hyper-Mo-enriched black shales from South China, suggesting a major role for Fe—Mn redox cycling in Mo capture.

The present study applies paired Mo and U isotope system records to investigate thin, hyper-enriched, transgressive black shales from nearshore areas of the Baltic Palaeobasin as potential trackers of Mo and U enrichment processes and environments. Mo and U isotope signatures are examined in black shales of the Tremadocian Türisalu Formation from the Aseri PH012B drillcore in NE Estonia, recently addressed by high-resolution geochemical investigations (Ndiaye et al., 2023b). These investigations revealed extreme enrichment of Mo (up to 2690 ppm) and U (up to 510 ppm), considerably exceeding values reported from coeval organic-rich facies from deeper basinal settings of the Baltic Palaeobasin where $Mo_{max} = 141$ ppm and $U_{max} = 70$ ppm have been reported by Bian et al. (2021). However, the peak enrichments of Mo and U are observed in different stratigraphic horizons. This study aims to determine if patterns of Mo and U enrichment correspond to shifts in the isotopic compositions of these trace metals and, if so, what information this provides about mechanisms of Mo and U sequestration in highly reducing facies. δ^{98}Mo and δ^{238}U data are interpreted along with selected trace and major elements and environmental proxies, based on what we propose a novel model to explain development of the observed patterns of Mo and U enrichment and isotopic variation.

1.2. Mo—U isotope overview

Stable isotopes of redox-sensitive elements and those with long half-lives, such as ^{98}Mo, ^{95}Mo, ^{238}U, and ^{235}U, and their isotopic ratios (δ^{98}Mo, δ^{238}U), can be used as tracers of various geological processes. Distributions of U and Mo, and more lately their isotopes, have been applied to reconstruct the redox conditions of marine palaeoenvironments, including those from the late Cambrian and Tremadocian (Algeo and Maynard, 2004; Algeo and Maynard, 2008; Arnold et al., 2004; Brüske et al., 2020; Dang et al., 2018; Kendall et al., 2015; Voegelin et al., 2009; Wang et al., 2015; Xu et al., 2012). The mobility and isotopic fractionation of multivalent Mo and U in surface waters are mainly dependent on redox state and local environmental conditions, typically resulting in high authigenic and low lithogenic fluxes of these elements to oxygen-depleted sediments (Calvert and Pedersen, 1993; Crusius et al., 1996; Nägler et al., 2005; Wilde et al., 2004). These elements exhibit relatively uniform isotopic compositions in the open ocean owing to their long residence times (~450 kyr for Mo: Dunk et al., 2002; Miller et al., 2011; Morford and Emerson, 1999; ~440 kyr for U: Calvert and Pedersen, 1993; Klinkhammer and Palmer, 1991) and high concentrations in oxygenated seawater (~110 nM for Mo, ~13 nM for U; Algeo and Tribovillard, 2009). The Mo and U isotopic compositions of ancient black shales record, foremost, the effects of redox-related fractionation (Arnold et al., 2004; Barling et al., 2001; Brennecka et al., 2011a; Dahl et al., 2014; Kendall et al., 2009; Scheiderich et al., 2010; Stirling et al., 2007; Weyer et al., 2008).

In oxic marine water masses, both Mo and U have valences of +6 (Algeo and Tribovillard, 2009; Asael et al., 2013) and predominantly exist as soluble molybdate ions (MoO_4^{2-}) and uranyl complexes (e.g., $UO_2(CO_3)_3^{4-}$), exhibiting conservative behaviour (Morford and Emerson, 1999). Under suboxic to sulfidic conditions, Mo and U are reduced to less soluble forms, driving their enhanced accumulation in sediments. When approaching an aquatic H_2S (H_2Saq) threshold value of approximately 11 μM, MoO_4^{2-} transforms into highly-particle-reactive thiomolybdate species or Fe–Mo–S phases, leading to effective Mo sequestration from seawater (Erickson and Helz, 2000; Helz et al., 1996; Nägler et al., 2011). This process introduces isotopic fractionation, causing measurable differences in Mo isotopic ratios ($\Delta^{98}Mo_{sediment-water} \approx -0.5$ ‰; Nägler et al., 2011). Under severely euxinic settings with closed-system effects, sedimentary Mo isotopes closely reflect seawater composition (Nägler et al., 2011).

The reduction and sequestration of U primarily occurs at redox potentials near those of Fe (III) reduction, thus under less reducing conditions compared to Mo reduction (Anderson et al., 1989). U reduction predominantly occurs within sediments and is strongly influenced by diffusive fluxes and biogeochemical interactions at the sediment-water interface, notably through microbial mediation involving iron- or sulfate-reducing bacteria (Abshire et al., 2020; Andersen et al., 2017; Andersen et al., 2015; Barnes and Cochran, 1993; Basu et al., 2014; Brennecka et al., 2011b; Brown et al., 2018; Bura-Nakić et al., 2018; Campbell et al., 2012; Goldmann et al., 2015; Holmden et al., 2015; Klinkhammer and Palmer, 1991; Somlyay et al., 2023; Stylo et al., 2015; Wang et al., 2015). Variations in pore-water δ^{238}U directly affect sediment compositions because U reduction predominantly takes place within sediment rather than in the overlying water column, meaning porewater isotopic signatures can be readily transferred to the solid sediment phases (Weyer et al., 2008). This transfer results in measurable and significant δ^{238}U fractionation (typically between 0.4 and 0.7 ‰ relative to seawater), thus imparting higher δ^{238}U values to sediments (Andersen et al., 2014; Bopp et al., 2010; Weyer et al., 2008). Nevertheless, under closed systems conditions with elevated dissolved sulfide concentrations, U is quantitatively scavenged from ambient water, reducing isotopic fractionation between seawater and sediment, and thereby complicating the interpretation of palaeoenvironmental conditions from δ^{238}U signatures (Chen et al., 2023; McManus et al., 2006; Yang et al., 2023; Zhao et al., 2023).

Additional factors can influence Mo and U isotopic fractionation patterns. In oxic and suboxic environments, preferential scavenging of Mo by Fe–Mn-(oxyhydr)oxide particles in the water column can enhance its sedimentary accumulation. Upon deposition in reducing organic-rich sediments, these phases undergo reductive dissolution, releasing Mo that may subsequently react with sulfide or organic matter, or diffuse back into the water column (Algeo and Lyons, 2006). The cycling of Fe–Mn-(oxyhydr)oxide particles in weakly restricted, redox-stratified marine settings typically produces sedimentary δ^{98}Mo values intermediate between seawater (+2.3 ‰) and ferromanganese concretions (~ −0.7 ‰), reflecting a large isotopic offset of approximately −3 ‰ from seawater (Kendall et al., 2017; Noordmann et al., 2015; Scholz et al., 2013). This significant fractionation aligns closely with experimental observations (Barling et al., 2001; Barling and Anbar, 2004; Siebert et al., 2003; Wasylenki et al., 2008). Moreover, while Mo generally behaves conservatively in the open ocean, notable non-conservative Mo dynamics have been documented in continental margin environments (Scholz et al., 2017), as well as in coastal and estuarine systems of open to semi-restricted shallow shelf seas like the Wadden Sea and Yellow Sea. In these areas, dissolved Mo dynamics are strongly linked to biologically driven nitrogen cycling, organic aggregate formation, and adsorption onto algal-derived organic matter (Dellwig et al., 2007; Fan et al., 2022). In productive marine systems, adsorption of Mo onto algal organic matter results in isotope fractionation, characterised by an enrichment factor (ε) of approximately −0.3 ‰ relative to seawater (Kowalski et al., 2013). In comparison, U isotope fractionation patterns differ from Mo due to distinct redox sensitivities and biogeochemical interactions. In marine settings, the cycling of Fe–Mn-(oxyhydr)oxides can influence U isotopes, but fractionation typically occurs upon U reduction within sediment porewaters rather than during water-column scavenging.

2. Geological background

Long-term transgression on Baltica with extensive facies migration and low clastic input to the innermost part of the inland sea make up the regional geological background for deposition of Tremadocian black shales. The Ordovician has been described as a “water world” with >80 % of the continental lithosphere submerged under shallow

epicontinental with an average depth of ~40 m (Scotese, 2023). In general, high sea levels and low-lying land areas on the major continents (i.e., Laurentia, Baltica and Gondwana) characterise the palaeogeography of the whole period (Fig. 1A). The Baltic Palaeobasin on Baltica has been investigated as a representative site for studying Cambrian to Lower Ordovician atmospheric, oceanic and biological turnovers (Bian et al., 2022; Gill et al., 2021; Gill et al., 2011; Nielsen and Schovsbo, 2015; Sturesson et al., 2005). During this interval, the epicontinental flat-bottomed sediment-starved Baltic Palaeobasin covered much of the Baltic Craton (Nielsen et al., 2020). In the outer and middle shelf of the basin, organic-rich metalliferous muds accumulated from the middle Cambrian to the Tremadocian, under extremely sluggish accumulation rates (Sørensen et al., 2020; Zhao et al., 2022). A transgression in the Furongian reinitiated sediment accumulation in the innermost part of Baltica after a long sedimentary hiatus (Fig. 1B). The study area in North Estonia is a part of the geotectonically extremely stable, rigid cratonic crust in the interior of Baltica located near the border of the Fennoscandian Shield and East European Platform with untectonized and unmetamorphosed Ediacaran and Lower Palaeozoic homoclinal strata above Palaeoproterozoic-Mesoproterozoic basement (Puura and Vaher, 1997). The nearby peneplained shield areas in southern Finland have been described as regions with ultra-slow denudation rates during the last >1 Gyr (Hall et al., 2021). Nevertheless, Fennoscandian and Ukrainian Siled, the only two land regions of Baltica during the Ordovician, acted as sole clastic supply areas for the East Baltic area of Baltic Palaeobasin (Nielsen and Schovsbo, 2015). There is no geological evidence of the existence of major river systems on Baltica during the Ordovician. Limited clastic supply and tectonic quietness prompted the accumulation of thin siliclastic ramp deposits and, later in Ordovician, condensed shallow water carbonate ramp sediments in the considered inner shelf region (Meidla et al., 2023). Nor is there evidence of syngenetic hydrothermal fluid intrusion, shown to be a significant driver of elevated productivity and metal enrichment in the case of some other highly metalliferous black shales (e.g., Zhang et al., 2022). The study area was located in the innermost part of Baltica far from distant stress fields possibly created at the N-NW margin of the continent due to the start of the closure of the Iapetus Ocean during the Furongian (Scotese, 2023). While low-temperature regional brines reached the area during the late Silurian to Middle Devonian interval in association with major phases of the Caledonian Orogeny, there are no known hydrothermal signatures recorded before that time in considered successions (Eensaar et al., 2017; Somelar et al., 2010).

In the study area in Estonia, nearby terrestrial landmasses of the Fennoscandian Shield, coastal to subtidal sands and silts with abundant detritus of phosphatic brachiopods (the Kallavere Formation) accumulated before the deposition of Tremadocian organic-rich muds (Artyushkov et al., 2000). This phosphate-rich lithofacies, which contains irregular lenticular bodies of phosphatic shelly coquinas and are known to hold the largest sedimentary phosphorite reserves in Europe, has been attributed to the upwelling of nutrient-rich waters at the Iapetus margin combined with coastal upwelling nearshore in the inner part of Baltica (Graul et al., 2023; Ilyin and Heinsalu, 1990). The Kallavere Formation, characterised by spatially highly variable thickness distribution (maximum thickness > 20 m), and its eastern counterparts, the Tosna Formation and Lomashka Formation (Kaljo et al., 1986), form a sandstone tongue along the margin of the assumed terrestrial landmasses of the Fennoscandian Siled but pinch out basinward. During their deposition, the area was dissected by moving sand ridges or islands (Heinsalu et al., 1994), and the complex siliciclastic facies show subaerial features such as palaeokarst (Popov et al., 2019), interbeds (up to 20 cm thick), thin drapes, and clasts of black shales, in some levels forming mud blankets above pyritized rippled surfaces, indicating organic-rich mud accumulation in a sediment-active shallow-water setting.

The Tremadocian black shales in Estonia form a non-contemporaneous lithostratigraphic unit known as the Türisalu Formation (Kaljo et al., 1986; Kaljo and Kivimägi, 1970). This longitudinal belt of inner shelf black shales continues eastward into Russia. The northern erosional boundary of the belt is the Baltic Klint. The maximum thickness (> 6 m) of the black shale succession is reached in NW Estonia; from there, the Türisalu Formation thins rapidly southward and eastward, pinching out around the middle of Estonia (Fig. 1C). Thin, thermally immature black shales present notable lithological complexity, including diagenetic limestone concretions, silty laminae, sandy pyritised and cyclic spiculite interbeds with heterogeneity generally increasing in thin eastward located and chronostratigraphically younger sections (Fig. 1D). The black shales of the Türisalu Formation contain sediment reactivation features, which points to the incomplete sedimentary record and relatively shallow sedimentary environment (Heinsalu, 1990; Hints et al., 2014a). Stratigraphic relationships between the black shale of the Türisalu Formation and those from the deeper shelf in Scandinavia are not well established due to the limited patchy preservation of Tremadocian sediments (Heinsalu and Bednarczyk, 1997). There is a hiatus in considered chronostratigraphic level in other parts of the East Baltic area of Baltic Palaeobasin, which stayed in the deeper part of the inner shelf during the Ordovician (Meidla et al., 2023). In the eastward, inland Moscow Basin, fine-grained offshore to basinal sandstones and dark grey shales accumulated at the start of Ordovician (Heinsalu and Bednarczyk, 1997).

The Türisalu Formation is characterised by remarkably high but spatially and vertically variable enrichment of V, Mo and U. The distribution profiles of those elements do not show clear overlap, however, the lower part of the Türisalu Formation, in general, tends to be more enriched in redox-sensitive elements (Hints et al., 2014b; Loog and Petersell, 1994; Pukkonen and Rammo, 1992; Vind et al., 2023). Pukkonen and Rammo (1992) divided the Türisalu Formation spatially into three geochemical zones based on the spatial variability of enrichment levels of redox-sensitive metals. The Aseri PH012B borehole, located in the northeastern part of Estonia (59.426053°N, 26.755267°E), belongs to the eastern geochemical zone, characterised by U and Mo hyper-enrichment. The U enrichment within the Türisalu Formation peaking in this area (the average U ~160 ppm, but sporadically U > 500 ppm; Hints et al., 2021; Petersell, 1997) has been generally attributed to the extremely slow net accumulation rates of the mud. In the study area, the thickness of the Türisalu Formation is approximately one meter, and the succession is composed of lithologically distinct horizons reflecting facies shift during transgression and highstand stages of development.

In the Aseri PH012B drillcore, the basal part of the Türisalu Formation consists of fine-grained laminated black shales. These are overlain by black shales displaying a cyclic occurrence of partly pyritised biosilica-rich interbeds and minor glendonite-like carbonate concretions. The uppermost, lighter-coloured part of the Türisalu Formation is thinly laminated and shows erosional features at bedding planes. Ndiaye et al. (2023b), which considered V hyper-enrichment mechanisms in black shales based on the same section, applied a tripartite division to the Türisalu Formation (Units I, II and III; note: previously called "zones" but revised here to "units" to avoid use of the term "zone" in multiple contexts) based on combined high-resolution geochemical data and novel and historic lithological studies (Kivimägi and Loog, 1972). The characteristic lithological–geochemical division into four subunits—comprising three black shale horizons and a major pyritized sandstone interbed with phosphatic detritus—was first established for these black shales during extensive phosphorite exploration and drilling campaigns in the 1970s at the nearby Toolse phosphorite deposit, located approximately 15 km west of the studied section (Kivimägi and Teedumäe, 1971). In addition to lithological variations, it was observed that V and Mo concentrations peaked in the lowermost unit (≈Unit I), while the highest average U content was recorded in the black shales of the middle part of the Türisalu Formation (≈Unit II). The black shales in the upper part of the formation (≈Unit III) were found to be depleted in these elements. The pyrite-rich siltstones of the Kallavere Formation below the Türisalu Formation (Orasoja Member) also contain interbeds

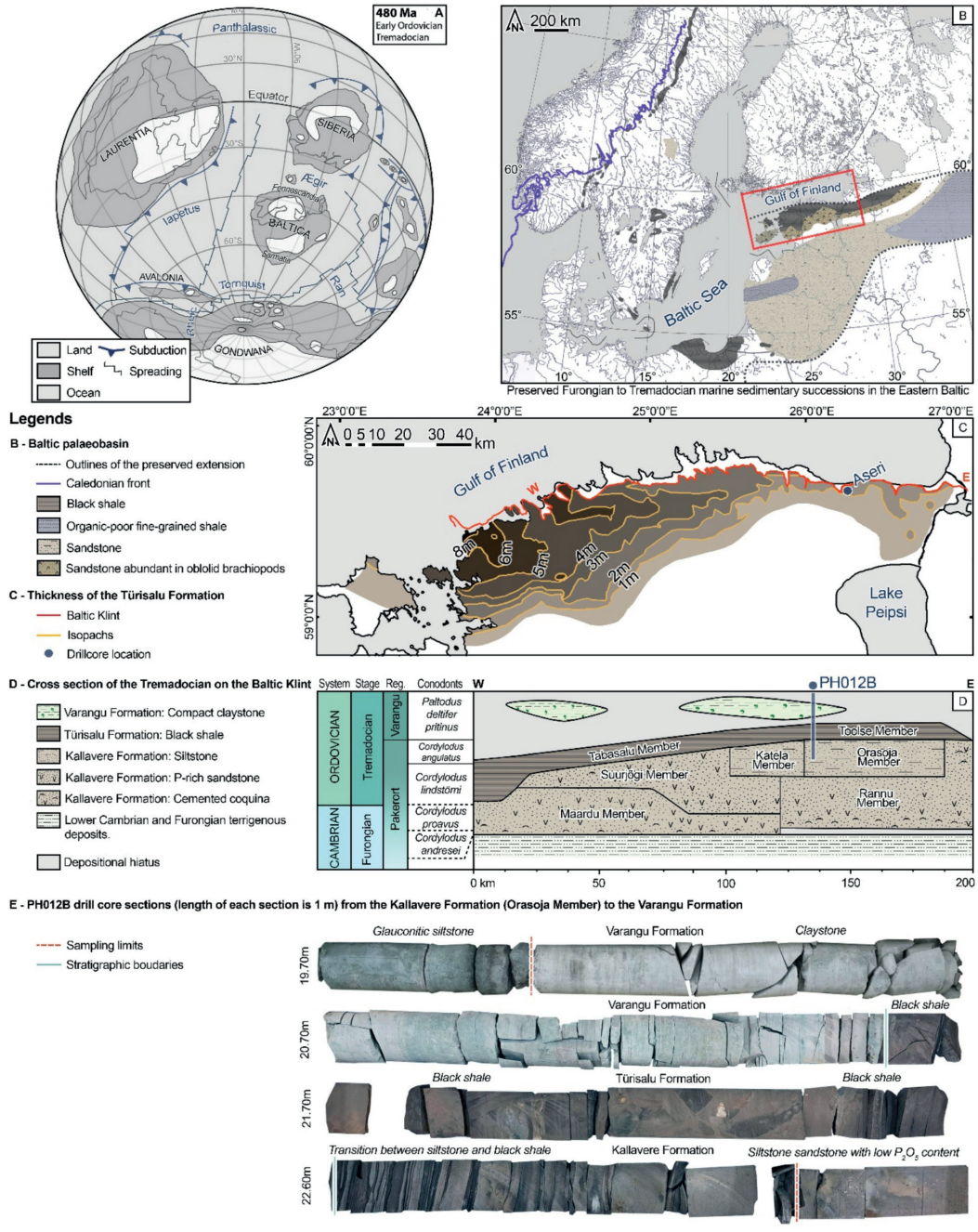

Fig. 1. (A) Relative position of the main palaeocontinents and Baltica during the Early Ordovician, after Cocks and Torsvik (2002). Extensively overflooded Baltica encompassed two land areas: the Fennoscandian Shield and the Ukrainian Shield. (B) Distribution area of Middle Cambrian to Lower Ordovician black shales and other siliciclastic facies of the Baltic Palaeobasin, after Schovsbo et al. (2018) and Popov et al. (2019). Note that black shales are preserved only in limited areas within the supposed original distribution limits of the organic-rich facies. (C) Location schema of the Türisalu Formation; isopach lines show formation thickness after Pukkonen (1989). (D) Lithostratigraphy and biostratigraphy of Furongian and Tremadocian deposits on the Baltic Klint section. The blue dot marks the location of core Aseri PH012B. (E) The drillcore section of Aseri PH012B. Stratigraphically, the oldest siltstone-fine-grained sandstone beds with phosphatic detritus belong to the Kallavere Formation. The upper part of the formation (Orasoja Member) shows the interfingering of siltstone and black shale laminae. The overlying Türisalu Formation contains black shales exhibiting distinct lithological changes (see text for further details). Grey silty claystones of the Varangu Formation cap the Türisalu Formation. (For interpretation of the references to colour in this figure legend, the reader is referred to the web version of this article.)

of organic-rich black shales, showing thus a gradual boundary between the Kallavere Formation and Türisalu Formation characterised by shift from silt-dominated horizons to black shale-dominated strata as the result of progressive transgression (Heinsalu et al., 2003). The Türisalu Formation is capped by lithologically similar but organic-poor grey mudstones of the Varangu Formation.

The hosts of redox-sensitive elements in the Türisalu Formation are not well defined due to the high organic matter content, low crystallinity, poorly characterised relationships between minerals and organic matter, and the finely dispersed nature of the mineralization. Mo is believed to occur as dispersed compounds in sulfides or bound to sulfidised organic matter. U is likely present mainly as U–organic complexes, and occasionally as U-rich apatite in the northeasternmost localities of the Türisalu Formation. V is either substituted into the crystal lattice of dioctahedral mixed-layered clays or bound to clay surfaces, possibly in the form of V–porphyrins (Baturin and Ilyin, 2013; Ndiaye et al., 2023b; Schulz et al., 2019; Shulga et al., 1987).

3. Materials and analytical methods

The sample set used for this study was collected during high-resolution geochemical profiling of black shales and associated beds from the Aseri PH012B core section ($n = 187$). Continuous sampling was employed, with each sample representing a 1-cm-thick core interval. X-ray fluorescence was used to obtain major and trace element compositions, and total organic carbon (TOC) content was analysed using a CHNS-O elemental analyser at the Tallinn University of Technology, Department of Geology. Detailed sample preparation, analytical procedures and selected results were previously published in Ndiaye et al. (2023b).

For analysis, all whole-rock samples (~20 g) were crushed and homogenised in an agate mortar using a tungsten carbide mill. For major element analysis, fused disks were prepared with a Claisse M4 Gas Fusion instrument. A 0.66 g portion of the crushed sample was fused in a platinum crucible using a flux of lithium metaborate: 49.75 % lithium tetraborate: 49.75 % lithium bromide 0.5 %. For trace element analysis, ~8 g of powder was pressed into a pellet using 5 % Mowiol solution (one drop per gram of sample). Pressed pellets and fused disks were analysed using a Bruker S4 spectrometer, with internal calibration based on six local in-house black shale reference samples (Pajusaar et al., 2021) and quality control using the GeoPT48/MzBP sample from the IAG proficiency testing series. The laboratory's analytical performance was confirmed as reliable for this rock type by results from the recent IAG testing round (GeoPT52), which used black shales from the Türisalu Formation. Loss-on-ignition measurements were conducted on all samples as follows: 1 g of material was placed in a crucible and heated in a Nabertherm furnace at 550 °C and 950 °C for 4 h. Samples were then cooled to room temperature in desiccators and weighed.

Total organic carbon was analysed by combustion in a FLASH 2000 organic elemental analyser. Approximately 8 mg of dried powdered sediment was placed in a silver container, pre-treated with 10 % HCl to remove inorganic carbon, and dried on a hotplate at 80 °C for 5 h. Once dry, the capsules were cooled and wrapped to form granules. Prior to analysis, silver capsules were packed into tin containers to facilitate combustion. Cystine (Thermo Fisher Scientific) was used as the standard, and high-organic sediment (IVA Analysentechnik e.K.) as the reference material.

The Mo and U isotopic analyses were conducted on selected samples from the same sample set. Sixteen samples from the Türisalu Formation were collected at intervals of 5 cm, except for five samples in Units II and III, which were collected at 10 cm intervals. Additionally, selected black shale interbeds from the Kallavere Formation ($n = 2$) and grey mudstones from the Varangu Formation ($n = 2$) were included in total twenty samples. Approximately 1 g of powdered material was used for isotopic analyses.

Samples for both Mo and U isotopic analyses were prepared using digestion with aqua regia (AR; a 3:1 mixture of concentrated HCl at 30 % and concentrated HNO_3 at 65 %) combined with hydrofluoric acid (HF; 48 %) to ensure complete digestion of refractory phases. Digestion was carried out at approximately 120 °C for 4 h in Teflon beakers. After complete dissolution was visually confirmed, the digests were evaporated to dryness. For U isotopic analysis specifically, the residue was refluxed overnight with 4 mL of aqua regia to remove excess fluoride, then evaporated again to dryness and re-dissolved in 6 M HNO_3. Subsequently, uranium was separated using pre-packed 2 mL TEVA resin columns. The purified U fraction was then evaporated to dryness and finally re-dissolved in 0.8 M HNO_3. For Mo isotope analyses, samples were digested exclusively with aqua regia under identical conditions due to the absence of Mo in the silicate fraction.

Mo and U isotopic compositions were determined using multi-collector inductively coupled plasma mass spectrometry (MC-ICP-MS) at ALS Scandinavia Laboratories (Luleå, Sweden), employing a Neptune PLUS (Thermo Fisher Scientific) instrument equipped with an OnToolBooster Jet interface pump (Pfeiffer). An external calibration method was utilized, using bracketed isotope standard reference materials (SRMs) to correct for instrumental mass bias. Analyses were carried out following ion-exchange separation using Chelex-100 resin for Mo and TEVA resin for U, both of which achieved analyte recoveries greater than 95 %.

For uranium isotope measurements ($\delta^{238/235}U$), sample introduction was via an Aridus II desolvating nebulizer, Jet sample cone, X-skimmer cone, and self-aspirated MicroMist nebulizer, achieving a sample uptake of ~70 μL min^{-1} and providing a $\delta^{238/235}U$ intensity of approximately 40 V per 80 μg L^{-1} (Pontér et al., 2021). All U isotope data are reported as per mille (‰) variation relative to the interpolated composition of the CRM-112a uranium isotope standard (National Institute of Standards and Technology, USA), analysed immediately before and after each sample. Analytical uncertainty was determined by calculating the standard deviation (SD) from two independent consecutive measurements, typically achieving reproducibility better than ±0.1 ‰ (Pontér et al., 2021). The isotopic composition ($\delta^{238}U$) is expressed using δ notation according to Eq. (1):

$$\delta^{238}U\ (‰) = 1000 \times \left[\left({}^{238/235}U \right)_{sample} \Big/ \left(\left({}^{238/235}U \right)_{CRM-112a} \right) - 1 \right] \quad (1)$$

Mo isotope measurements followed the protocol described by Malinovsky et al. (2005). Mo isotopic compositions ($\delta^{98}Mo$) were measured against an in-house standard, then corrected and reported relative to the NIST SRM 3134 standard according to Eq. (2) (Malinovsky et al., 2005). Analytical reproducibility, assessed through replicate analyses of standards and secondary reference materials, demonstrated long-term precision (2σ) of ±0.08 ‰ or better for $\delta^{98/95}Mo$. Tabulated δ-values for Mo and U certified reference materials (CRMs) were taken from the GeoReM database (Jochum et al., 2005).

$$\delta^{98}Mo\ (‰) = 1000 \times \left[\left({}^{98/95}Mo \right)_{sample} \Big/ \left({}^{98/95}Mo_{NIST\ SRM\ 3134} \right) - 1 \right] + 0.25 \quad (2)$$

To define the contribution of $\delta^{98}Mo$ and $\delta^{238}U$ from lithogenic and authigenic sources to the measured total isotopic signatures, the authigenic proportion of isotopic compositions was estimated using the following equations for the bulk rock (bulk) and authigenic (auth) and detrital (det) fractions; Eqs. (3) and (4)):

$$\delta^{98}Mo_{auth} = \delta^{\frac{98}{95}}Mo_{bulk} - \left(\frac{Al}{Mo} \right)_{bulk} \times \left\{ \frac{\delta^{\frac{98}{95}}Mo_{det} - \delta^{\frac{98}{95}}Mo_{bulk}}{\left(\frac{Al}{Mo} \right)_{det} - \left(\frac{Al}{Mo} \right)_{bulk}} \right\} \quad (3)$$

$$\delta^{238}U_{auth} = \delta^{238}U_{bulk} - \left(\frac{Al}{U} \right)_{bulk} \times \left\{ \frac{\delta^{238}U_{det} - \delta^{238}U_{bulk}}{\left(\frac{Al}{U} \right)_{det} - \left(\frac{Al}{U} \right)_{bulk}} \right\} \quad (4)$$

We assumed that the detrital fraction had the same Mo (1.1 ppm), U (2.7 ppm) and Al (8.15 wt%) contents and the same δ^{98}Mo (+0.3 ‰) and δ^{238}U (−0.3 ‰) isotopic ratios as the average upper continental crust (Noordmann et al., 2016; Rudnick and Gao, 2003; Tissot and Dauphas, 2015; Voegelin et al., 2014).

Enrichment factors (X_{EF}) for trace elements (X) were calculated according to the procedure of Tribovillard et al. (2006). The element concentrations were first normalised to the Al content of the sample and divided by the appropriate trace element-to-Al ratio in the Post-Archean Australian Shale (PAAS) standard (Taylor and McLennan, 1985) (Eq. (5)):

$$X_{EF} = (X/Al)_{sample} \Big/ (X/Al)_{PAAS} \quad (5)$$

4. Results

4.1. Major and trace elemental records

The obtained isotopic δ^{98}Mo and δ^{238}U data for the Aseri PH012B drillcore, as well as Mo, U and V concentrations and other selected geochemical variables, are presented in Table 1 and illustrated in Fig. 2. The stratigraphic framework for the Türisalu Formation is the same as that used by Ndiaye et al. (2023b), although we further divided Unit I into two subunits: lower (I_L) and transitional (I_T). Figs. 2 and 3 show commonly used geochemical indices for oxygen-depleted deposits based on the collected analytical data. Only samples with $Al_2O_3 > 9$ wt% were included in the presented dataset to avoid possible biases introduced by samples with mixed lithologies. The applied threshold value is empirical. It was originally used by Ndiaye et al. (2023b) on the same dataset to distinguish pure black shale samples from a broader whole-rock set that included coarse-grained siliciclastic, carbonate-rich, and mixed lithologies. The threshold was chosen based on major element profiles from two drillcores, including 187 samples from the Aseri PH012B core, to ensure inclusion of coarse-grained but organic-rich black shales, as well as samples with moderate biosilica content and elevated pyrite. The complete geochemical dataset and distribution ranges for each interval are provided in the supplementary material.

A distinctive feature of the dataset is the extreme Mo enrichment of samples from Unit I_L of the Türisalu Formation. On Mo_{EF} vs. U_{EF} (Fig. 4A) and Mo vs. TOC (Fig. 4B) discriminant diagrams, samples of Units I_T and II also show high levels of Mo and U enrichment, although to levels closer to some other Phanerozoic metalliferous black shales (cf. Algeo and Lyons, 2006; Algeo and Tribovillard, 2009). In contrast, samples from Unit I_L show Mo enrichments up to ~10× greater than are typically encountered, yielding Mo_{EF} values as high as 3300–4700. The black shales from the Mo hyper-enriched Unit I_L stand out by their fine-grained nature, as reflected in Al concentrations (avg 15.0 %, std. 1.37 %) higher than those of Unit I_T (avg 12.0 %, std. 3.66 %) and Unit II (avg 13.1 %, std. 3.04 %). The boundary between the Kallavere Formation and Unit I_L exhibits a sharp rise in Mo enrichment in black shales compared to a more modest increase in U (Mo_{EF}/U_{EF} rise from <10 to >30) (Figs. 3A, 4B), resembling Mo sequestration fingerprint commonly attributed to the particulate shuttle process. However, unlike modern open-marine anoxic settings where Mn—Fe shuttles control Mo accumulation, the hyper-enrichment of Mo in Unit I_L falls into the severe euxinic range on the Mo_{EF} vs. U_{EF} diagram. This appears to align with the sharp increase in the Mo/S ratio in the lower Türisalu black shales, suggesting that mud accumulation was accompanied by extensive organic matter degradation, enhanced sulfide production and possibly steep redox gradients near the sediment-water interface (Fig. 3E). Other geochemical features include uniform P/Al (Fig. 3F) values in Unit I_L, varying from 0.27 to 0.29 and from 0.95 to 2.26, respectively, while Mo/Mn (Fig. 3C) shows a general upward increase from 3 to >10.

Unit I_T, hyper-enriched with both Mo and U, presents several specific geochemical signatures – these features include 1) a drop in TOC and Al

Table 1
The table presents the geochemical and isotopic data of Aseri PH012B samples collected at different depth. Isotopic compositions are shown for δ^{98}Mo (measured and authigenic), δ^{238}U (measured and authigenic), and their associated uncertainties (2σ), as well as calculated detrital proportion of Mo and U from the total Mo and U content.

Depth (m)	Al_2O_3 (wt %)	Fe_2O_3 (wt %)	MnO (wt %)	S (wt %)	Mo (ppm)	U (ppm)	V (ppm)	TOC (wt %)	$\delta^{98/95}Mo_{measured}$ (‰)	2 σ	$Mo_{detrital}$ (wt %)	$\delta^{98}Mo_{authigenic}$ (‰)	$\delta^{238}U_{measured}$ (‰)	2 σ	$U_{detrital}$ (wt %)	$\delta^{238}U_{authigenic}$ (‰)
21.49	15.88	4.20	0.02	1.20	9	16	355	2.16	0.77	*0.06*	1.13	0.84	0.19	0.02	2.78	0.17
21.53	1.41	60.33	0.00	32.25	121		44	1.05	−0.89	*0.07*	0.10	−0.89	0.12	0.03	0.25	0.30
21.58	15.77	5.90	0.03	3.75	44	60	672	12.80	0.57	*0.07*	1.13	0.58	0.15	0.02	2.77	0.14
21.63	15.65	6.85	0.03	4.30	38	40	795	14.10	0.57	*0.06*	1.12	0.58	0.15	0.02	2.74	0.13
21.68	14.59	6.66	0.03	4.77	446	252	1288	13.68	0.54	*0.07*	1.04	0.54	0.10	0.03	2.56	0.10
21.78	15.31	6.33	0.03	4.61	536	322	1782	14.97	0.81	*0.07*	1.09	0.82	0.09	0.02	2.68	0.09
21.88	4.42	14.49	0.10	7.74	50	74	283	2.04	0.97	*0.08*	0.32	0.98	0.33	0.02	0.78	0.33
21.98	13.88	8.76	0.02	7.18	123	83	1419	9.68	−0.01	*0.06*	0.99	−0.01	0.33	0.02	2.43	0.33
22.08	14.50	6.08	0.02	4.83	520	325	1388	10.23	−0.39	*0.08*	1.04	−0.39	0.16	0.03	2.54	0.16
22.18	13.90	6.37	0.04	4.79	453	214	1470	10.16	1.74	*0.08*	0.99	1.75	0.10	0.02	2.44	0.10
22.23	13.95	6.08	0.02	4.70	475	220	1308	8.75	1.79	*0.07*	1.00	1.79	0.10	0.02	2.45	0.10
22.28	14.13	6.40	0.06	4.68	708	360	1503	11.06	2.03	*0.08*	1.01	2.04	−0.28	0.03	2.48	−0.28
22.33	13.87	5.86	0.02	4.62	1360	511	1466	10.02	1.53	*0.08*	0.99	1.53	0.01	0.02	2.43	0.01
22.38	11.76	5.36	0.02	4.36	1864	401	1260	0.72	1.29	*0.08*	0.84	1.29	0.52	0.03	2.06	0.52
22.43	15.43	6.84	0.03	4.98	2510	102	2265.50	13.40	1.07	*0.07*	1.10	1.07	0.38	0.03	2.71	0.38
22.48	14.98	7.76	0.03	6.04	1203	105	2191.20	14.71	0.90	*0.06*	1.07	0.90	0.34	0.03	2.63	0.34
22.53	15.57	6.96	0.03	5.03	1661	117	2246.70	14.68	0.55	*0.07*	1.11	0.55	0.46	0.02	2.73	0.47
22.58	15.23	7.19	0.03	5.48	1943	93	2132.60	13.52	−0.49	*0.08*	1.09	−0.49	0.46	0.03	2.67	0.46
22.63	6.94	0.00	0.01	17.09	44	21	833.80	5.89	−0.85	*0.08*	0.50	−0.86	0.40	0.03	1.22	0.41
22.68	10.41	9.29	0.02	9.71	51	36	854.10	3.99	−0.61	*0.09*	0.74	−0.62	0.35	0.03	1.82	0.35

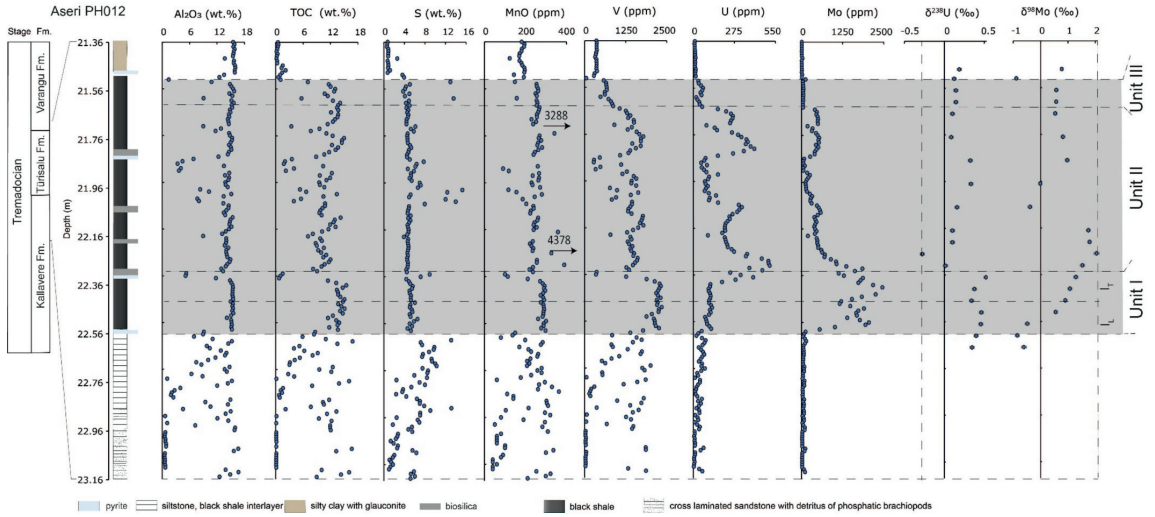

Fig. 2. Lithostratigraphic column and geochemical profiles for selected major elements, TOC, enriched redox-sensitive elements and U, Mo isotope data from black shales through the Tremadocian section of the Aseri PH012B core.

content compared to Unit I_L, 2) a more than twofold drop in Mo_{EF}/U_{EF} ratios, 3) an almost twofold drop in V concentrations, 4) the highest Mo/TOC ratios (extreme values up to 2590 in a few TOC-poor samples), 5) a significant increase in Mo/Mn and P/Al values and dispersion range compared to Unit I_L.

Unit II exhibits exceptionally high U enrichment with cyclic variability and a lack of distinct preferential Mo enrichment. Observed Mo_{EF}/U_{EF} trends generally follow those of average seawater, while Mo/TOC ratios mostly remain >25, higher than the modern semi-restricted Cariaco Basin. The Mo_{EF}/U_{EF} ratios of metal-poor Unit III cluster slightly below normal seawater, and samples display a homogeneous low Mo/TOC ratio of ~4, close to the Mo/TOC signal reported for the severely restricted Black Sea.

4.2. Mo and U isotope records

The black shales of the Türisalu Formation underlying and overlying rock beds exhibit substantial Mo and U isotopic variation, with $\delta^{98}Mo$ ranging from −0.89 to +2.03‰ (median + 0.67‰, $n = 16$) and $\delta^{238}U$ from −0.27 to +0.52‰ (median + 0.17‰, $n = 16$). The black shale samples that consistently show anomalously high $\delta^{238}U$ values (from +0.33 to +0.46‰) belong to the Kallavere Formation and Units I_L and I_T of the Türisalu Formation. The sample with the highest $\delta^{98}Mo$ value (+2.03 ‰) had the lowest $\delta^{238}U$ value (−0.27‰). The isotopic signals from Units II and III for $\delta^{98}Mo$ and $\delta^{238}U$ were − 0.89 to +2.03 ‰ and − 0.27 to +0.33‰, respectively.

The calculated detrital contributions to the U and Mo budgets were low (Table 1) for all study samples, resulting in authigenic $\delta^{98}Mo$ and $\delta^{238}U$ values that closely matched the measured values. This confirms that the measured isotopic signals reflect hydrogenous up take and related fractionation.

5. Discussion

5.1. Influence of sedimentation rates and rising sea level

Aqueous trace-metal concentrations and sedimentation rates can influence the authigenic accumulation of redox-sensitive trace metals in sediments, but these factors have been less addressed compared to redox control. Recent research by Liu and Algeo (2020) highlights the potential impact of watermass chemistry and sedimentation rates on trace-metal enrichment in anoxic marine environments. In their study of the Devonian-Carboniferous boundary, they found that slow sedimentation rates were likely the primary control on authigenic Mo and U enrichment. Considering those findings and geological background of the study area, one can assume that the primary mud beds of the Türisalu Formation formed under extremely slow long-term sediment accumulation rates, comparable to those calculated for the Alum Shale succession in Scandinavian successions (Sørensen et al., 2020; Zhao et al., 2022). Based on extensive biostratigraphic studies, the Türisalu Formation in NE Estonia was likely deposited entirely within the *Paltodus deltifer pristinus* Biozone, which is estimated to span approximately one million years (Goldman et al., 2023; Heinsalu et al., 2003; Kaljo et al., 1988; Kaljo and Kivimägi, 1970; Kaljo and Viira, 1989). While the geochronological framework for basinal Alum Shale settings has recently improved through integrated bio-, cyclo-, and chemostratigraphy, thin metalliferous NE Estonian black shale poses challenges for further refinement due to limited biostratigraphic range, poor fossil preservation, and erosional features. However, several indirect indicators support highly limited long-term terrigenous input to the considered setting. The entire Ordovician succession in North Estonia is highly condensed, with frequent gaps yet a remarkably complete stratigraphic record (Meidla et al., 2023). Indicators of extremely low net sedimentation during the Tremadocian include extensive pyritized hardgrounds below the Türisalu Formation, glauconitic sandstone development, and micrometeorite abundance in the late Tremadocian. Also, the high sulfur content in the black shales of the Türisalu Formation (4–10 %, Fig. 2) supports a slow sedimentation rate, as significant time is needed for sufficient sulfate to diffuse downward into the sediment to generate the observed amounts of H_2S and pyrite (Zaback et al., 1993). In the Türisalu Formation and the underlying Kallavere Formation, pyrite morphology is complex, suggesting the presence of syngenetic, early diagenetic, reworked detrital, and possibly late diagenetic varieties, though the available information remains poorly constrained. Disseminated framboidal pyrite and microcrystalline subhedral diagenetic pyrite are ubiquitous in the black shales. Commonly, thin, massive diagenetic pyrite laminae and less frequently flat pyrite nodules occur at the boundaries of lamina sets. Organic-poor siliciclastic

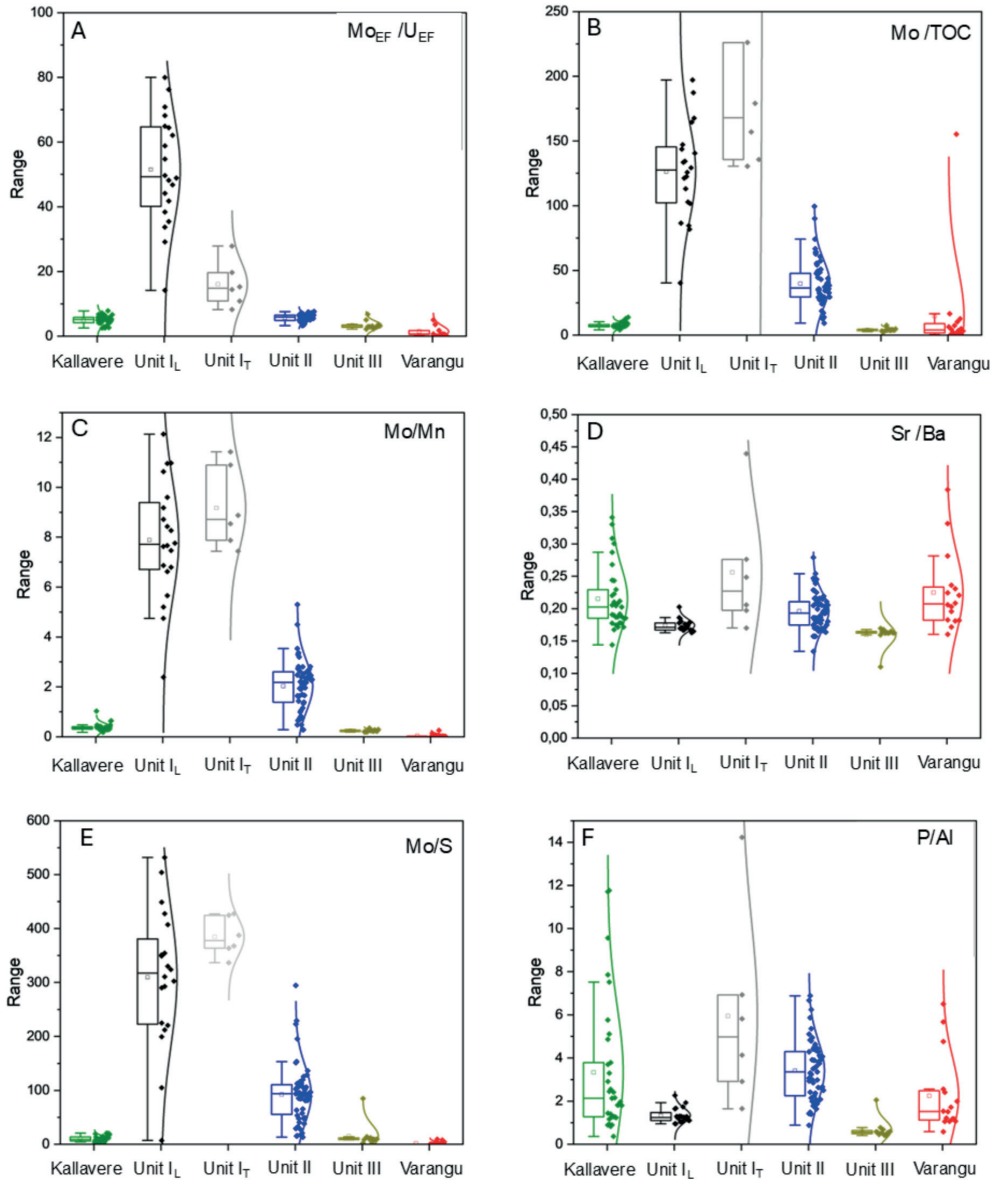

Fig. 3. Boxplots showing the median, quartiles and outliers, with individual data points overlaid. The plots highlight geochemical variation across different horizons in the Aseri PH012B core.

interbeds within the black shales are often partially or internally cemented with pyrite or may contain pyritized organic fragments (Schieber, 1990; Wilkin and Barnes, 1997; Schieber and Baird, 2001). In the Kallavere Formation, thick pyrite-cemented hardgrounds can be observed, where the cement likely formed by the replacement of primary metastable sulfides (Nemliher and Puura, 1996). Additionally, transgressive events generally promote slow sedimentation by trapping detrital siliciclastic sediments in coastal areas that retreat from open shelves (Cattaneo and Steel, 2003; Hein et al., 2014). Similar organic-rich black shales have been described from other palaeosettings, such as core shales of the Upper Pennsylvanian in the Midcontinent region of North America, containing up to 40 % TOC despite being deposited under exceedingly slow sedimentation rates (Algeo and Maynard, 2004; Cruse and Lyons, 2004; Heckel, 1977, 1986).

As redox-sensitive elements exhibit different solubilities and particle affinities depending on their oxidation state, their reductive uptake leads to distinct patterns of authigenic enrichment (Tribovillard et al., 2006). The non-matching hyper-enrichment patterns of redox-sensitive elements recorded in the study profile beginning with V hyper-enrichment during the deposition of the siltstone-black shale succession of the Kallavere Formation and followed by Mo and U hyper-enrichment (Fig. 2) can further reflect influence of rising sea level.

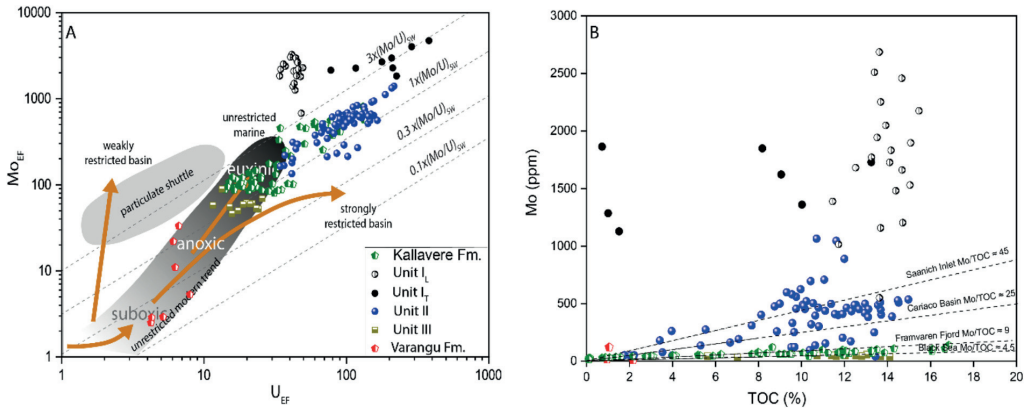

Fig. 4. (A) U_{EF} vs. Mo_{EF}, and (B) TOC vs. Mo diagrams for Aseri PH012B drillcore samples. The diagonal lines represent multiples (0.1, 0.3, 1 and 3) of the Mo/U ratio of present-day seawater (after Algeo and Tribovillard, 2009). The Mo enrichment factor (Mo_{EF}) vs U enrichment factor (U_{EF}) illustrates redox conditions (oxic, suboxic and anoxic) in data from the Kallavere Formation (green diamonds), Unit I_T (black circles), Unit I_L (open black circles), Unit II (blue circles), Unit III (blue squares) and the Varangu Formation (red diamonds). Shaded areas and arrows denote particulate shuttling and basinal restriction pathways in panel A. Reference lines for Mo/TOC ratios in panel B from Saanich Inlet, Cariaco Basin and Framvaren Fjord show varying Mo enrichment levels relative to TOC for various depositional settings (Algeo and Lyons, 2006; Algeo and Rowe, 2012). (For interpretation of the references to colour in this figure legend, the reader is referred to the web version of this article.)

Thus, V hyper-enrichment in the black shale intercalations of the Kallavere Formation likely began with initial V uptake occurring in a shallow suboxic-anoxic zone, controlled by the scavenging of V-organic complexes by clay particles (Ndiaye et al., 2023b). The water depth increase shift sedimentary condition to organic-rich mud accumulation field of the inner shelf, enhancing sulfide production due to organic matter mineralization at the shallow sea bottom and leading to Mo and U hyper-enrichment. The reasons behind the non-simultaneous hyper-enrichment of the latter, which considerably exceeds that observed in modern anoxic settings, remain poorly understood. Commonly used redox indices, such as Mo_{EF}/U_{EF} and Mo/S, suggest the dominance of euxinic conditions in the sedimentary setting, but the recorded variance ranges fall outside those observed in modern euxinic basins. Notably, in the studied black shale profile Mo enrichment sharply decreases above 22.30 m, precisely at the level at which U sever hyper-enrichment emerges (Figs. 2 and 3), possibly indicating a drawdown of aqueous Mo in primary seawater. The decline in all trace metals around 21.60 m, simultaneous with a sequence stratigraphic change from highstand to early regressive systems tracts, may suggest a shift toward less persistent anoxia in the water column.

5.2. Isotopic fractionation and $\delta^{98}Mo$–$\delta^{238}U$ covariation

Recorded $\delta^{98}Mo$–$\delta^{238}U$ data present in general inverse trend (Fig. 5A). As the fractionation processes at low temperatures are dominated by mass-dependent fractionation in the case of Mo isotopes and by nuclear shift type fractionation in the case of U isotopes, $\delta^{98}Mo$ and $\delta^{238}U$ commonly exhibit such inverse isotopic patterns in nature (Fig. 5B, C, D and E) (Abe et al., 2008; Bigeleisen, 1996; Brüske et al., 2020; Schauble, 2007). Modern seawater exhibits a high $\delta^{98}Mo$ value (+2.34 ‰; Barling et al., 2001; Nägler et al., 2005; Nakagawa et al., 2012; Siebert et al., 2003) compared to average inputs from rivers ($\delta^{98}Mo_{rivers}$ = +0.7 ‰; Archer and Vance, 2008). In contrast, $\delta^{238}U_{seawater}$ (∼−0.39 ‰; Tissot and Dauphas, 2015) is slightly lower than that of

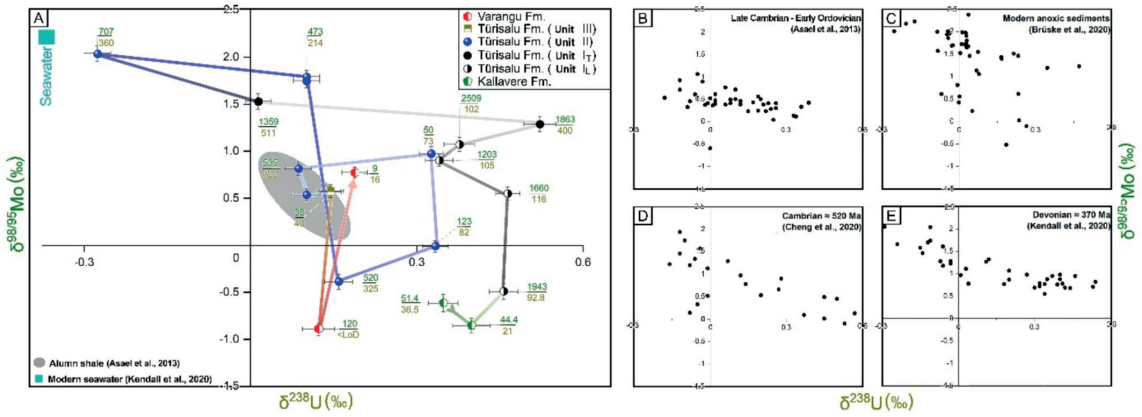

Fig. 5. (A) $\delta^{98}Mo$–$\delta^{238}U$ covariation for the Aseri PH012B study core, as well as Mo—U enrichment signatures (Mo (ppm) = green; U (ppm) = greenish beige), highlighting distinct evolutionary trends. (B-E) Selected $\delta^{98}Mo$–$\delta^{238}U$ reference data from modern and ancient oxygen-deficient marine deposits demonstrate general patterns of negative covariance between $\delta^{98}Mo$ and $\delta^{238}U$.

riverine inputs and the upper crust (∼−0.29 ‰) (Andersen et al., 2017). Although seawater Mo and U isotopic compositions may have been considerably different in poorly oxygenated palaeo-oceans in which anoxic sinks dominated (Dickson, 2017), the highest δ^{98}Mo and lowest δ^{238}U values from the Türisalu Formation are close to those of modern seawater and possibly representative of average Tremadocian seawater. Consequently, there is no isotopic evidence indicating long-term, widespread oceanic anoxia or altered isotopic composition of average global seawater. Nevertheless, this interpretation remains superficial given the influence of local fractionation pathways and the observed hyper-enrichment.

δ^{98}Mo–δ^{238}U covariation in the study succession shows remarkable shifts in isotopic composition, most likely indicating changes in the dominant isotope fractionation mechanisms. Furthermore, the values recorded from the lower part of the section clearly differentiate from typical range recorded from the Scandinavian Alum Shale successions. Thus, low δ^{98}Mo and high δ^{238}U signatures appear in moderately U- and Mo-enriched black shale beds of the Kallavere Formation. Comparable isotopic features have been reported from specific palaeosettings such as the Holocene Black Sea/Mediterranean sapropels (Unit II) and the mid-Cretaceous pre-Oceanic Anoxic Event 2 deposits (Anbar and Rouxel, 2007; Andersen et al., 2020; Asael et al., 2013; Neubert et al., 2008).

Modern high δ^{98}Mo in seawater is attributed to the preferential adsorption of light Mo isotopes from oxic seawater onto Mn oxides (Kendall et al., 2015), possibly controlled by a shift in Mo coordination geometry (Wasylenki et al., 2008). A comparable selective uptake mechanism but with a less pronounced fractionation effect is also suggested in the case of Fe-oxyhydroxides (Goldberg et al., 2009; Wasylenki et al., 2008). Alternative scenarios invoking preferential uptake of light Mo isotopes have been proposed for euxinic and anoxic-ferruginous settings, such as non-quantitative scavenging of Mo by intermediate thiomolybdates (Kendall et al., 2017; Neubert et al., 2008) or adsorption of Mo complexes onto organic particles (Dahl et al., 2017; King et al., 2018). Nevertheless, the molecular mechanisms for the latter are still unknown (Helz and Vorlicek, 2019).

In the case of δ^{238}U, atypical high values (> + 0.35 ‰), i.e., above those attributed to diffusion-controlled U isotope fractionation, can point to U fractionation in open-system settings (Xu et al., 2024), e.g., reduction of U by organic matter in the marine water column or the fluffy flocculant layer on the seafloor (Andersen et al., 2020; Cheng et al., 2020; Clarkson et al., 2023). It has been suggested that the resulting U isotope fractionation relative to seawater should be close to the total isotope fractionation factor of ∼0.8 to 1.6 ‰ (Andersen et al., 2017).

Mo hyper-enriched Units I_L and I_T in the Türisalu Formation show a well-defined stratigraphic trend: a gradual shift of δ^{98}Mo toward higher (non-fractionated) values, whereas δ^{238}U remains relatively high and similar to that of the Kallavere Formation. The low δ^{98}Mo at the contact between the Kallavere and the Türisalu Formation, as well as a sharp increase in Mo/Mn (Fig. 3C), suggests Mo uptake primarily via adsorption to Fe–Mn-(oxyhydr)oxides. This assumption primarily stems from the observed δ^{98}Mo range, as uptake by Fe—Mn (oxyhydr)oxides—during which isotopically light Mo is preferentially adsorbed—results in the largest seawater–solid isotopic offset (up to 3 ‰), which is not observed with other uptake mechanisms (Barling and Anbar, 2004; Goldberg et al., 2009; Wasylenki et al., 2008). Additional indirect evidence—such as the abundance of iron-rich lithologies in sedimentary successions and the presence of middle rare earth element enrichment in phosphorites of the Kallavere Formation, attributed to primary REE scavenging by Fe—Mn (oxyhydr)oxides—supports the assumption that shallow inner shelf settings of Baltica were a locus for redox cycling of Fe and Mn during the Early Ordovician. However, there is no significant change in δ^{98}Mo values at that contact of the Kallavere and the Türisalu Formation. These patterns might reflect buildup of H_2S_{aq} to >11 μm near the sediment-water interface or in the lower water column, thus initiating efficient conversion of Mo to thiomolybdates and preventing its recycling after the reductive dissolution of Fe–Mn-(oxyhydr)oxides. Despite the gradual decrease of δ^{98}Mo values upwards in the basal transgressive part of the Türisalu Formation, Mo remains severely hyper-enriched throughout this interval.

In case of the U—Mo hyper-enriched Unit I_T, isotopic signals align with an effective quantitative capture scenario for the uptake of dissolved Mo and U (Brüske et al., 2020), possibly due to elevated free sulfides (H_2S, HS^- and S^{2-}) in the water column or pore-water (Arnold et al., 2004; Barling et al., 2001; Neubert et al., 2008; Poulson Brucker et al., 2009) and quantitative conversion of molybdate into tetrathiomolybdate and polysulfides (Erickson and Helz, 2000; Helz et al., 2011; Helz and Vorlicek, 2019; Nägler et al., 2011; Scholz et al., 2013). Near-complete capture of such species by S-rich organic matter and iron sulfides could have ensured the sequestration of almost all Mo from the lower water column to the sediment, with minimal to no isotopic fractionation observed (Fig. 5A) (Erickson and Helz, 2000; Neubert et al., 2008; Tossell, 2005). This is because, in the case of near-total conversion of dissolved Mo to poorly soluble Mo species—at observed H_2S_{aq} concentrations >11 μM—these species should inherit an isotope composition similar to that of the source (seawater).

Indeed, the progressive decrease in Mo within Unit I_T, accompanied by a slight but noticeable increase in δ^{98}Mo values, supports the drawdown of dissolved Mo in the lower water column. This suggests that nearly complete thiolation of Mo and its conversion to refractory sulfidic compounds likely outpaced the input of Mo to the benthic water mass. The exhaustion of dissolved Mo, resulting in minimal isotope fractionation in precipitates, could also have extended into the pore water within the upper few centimetres below the sediment–water interface—i.e., into the active diffusion zone of muddy sediments (Neubert et al., 2008). Importantly, although later diagenetic modification of the observed Mo and U isotope signals cannot be entirely ruled out, it appears unlikely. Large-scale diagenetic alteration of Mo isotopic composition is not supported by the refractory nature of Mo-sulfidic compounds, the lack of potential Mo sources in host complexes, and limited evidence for Mo mobility with low-temperature fluids (Vorlicek et al., 2004; Wheat et al., 2002). U remobilization by oxic late diagenetic or recent glacial meltwater remains a somewhat more plausible scenario, with the potential for preferential removal of isotopically light U (Andersen et al., 2017). Still, the overlap of isotopically heavy U and peak Mo hyper-enrichment patterns in Unit I rather supports syngenetic processes as the primary control on the development of both signals. Despite slight decrease in Mo concentrations in Unit I_T, the Mo/TOC ratios recorded remain consistent with those typically observed in productive open-water euxinic environments (Algeo and Lyons, 2006; Algeo and Rowe, 2012; Helz and Vorlicek, 2019; Neubert et al., 2008). The occurrence of the pyritised horizon and a general increase of S/TOC values in Unit I_T compared to Unit I_L agree with extremely slow sediment accumulation rates (e.g., Zaback et al., 1993), thus suggesting complex environmental control behind shifts in isotopic and hyper-enrichment patterns.

Unit II, interpreted as the transgressive-highstand stage of the study succession (based on 1) absence of coarse-grained silty interbeds with brachiopod detritus present in Unit I and between Unit II and Unit III in the nearby Toolse area, and 2) absence of distinct erosional upper boundaries of lamina sets unlike those occasionally observed in Units I and III), lacked clear stratigraphic trends and presented fluctuating δ^{98}Mo and δ^{238}U signatures (Figs. 2 and 5) in a range comparable to that reported from the outer shelf Alum Shale settings. Still, most δ^{238}U values remained near ∼ + 0.1 ‰, which aligns with the isotopic ranges typical for the diffusion-controlled sequestration of U. Also, U enrichment peaking in this unit agrees with prolonged uptake controlled by the diffusion of dissolved U(VI) species across the sediment-water interface, which points to ultra-slow sediment accumulation rates, considerably below 3.1–5.6 mm kyr^{-1} estimated for the Tremadocian Alum Shale succession in the outer shelf of the basin (Zhao et al., 2022; Supplementary Table 1). If similar uptake conditions for U (e.g., redox

environments and diffusional flux of U across the sediment-water interface) are considered for the inner and outer shelf of the basin, estimated sediment accumulation rates between 0.6 and 1 mm kyr^{-1} can be inferred for Unit II. The extreme U enrichment might thus reflect the dwindling out of clastic supply to the more distal inner shelf in the Eastern Baltic area under the highstand conditions. On the other hand, if one considers recorded fluctuating isotopic signatures, the uptake of U in ferruginous environments has been shown to result in much more variable isotope fractionation signals compared to permanent euxinic settings (Cole et al., 2020), probably due to competing reduction rates and isotope effects. At the same time, high S content was recorded in specific intervals of Unit II. However, this may be likely attributed to extremely slow net burial rates or sediment gaps, rather than to persistent euxinic conditions in the lower water column (Algeo and Maynard, 2004; Liu and Algeo, 2020). Furthermore, the δ^{98}Mo of Unit II, ranging from +0.06 ‰ to +2.03 ‰, aligns with the variance attributed to nonquantitative scavenging of Mo under suboxic to anoxic-ferruginous settings (Kendall et al., 2017; Neubert et al., 2008)and possibly two-component fractionation pathway reflecting cumulative effect of uptake by Mn oxides and redox fractionation (Scholz et al., 2013, 2018). Considering other indicators of physicochemical stratification in the water column beside those derived from isotopic compositions, one may assume that if a semi-permanent chemocline—controlled by density stratification—characterised the transgressive systems in question, similar Mo and U isotope trends might be expected to recur in chronostratigraphically discordant settings (Dahl et al., 2010; Andersen et al., 2018; Chiu et al., 2022). This seems to hold true for enrichment patterns of redox-sensitive elements: both stratigraphically older black shales in western and northwestern Estonia and younger ones in northeastern Estonia typically show enrichment peaking in the lowermost part of the formation (Pukkonen and Rammo, 1992; Vind et al., 2023). A single sample from the redox-sensitive metal-poor Unit III, likely representing the early regressive stage of mud accumulation, produced isotopic signatures in the same range as Unit II.

5.3. Metallogeny linked to transgression and redox dynamics of shallow sea

The recorded geochemical signatures indicate the existence of steep environmental gradients in the inner shelf of the Baltic Palaeobasin. In modern anoxic (semi-)restricted basins, a chemocline separates the lower water column from upper oxygenated waters, maintained by a physical mixing barrier such as a halocline or thermocline at a similar depth. The development of a persistent chemocline in the shallow water column of an epicontinental sea (<100 m), excluding sheltered embayment, is usually prohibited by wind- and tide-driven mixing. However, seasonal density stratification, which can produce a seasonal pycnocline as shallow as <40 m (e.g., Li et al., 2020), is a widespread phenomenon in present-day shelf seas and is projected to increase due to global warming driven by the increasing buoyancy of heated-up upper layers (Holt and Umlauf, 2008).

Regarding the Tremadocian, oxygen isotope studies suggest extremely hot surface temperatures in tropical seas exceeding 40 °C at that time (Trotter et al., 2008). Elevated surface temperatures also likely applied to Baltica, which was positioned in mid-latitudes during this period (Scotese, 2023). Salinity stratification trends that might have favoured general density stratification under a super greenhouse climate include increased freshwater input to climatologically favourable areas (e.g., Pagani et al., 2006; Yamaguchi and Suga, 2019) under a warm 'wet' atmosphere, as well as the incursion of cold/more saline (Hay et al., 2006) ocean water into the deep layer of the sea due to upwelling at the western border of Baltica.

Although there is no consensus on the redox state of the deep ocean during the Tremadocian (Neubert et al., 2008), there are widely recognised circulation scenarios for a super greenhouse climate (Manabe and Stouffer, 1993) that foresee reduced thermohaline circulation and limited deepwater ventilation, favouring the generally oxygen-poor nature of deep upwelled water. Several studies (Herrmann et al., 2012; Algeo and Herrmann, 2018) have also stressed the importance of freshening the surface layer due to river runoff for the development of a shallow stratified water column in epicontinental seas. All the factors mentioned above may thus have contributed to the physicochemical stratification of the water column of the Baltic Palaeobasin.

The robust and permanent stratification in the water column of the Baltic Palaeobasin aligns well with the recorded U hyper-enrichment and U isotope range in Unit II, implying diffusion-controlled capture under extremely low sedimentation rates. Notably, significant diffusional uptake of U has been shown to occur only under a water column that remains anoxic for extended periods (Bone et al., 2017). Nevertheless, the unit contains spiculite interbeds, which point to the short benthic oxygenation episodes. Dahl et al. (2019) suggested that the prevalent anoxic-sulfidic benthic conditions during Alum Shale deposition in mid-shelf settings of the Baltic Palaeobasin (~501–494 million years ago) were disrupted by brief (600 to 3000 years) cyclic oxygenation events and recorded fluctuations in Mo concentrations concerning such intervals. They implied that oxygenation episodes were controlled by the intermittent inflow of dense salty cold ocean water to the shelf based on an analogue of the modern strongly stratified semi-restricted brackish water Baltic Sea. Indeed, in the latter, short incursion events of deep water have been observed to enhance Fe–Mn-(oxyhydr)oxide recycling and preferential delivery of lighter Mo isotopes to sediments (Dellwig et al., 2010; Goldberg et al., 2009).

Low δ^{98}Mo values (~ + 0.6 ‰) can also potentially develop due to redox cycling of Mn triggered by extensive estuarine circulation and entrapment of shelf anoxic waters under the riverine freshwater outflows, as shown by Herrmann et al. (2012) in their study of the thin transgressive Hushpuckney Shale from the Late Pennsylvanian Midcontinent Sea. Relatively low Sr/Ba values (<0.5, Fig. 3D) in the Tremadocian black shale appear to corroborate the lowered salinity concept in contemporaneous seawater (Wei and Algeo, 2020). Furthermore, the δ^{18}O signals from glendonite from the Kallavere and Türisalu Formations have been interpreted to indicate density stratification in the inner shelf of Baltica triggered either by freshwater flushing or high surface temperatures (Popov et al., 2019).

Still, the physiography of the Baltic Palaeobasin is hardly comparable to modern or ancient landlocked anoxic waterbodies as pointed out earlier. The geochemical indices from the Alum Shale Formation (Zhao et al., 2023) and the hyper-enrichment of redox-sensitive metals in the shallow inner shelf indicate largely unrestricted exchange of watermasses between the Baltic Palaeobasin and the Iapetus Ocean. Also, lithostratigraphic relations suggest existence of siliciclastic P-rich facies shoreward from the organic-rich mud facies on the inner shelf, requiring efficient delivery of P to coastal oxic zone. The latter is consistent with δ^{15}N isotope values (−2.5 to +0.2 ‰) in the Kallavere and Türisalu formations, indicating primary production patterns dominated by N-fixation and abundance of dissolved P (Ndiaye et al., 2023a). The laterally advected subpycnocline water from the deeper shelf has been seen as a major source of P flux for phosphorite development in the considered settings (Ilyin and Heinsalu, 1990).

We propose persistent shallow stratification with enhanced cross-boundary mixing between lower and upper water columns in the innermost shelf could explain the non-matching hyper-enrichment signatures and isotopic trends of δ^{98}Mo and δ^{238}U in the Tremadocian black shales (Fig. 6). Other key factors for the hyper-enrichment of U and Mo include sea-level rise and extremely slow sedimentation rates (~1 mm kyr^{-1}). Ultraslow sedimentation rates are known to result in trace-metal enrichments up to 100 times greater than in typical black shales, as demonstrated by Liu and Algeo (2020). The slow rates allowed prolonged exposure of the sediments to the overlying water column, facilitating extensive interaction between trace metal source (seawater) and organic-rich sediments, enabling diffusion-controlled uptake of U and Mo.

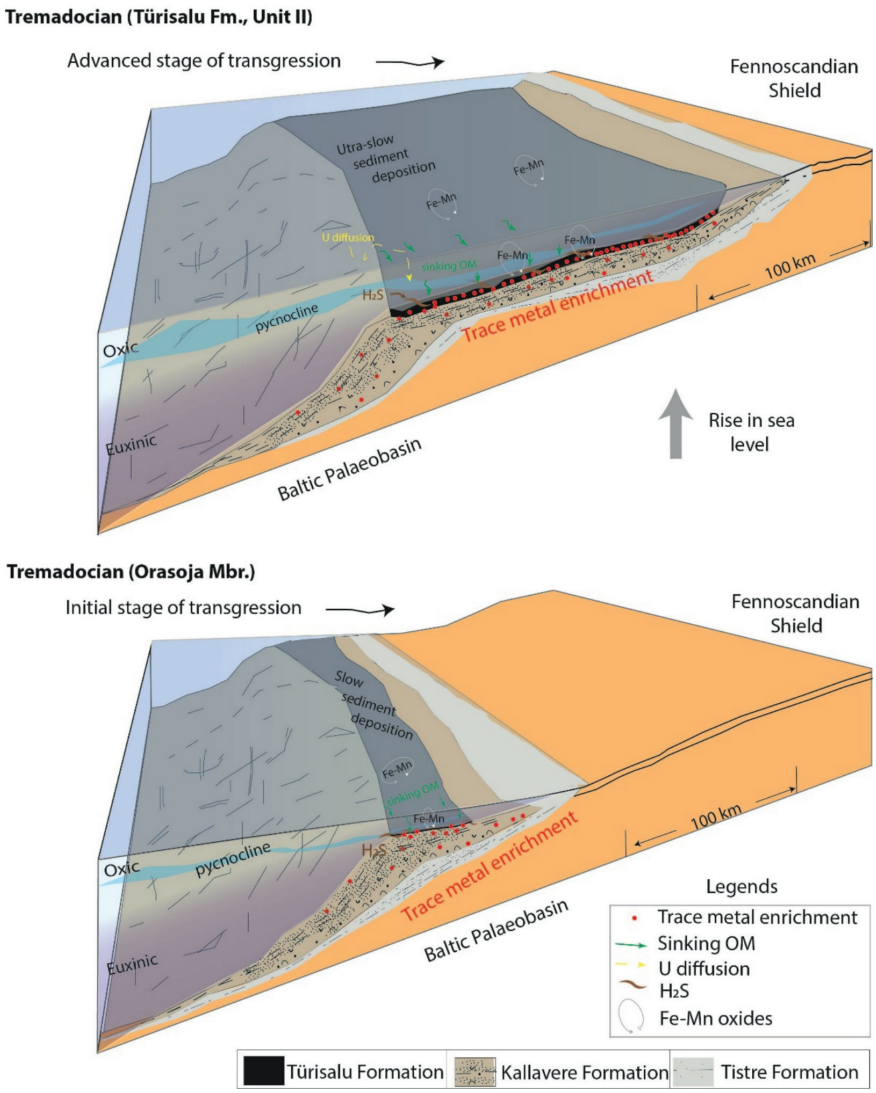

Fig. 6. Conceptual model of redox conditions and trace metal enrichment during the Tremadocian transgression in the Baltic Palaeobasin. The lower panel represents the initial stage of transgression (Kallavere Formation, Orasoja Member – Türisalu Formation), characterised by a shallow water column with slow sediment deposition, localized euxinic conditions near the seafloor, and the onset of trace metal enrichment on the inner shelf. The upper panel shows the advanced stage of transgression (Türisalu Formation, Unit II), during which sea level rise led to more stratified water column on the inner shelf, with ultra-slow sedimentation and expanded euxinia. Enhanced organic matter flux and uranium diffusion promoted widespread trace metal enrichment in sediments. Geochemical processes depicted include organic matter sinking, hydrogen sulfide formation, uranium diffusion across the redoxcline, and cycling of Fe—Mn oxides.

The transgressive nature of the succession and related landward shift of facies and upward deepening trend also played a critical role in metal enrichment. As sea levels rose, detrital siliciclastic input was preferentially trapped in coastal areas (Cattaneo and Steel, 2003), resulting in the progressive drop of sedimentation rates and extremely low clastic dilution of organic-rich sediments deposited in more distal parts of the inner shelf. The observed non-matching successive hyper-enrichment trends of redox-sensitive metals, starting with hyper-enrichment of V, followed by Mo and U, most likely reflect the progressive expansion of oxygen-deficient subpycnoclinal waters due to sea-level rise. Thus, during the early stages of organic-rich mud sedimentation (Kallavere Formation), V began to accumulate under suboxic conditions. Due to the shallow position of pycnocline and associated steep redoxcline in the water column, redox conditions shifted to the euxinic field in the study locality because of transgression, thus triggering hyper-enrichment of Mo and U. The sharp decline in Mo enrichment above 22.30 m in the Aseri PH012B core section, concurrent with further U enrichment, likely points to aqueous Mo depletion in the subpycnoclinal watermass (Liu and Algeo, 2020).

The isotopic patterns for Mo and U should be interpreted within the established context of slow sedimentation and redox stratification. The observed isotopic trends are consistent with the locally controlled redox-driven fractionation during trace-metal uptake. Thus, higher δ^{98}Mo values in more distal inner shelf settings reflect Mo sequestration under

dominantly euxinic conditions, while the $\delta^{238}U$ values point to continued U uptake from a Mo-depleted watermass. Development of low $\delta^{98}Mo$ values along with initiation of Mo hyper-enrichment in the lowermost part of the Türisalu Formation is, however, most likely a combined effect of Mo adsorption and release in cause of vigorous Mn—Fe recycling at or near chemocline and Mo subsequent uptake under sulfidic conditions. In the latter case, Mo source is likely a suboxic watermass close to chemocline supporting the genesis of neoformed Fe-Mn-(oxyhydr)oxides. Significant cross-boundary exchange between stratified surface and lower water column, likely prerequisite for effective Fe—Mn recycling, might have been favoured by different local and distal forcing mechanisms in inner shelf such as diapycnal mixing due to estuarian circulation, turbulence created by local wind-forcing, wave and tide shoaling or seasonal variations in thermohaline structure of the watermasses (Algeo and Herrmann, 2018; Richards et al., 2013; Rippeth, 2005).

6. Conclusions

This study investigated coupled $\delta^{98}Mo$ and $\delta^{238}U$ signals in thin transgressive Mo-U-V hyper-enriched Tremadocian black shales from the inner shelf of the Baltic Palaeobasin, revealing a wide range of isotopic compositions with well-defined covariation patterns in a single drillcore from NE Estonia, starting from highly fractionated to essentially non-fractionated values compared to modern seawater. Notably low $\delta^{98}Mo$ (−0.86 ‰) and high $\delta^{238}U$ (+0.52 ‰) compositions were recorded in the basal Mo hyper-enriched part of the transgressive black shales. In contrast, the upward sharp shift to the U—Mo hyper-enriched horizon was marked by a sharp decrease of $\delta^{238}U$ values. These variations demonstrate facies-specific control on isotopic fractionation patterns and alteration on U and Mo sequestration pathways in the inner shelf organic-rich facies under extremely low sediment accumulation rates. This study highlights the influence of local factors such as sedimentation rate and watermass architecture on the development of trace-metal hyper-enrichment and related isotopic patterns in black shales from the shallow epicontinental sea. High global temperatures at the start of the Ordovician contributed to development of a density-stratified water column with a shallow pycnocline in the inner shelf of the Baltic Palaeobasin, while progressive transgression trapped siliciclastic input in nearshore areas, favouring organic-rich mud accumulation offshore. Ultraslow sedimentation rates in the distal inner shelf allowed prolonged diffusion of redox-sensitive metals (Mo, U, V) into the sediment and development of hyper-enrichment. The co-occurrence of low $\delta^{98}Mo$ and Mo hyper-enrichment suggests that recycling of Fe—Mn species near the chemocline was critical in Mo capture. Together, these factors reveal the nuanced local controls on trace-metal enrichment in this ancient shallow-water epicontinental sea.

A more extensive isotopic dataset with broader spatial coverage is needed to further evaluate the proposed development scenario. It is worth stressing that similar abrupt changes and non-simultaneous hyper-enrichment patterns of U and Mo have been widely recorded in the Tremadocian inner shelf black shales in the Baltic Palaeobasin. In more general terms, this study demonstrates the potential of tracking isotopic signatures to uncover unique genetic aspects of metalliferous black shales.

CRediT authorship contribution statement

Mawo Ndiaye: Writing – review & editing, Writing – original draft, Visualization, Validation, Supervision, Software, Resources, Project administration, Methodology, Investigation, Funding acquisition, Formal analysis, Data curation, Conceptualization. **Sophie Graul:** Visualization, Data curation, Conceptualization. **Merlin Liiv:** Data curation. **Toivo Kallaste:** Visualization, Validation, Data curation. **Thomas J. Algeo:** Writing – review & editing, Writing – original draft, Visualization, Validation, Supervision, Methodology, Formal analysis, Data curation, Conceptualization. **Rutt Hints:** Writing – review & editing, Writing – original draft, Visualization, Supervision, Software, Resources, Project administration, Funding acquisition, Data curation, Conceptualization.

Declaration of competing interest

The authors declare that they have no known competing financial interests or personal relationships that could have appeared to influence the work reported in this paper.

Acknowledgments

We highly appreciate the comments from the two anonymous reviewers, which helped improve the quality of the manuscript. This study was co-funded by the European Union and the Estonian Research Council through project TEM-TA100. We gratefully acknowledge their financial support, which made this research possible.

Appendix A. Supplementary data

Supplementary data to this article can be found online at https://doi.org/10.1016/j.chemgeo.2025.122910.

Data availability

Data will be made available on request.

References

Abe, M., Suzuki, T., Fujii, Y., Hada, M., Hirao, K., 2008. An ab initio molecular-orbital study of the nuclear-volume effects in uranium-isotope fractionations. J. Chem. Phys. 129, 124102. https://doi.org/10.1063/1.2992616.

Abshire, M.L., Romaniello, S.J., Kuzminov, A.M., Cofrancesco, J., Severmann, S., Riedinger, N., 2020. Uranium isotopes as a proxy for primary depositional redox conditions in organic-rich marine systems. Earth Planet. Sci. Lett. 529, 115878. https://doi.org/10.1016/j.epsl.2019.115878.

Algeo, T.J., Herrmann, A.D., 2018. An ancient estuarine-circulation nutrient trap: the Late Pennsylvanian Midcontinent Sea of North America. Geology 46, 143–146. https://doi.org/10.1130/G39804.1.

Algeo, T.J., Lyons, T.W., 2006. Mo–total-organic-carbon covariation in modern anoxic marine environments: implications for analysis of paleoredox and paleohydrographic conditions. Paleoceanography 21, PA1016. https://doi.org/10.1029/2004PA001112.

Algeo, T.J., Maynard, J.B., 2004. Trace-element behaviour and redox facies in core shales of Upper Pennsylvanian Kansas-type cyclothems. Chem. Geol. 206, 289–318. https://doi.org/10.1016/j.chemgeo.2003.12.009.

Algeo, T.J., Maynard, J.B., 2008. Trace-metal covariation as a guide to water-mass conditions in ancient anoxic marine environments. Geosphere 4, 872–887. https://doi.org/10.1130/GES00174.1.

Algeo, T.J., Rowe, H., 2012. Paleoceanographic applications of trace-metal concentration data. Chem. Geol. 324, 6–18. https://doi.org/10.1016/j.chemgeo.2011.09.002.

Algeo, T.J., Tribovillard, N., 2009. Environmental analysis of paleoceanographic systems based on molybdenum–uranium covariation. Chem. Geol. 268, 211–225. https://doi.org/10.1016/j.chemgeo.2009.09.001.

Anbar, A.D., Rouxel, O., 2007. Metal stable isotopes in paleoceanography. Annu. Rev. Earth Planet. Sci. 35, 717–746. https://doi.org/10.1146/annurev.earth.34.031405.125029.

Andersen, M.B., Matthews, A., Vance, D., Bar-Matthews, M., Archer, C., de Souza, G.F., 2018. A 10-fold decline in the deep Eastern Mediterranean thermohaline overturning circulation during the last interglacial period. Earth Planet. Sci. Lett. 503, 58–67. https://doi.org/10.1016/j.epsl.2018.09.013.

Andersen, M.B., Romaniello, S., Vance, D., Little, S.H., Herdman, R., Lyons, T.W., 2014. A modern framework for interpreting 238U/235U in studies of ancient ocean redox. Earth Planet. Sci. Lett. 400, 184–194. https://doi.org/10.1016/j.epsl.2014.05.051.

Andersen, M.B., Elliott, T., Freymuth, H., Sims, K.W.W., Niu, Y., Kelley, K.A., 2015. The terrestrial uranium-isotope cycle. Nature 517, 356–359. https://doi.org/10.1038/nature14062.

Andersen, M.B., Stirling, C.H., Weyer, S., 2017. Uranium isotope fractionation. In: Johnson, C.M., Beard, B., Albarède, F. (Eds.), Non-Traditional Stable Isotopes, Rev. Mineral. Geochem, vol. 82, pp. 799–850. https://doi.org/10.2138/rmg.2017.82.19.

Andersen, M.B., Matthews, A., Bar-Matthews, M., Vance, D., 2020. Rapid onset of ocean anoxia shown by high U and low Mo isotope compositions of sapropel S1. Geochem. Perspect. Lett. 15, 8–12. https://doi.org/10.7185/geochemlet.2027.

Anderson, R.F., Fleisher, M.Q., LeHuray, A.P., 1989. Concentration, oxidation state and particulate flux of uranium in the Black Sea. Geochim. Cosmochim. Acta 53, 2215–2224. https://doi.org/10.1016/0016-7037(89)90345-1.

Archer, C., Vance, D., 2008. The isotopic signature of the global riverine molybdenum flux and anoxia in the ancient oceans. Nature Geoscience 1 (9), 597–600. https://doi.org/10.1038/ngeo282.
Arnold, G.L., Anbar, A.D., Barling, J., Lyons, T.W., 2004. Molybdenum isotope evidence for widespread anoxia in mid-Proterozoic oceans. Science 304, 87–90. https://doi.org/10.1126/science.1091785.
Artyushkov, E.A., Lindström, M., Popov, L.E., 2000. Relative sea-level changes in Baltoscandia in the Cambrian and early Ordovician: predominance of tectonic factors and absence of large-scale eustatic fluctuations. Tectonophysics 320, 375–407. https://doi.org/10.1016/S0040-1951(00)00038-X.
Asael, D., Tissot, F.L.H., Reinhard, C.T., Rouxel, O., Dauphas, N., Lyons, T.W., Ponzevera, E., Liorzou, C., Chéron, S., 2013. Coupled molybdenum, iron and uranium stable isotopes as oceanic paleoredox proxies during the Paleoproterozoic Shunga Event. Chem. Geol. 362, 193–210. https://doi.org/10.1016/j.chemgeo.2013.08.003.
Barling, J., Anbar, A.D., 2004. Molybdenum isotope fractionation during adsorption by manganese oxides. Earth Planet. Sci. Lett. 217, 315–329. https://doi.org/10.1016/S0012-821X(03)00608-3.
Barling, J., Arnold, G.L., Anbar, A.D., 2001. Natural mass-dependent variations in the isotopic composition of molybdenum. Earth Planet. Sci. Lett. 193, 447–457. https://doi.org/10.1016/S0012-821X(01)00514-3.
Barnes, C.E., Cochran, J.K., 1993. Uranium geochemistry in estuarine sediments: controls on removal and release processes. Geochim. Cosmochim. Acta 57, 555–569. https://doi.org/10.1016/0016-7037(93)90367-6.
Basu, A., Sanford, R.A., Johnson, T.M., Lundstrom, C.C., Löffler, F.E., 2014. Uranium-isotopic fractionation factors during U(VI) reduction by bacterial isolates. Geochim. Cosmochim. Acta 136, 100–113. https://doi.org/10.1016/j.gca.2014.02.041.
Baturin, G.N., Ilyin, A.V., 2013. Comparative geochemistry of shell phosphorites and Dictyonema shales of the Baltic. Geochem. Int. 51, 23–32. https://doi.org/10.1134/S0016702913010023.
Bian, L., Schovsbo, N.H., Chappaz, A., Zheng, X., Nielsen, A.T., Ulrich, T., Wang, X., Dai, S., Galloway, J.M., Małachowska, A., Xu, X., Sanei, H., 2021. Molybdenum–uranium–vanadium geochemistry in the Lower Paleozoic Alum Shale of Scandinavia: implications for vanadium exploration. Int. J. Coal Geol. 239, 103730. https://doi.org/10.1016/j.coal.2021.103730.
Bian, L., Chappaz, A., Schovsbo, N.H., Sanei, H., 2022. A new vanadium species in black shales: updated burial pathways and implications. Geochim. Cosmochim. Acta 338, 1–10. https://doi.org/10.1016/j.gca.2022.09.035.
Bigeleisen, J., 1996. Temperature dependence of the isotope chemistry of the heavy elements. Proc. Natl. Acad. Sci. USA 93, 9393–9396. https://doi.org/10.1073/pnas.93.18.9393.
Bone, S.E., Cahill, M.R., Jones, M.E., Fendorf, S., Davis, J., Williams, K.H., Bargar, J.R., 2017. Oxidative uranium release from anoxic sediments under diffusion-limited conditions. Environ. Sci. Technol. 51, 11039–11047. https://doi.org/10.1021/acs.est.7b02241.
Bopp, C.J., Lundstrom, C.C., Johnson, T.M., Sanford, R.A., Long, P.E., Williams, K.H., 2010. Uranium 238U/235U isotope ratios as indicators of reduction: results from an in situ biostimulation experiment at Rifle, Colorado, U.S.A. Environ. Sci. Technol. 44, 5927–5933. https://doi.org/10.1021/es100643v.
Brennecka, G.A., Herrmann, A.D., Algeo, T.J., Anbar, A.D., 2011a. Rapid expansion of oceanic anoxia immediately before the end-Permian mass extinction. Proc. Natl. Acad. Sci. USA 108, 17631–17634. https://doi.org/10.1073/pnas.1106039108.
Brennecka, G.A., Wasylenki, L.E., Bargar, J.R., Weyer, S., Anbar, A.D., 2011b. Uranium isotope fractionation during adsorption to Mn-oxyhydroxides. Environ. Sci. Technol. 45, 1370–1375. https://doi.org/10.1021/es103061v.
Brown, S.T., Basu, A., Ding, X., Christensen, J.N., DePaolo, D.J., 2018. Uranium isotope fractionation by abiotic reductive precipitation. Proc. Natl. Acad. Sci. USA 115, 8688–8693. https://doi.org/10.1073/pnas.1805234115.
Brüske, A., Weyer, S., Zhao, M.Y., Planavsky, N.J., Wegwerth, A., Neubert, N., Dellwig, O., Lau, K.V., Lyons, T.W., 2020. Correlated molybdenum and uranium isotope signatures in modern anoxic sediments: implications for their use as palaeoredox proxies. Geochim. Cosmochim. Acta 270, 449–474. https://doi.org/10.1016/j.gca.2019.11.031.
Bura-Nakić, E., Andersen, M.B., Archer, C., de Souza, G.F., Marguš, M., Vance, D., 2018. Coupled Mo–U abundances and isotopes in a small marine euxinic basin: constraints on processes in euxinic basins. Geochim. Cosmochim. Acta 222, 212–229. https://doi.org/10.1016/j.gca.2017.10.023.
Calvert, S.E., Pedersen, T.F., 1993. Geochemistry of recent oxic and anoxic marine sediments: implications for the geological record. Mar. Geol. 113, 67–88. https://doi.org/10.1016/0025-3227(93)90150-T.
Campbell, K.M., Kukkadapu, R.K., Qafoku, N.P., Peacock, A.D., Lesher, E., Williams, K.H., Bargar, J.R., Wilkins, M.J., Figueroa, L., Ranville, J., Davis, J.A., Long, P.E., 2012. Geochemical, mineralogical and microbiological characteristics of sediment from a naturally reduced zone in a uranium-contaminated aquifer. Appl. Geochem. 27, 1499–1511. https://doi.org/10.1016/j.apgeochem.2012.04.013.
Cattaneo, A., Steel, R.J., 2003. Transgressive deposits: a review of their variability. Earth Sci. Rev. 62, 187–228. https://doi.org/10.1016/S0012-8252(02)00134-4.
Chen, X., Shields, G.A., Andersen, M.B., Qiu, C., Min, S.Y., Shao, Q.F., Ling, H.F., 2023. Oceanic redox conditions during the terminal Cambrian extinction event. Chem. Geol. 626, 121456. https://doi.org/10.1016/j.chemgeo.2023.121456.
Cheng, M., Li, C., Jin, C., Wang, H., Algeo, T.J., Lyons, T.W., Zhang, F., Anbar, A., 2020. Evidence for high organic-carbon export to the early Cambrian seafloor. Geochim. Cosmochim. Acta 287, 125–140. https://doi.org/10.1016/j.gca.2020.01.050.
Chiu, C.F., Sweere, T.C., Clarkson, M.O., de Souza, G.F., Hennekam, R., Vance, D., 2022. Co-variation systematics of uranium and molybdenum isotopes reveal pathways for descent into euxinia in Mediterranean sapropels. Earth Planet. Sci. Lett. 585, 117527. https://doi.org/10.1016/j.epsl.2022.117527.
Clarkson, M.O., Sweere, T.C., Chiu, C.F., Hennekam, R., Bowyer, F., Wood, R.A., 2023. Environmental controls on very high δ238U values in reducing sediments: implications for Neoproterozoic seawater records. Earth Sci. Rev. 237, 104306. https://doi.org/10.1016/j.earscirev.2022.104306.
Cocks, L.R.M., Torsvik, T.H., 2002. Earth geography from 500 to 400 Ma: a faunal and palaeomagnetic review. J. Geol. Soc. Lond. 159, 631–644. https://doi.org/10.1144/0016-764901-118.
Cole, D.B., Planavsky, N.J., Longley, M., Böning, P., Wilkes, D., Wang, X., Swanner, E.D., Wittkop, C., Loydell, D.K., Busigny, V., Knudsen, A.C., Sperling, E.A., 2020. Uranium isotope fractionation in non-sulfidic anoxic settings and the global uranium isotope mass balance. Glob. Biogeochem. Cycles 34, e2020GB006649. https://doi.org/10.1029/2020GB006649.
Cruse, A.M., Lyons, T.W., 2004. Trace-metal records of regional palaeoenvironmental variability in Pennsylvanian (Upper Carboniferous) black shales. Chem. Geol. 206, 319–345. https://doi.org/10.1016/j.chemgeo.2003.12.010.
Crusius, J., Calvert, S., Pedersen, T., Sage, D., 1996. Rhenium and molybdenum enrichments in sediments as indicators of oxic, suboxic and sulfidic conditions of deposition. Earth Planet. Sci. Lett. 145, 65–78. https://doi.org/10.1016/S0012-821X(96)00204-X.
Dahl, T.W., Anbar, A.D., Gordon, G.W., Rosing, M.T., Frei, R., Canfield, D.E., 2010. The behavior of molybdenum and its isotopes across the chemocline and in the sediments of sulfidic Lake Cadagno, Switzerland. Geochim. Cosmochim. Acta 74, 144–163. https://doi.org/10.1016/j.gca.2009.09.018.
Dahl, T.W., Boyle, R.A., Canfield, D.E., Connelly, J.N., Gill, B.C., Lenton, T.M., Bizzarro, M., 2014. Uranium isotopes distinguish two geochemically distinct stages during the later Cambrian SPICE event. Earth Planet. Sci. Lett. 401, 313–326. https://doi.org/10.1016/j.epsl.2014.05.043.
Dahl, T.W., Chappaz, A., Hoek, J., McKenzie, C.J., Svane, S., Canfield, D.E., 2017. Evidence of molybdenum association with particulate organic matter under sulfidic conditions. Geobiology 15, 311–323. https://doi.org/10.1111/gbi.12220.
Dahl, T.W., Siggaard-Andersen, M.-L., Schovsbo, N.H., Persson, D.O., Husted, S., Hougård, I.W., et al., 2019. Brief oxygenation events in locally anoxic oceans during the Cambrian solve the animal breathing paradox. Scientific Reports 9, 11669. https://doi.org/10.1038/s41598-019-48123-2.
Dang, D.H., Evans, R.D., Wang, W., Omanović, D., El Houssainy, A., Lenoble, V., Mullot, J.U., Mounier, S., Garnier, C., 2018. Uranium isotope geochemistry in modern coastal sediments: insights from Toulon Bay, France. Chem. Geol. 481, 133–145. https://doi.org/10.1016/j.chemgeo.2018.01.032.
Dellwig, O., Beck, M., Lemke, A., Lunau, M., Kolditz, K., Schnetger, B., Brumsack, H.J., 2007. Non-conservative behaviour of molybdenum in coastal waters: coupling geochemical, biological and sedimentological processes. Geochim. Cosmochim. Acta 71, 2745–2761. https://doi.org/10.1016/j.gca.2007.03.014.
Dellwig, O., Leipe, T., März, C., Glockzin, M., Pollehne, F., Schnetger, B., Yakushev, E.V., Böttcher, M.E., Brumsack, H.J., 2010. A new particulate Mn–Fe–P shuttle at the redoxcline of anoxic basins. Geochim. Cosmochim. Acta 74, 7100–7115. https://doi.org/10.1016/j.gca.2010.09.017.
Dickson, A.J., 2017. A molybdenum-isotope perspective on Phanerozoic deoxygenation events. Nat. Geosci. 10, 721–726. https://doi.org/10.1038/ngeo3028.
Dunk, R.M., Mills, R.A., Jenkins, W.J., 2002. A re-evaluation of the oceanic uranium budget for the Holocene. Chem. Geol. 190, 45–67. https://doi.org/10.1016/S0009-2541(02)00110-9.
Eensaar, J., Gaškov, M., Pani, T., Sepp, H., Somelar, P., Kirsimäe, K., 2017. Hydrothermal fracture mineralization in the stable cratonic northern part of the Baltic Paleobasin: sphalerite fluid-inclusion evidence. GFF 139, 52–62. https://doi.org/10.1080/11035897.2016.1196499.
Erickson, B.E., Helz, G.R., 2000. Molybdenum(VI) speciation in sulfidic waters: stability and lability of thiomolybdates. Geochim. Cosmochim. Acta 64, 1149–1158. https://doi.org/10.1016/S0016-7037(99)00423-8.
Fan, J., Duan, L., Yin, M., Yuan, H., Li, X., 2022. Non-conservative behaviour of dissolved molybdenum and its potential role in nitrogen cycling in the Bohai and Yellow Seas. Front. Mar. Sci. 9, 1094846. https://doi.org/10.3389/fmars.2022.1094846.
Gill, B.C., Lyons, T.W., Young, S.A., Kump, L.R., Knoll, A.H., Saltzman, M.R., 2011. Geochemical evidence for widespread euxinia in the later Cambrian Ocean. Nature 469, 80–83. https://doi.org/10.1038/nature09700.
Gill, B.C., Dahl, T.W., Hammarlund, E.U., LeRoy, M.A., Gordon, G.W., Canfield, D.E., Anbar, A.D., Lyons, T.W., 2021. Redox dynamics of later Cambrian oceans. Palaeogeogr. Palaeoclimatol. Palaeoecol. 581, 110623. https://doi.org/10.1016/j.palaeo.2021.110623.
Goldberg, T., Archer, C., Vance, D., Poulton, S.W., 2009. Mo isotope fractionation during adsorption to Fe(oxyhydr)oxides. Geochim. Cosmochim. Acta 73, 6502–6516. https://doi.org/10.1016/j.gca.2009.08.004.
Goldman, D., Leslie, S.A., Liang, Y., Bergström, S.M., 2023. Ordovician biostratigraphy: index fossils, biozones and correlation. Geological Society, London, Special Publications 532, 31–62. https://doi.org/10.1144/SP532-2022-49.
Goldmann, A., Brennecka, G., Noordmann, J., Weyer, S., Wadhwa, M., 2015. The uranium isotopic composition of the Earth and the Solar System. Geochim. Cosmochim. Acta 148, 145–158. https://doi.org/10.1016/j.gca.2014.09.008.
Graul, S., Kallaste, T., Pajusaar, S., Urston, K., Gregor, A., Moilanen, M., Ndiaye, M., Hints, R., 2023. REE + Y distribution in Tremadocian shelly phosphorites (Toolse, Estonia): multi-stage enrichment in shallow-marine sediments during early diagenesis. J. Geochem. Explor. 254, 107311. https://doi.org/10.1016/j.gexplo.2023.107311.
Hall, A.M., Putkinen, N., Hietala, S., Lindsberg, E., Holma, M., 2021. Ultra-slow cratonic denudation in Finland since 1.5 Ga indicated by tiered unconformities and impact

structures. Precambrian Res. 352, 106000. https://doi.org/10.1016/j.precamres.2020.106000.
Hay, W.W., Flögel, F., Söding, E., 2006. Evaporites and the salinity of the ocean during the Phanerozoic: implications for climate, ocean circulation and life. Palaeogeogr. Palaeoclimatol. Palaeoecol. 240, 3–46. https://doi.org/10.1016/j.palaeo.2006.03.044.
Heckel, P.H., 1977. Origin of phosphatic black-shale facies in Pennsylvanian cyclothems of mid-continent North America. AAPG Bull. 61, 1045–1068. https://doi.org/10.1306/C1EA43C4-16C9-11D7-8645000102C1865D.
Heckel, P.H., 1986. Sea-level curve for Pennsylvanian eustatic marine transgressive-regressive depositional cycles along mid-continent outcrop belt, North America. Geology 14, 330–334. https://doi.org/10.1130/0091-7613(1986)14<330:SCFPEM>2.0.CO;2.
Hein, C.J., FitzGerald, D.M., de Menezes, J.T., Cleary, W.J., Klein, A.H.F., Albernaz, M.B., 2014. Coastal response to late-stage transgression and sea-level highstand. Geol. Soc. Am. Bull. 126, 459–480. https://doi.org/10.1130/B30836.1.
Heinsalu, H., 1990. On the lithology and stratigraphy of Late Tremadoc graptolitic argillites of north-West Estonia. Proc. Est. Acad. Sci. Geol. 39, 142–151.
Heinsalu, H., Bednarczyk, W., 1997. Tremadoc of the East European Platform: lithofacies and palaeogeography. Proc. Est. Acad. Sci. Geol. 46, 59–74.
Heinsalu, H., Raudsep, R., Viira, V., 1994. Environmental conditions of shelly phosphorite accumulation in the Rakvere phosphorite region, northern Estonia. Proc. Est. Acad. Sci. Geol. 43, 109–122. https://doi.org/10.3176/geol.1994.3.01.
Heinsalu, H., Kaljo, D., Kurvits, T., Viira, V., 2003. The stratotype of the Orasoja Member (Tremadocian, Northeast Estonia): lithology, mineralogy and biostratigraphy. Proc. Est. Acad. Sci. Geol. 52, 135–154.
Helz, G.R., Vorlicek, T.P., 2019. Precipitation of molybdenum from euxinic waters and the role of organic matter. Chem. Geol. 509, 178–193. https://doi.org/10.1016/j.chemgeo.2019.02.001.
Helz, G.R., Miller, C.V., Charnock, J.M., Mosselmans, J.F.W., Pattrick, R.A.D., Garner, C. D., Vaughan, D.J., 1996. Mechanism of molybdenum removal from the sea and its concentration in black shales: EXAFS evidence. Geochim. Cosmochim. Acta 60, 3631–3642. https://doi.org/10.1016/0016-7037(96)00195-0.
Helz, G.R., Bura-Nakić, E., Mikac, N., Ciglenečki, I., 2011. New model for molybdenum behaviour in euxinic waters. Chem. Geol. 284, 323–332. https://doi.org/10.1016/j.chemgeo.2011.03.012.
Herrmann, A.D., Kendall, B., Algeo, T.J., Gordon, G.W., Wasylenki, L.E., Anbar, A.D., 2012. Anomalous molybdenum-isotope trends in Upper Pennsylvanian euxinic facies: significance for use of δ98Mo as a global marine redox proxy. Chem. Geol. 324–325, 87–98. https://doi.org/10.1016/j.chemgeo.2012.05.013.
Hints, R., Hade, S., Soesoo, A., Voolma, M., 2014a. Depositional framework of the East Baltic Tremadocian black shale revisited. GFF 136, 464–482. https://doi.org/10.1080/11035897.2013.866978.
Hints, R., Soesoo, A., Voolma, M., Tarros, S., Kallaste, T., Hade, S., 2014b. Centimetre-scale variability of redox-sensitive elements in Tremadocian black shales from the eastern Baltic Palaeobasin. Est. J. Earth Sci. 63, 233–239. https://doi.org/10.3176/earth.2014.24.
Hints, R., Pajusaar, S., Urtson, K., Liiv, M., Kallaste, T., 2021. Metal enrichment in lithologically complex black shales: a case study from the Tremadocian of NE Estonia. Est. J. Earth Sci. 70, 36. https://doi.org/10.3176/earth.2021.04.
Holmden, C., Amini, M., Francois, R., 2015. Uranium isotope fractionation in Saanich Inlet: a modern analogue study of a palaeoredox tracer. Geochim. Cosmochim. Acta 153, 202–215. https://doi.org/10.1016/j.gca.2014.11.012.
Holt, J.T., Umlauf, L., 2008. Modelling the tidal-mixing fronts and seasonal stratification of the northwest European continental shelf. Cont. Shelf Res. 28, 887–903. https://doi.org/10.1016/j.csr.2008.01.012.
Ilyin, A.V., Heinsalu, H.N., 1990. Early Ordovician shelly phosphorites of the Baltic phosphate Basin. Geol. Soc. Lond. Spec. Publ. 52, 253–259. https://doi.org/10.1144/gsl.sp.1990.052.01.18.
Jochum, K.P., Nohl, U., Herwig, K., Lammel, E., Stoll, B., Hofmann, A.W., 2005. GeoReM: a new geochemical database for reference materials and isotopic standards. Geostand. Geoanal. Res. 29, 333–338. https://doi.org/10.1111/j.1751-908X.2005.tb00904.x.
Kaljo, D., Kivimägi, E., 1970. Distribution of graptolites in the Dictyonema shale of Estonia and on the uncontemporaneity of its different facies. Proc. Acad. Sci. Est. SSR Chem. Geol. 19, 334–341.
Kaljo, D., Viira, V., 1989. Co-occurrences of conodonts and graptolites in the Estonian early Tremadoc. Proc. Est. Acad. Sci. Geol. 38, 97–100.
Kaljo, D., Borovko, N., Heinsalu, H., Khazanovich, K., Mens, K., Popov, L.E., Sergeyeva, S., Sobolevskaya, R., Viira, V., 1986. The Cambrian-Ordovician boundary in the Baltic–Ladoga clint area (North Estonia and Leningrad Region, USSR). Proc. Est. Acad. Sci. Geol. 35, 97–108.
Kaljo, D., Heinsalu, H., Mens, K., Puura, I., Viira, V., 1988. Cambrian–Ordovician boundary beds at Tõnismägi, Tallinn, North Estonia. Geol. Mag. 125, 457–463. https://doi.org/10.1017/S001675680001308X.
Kendall, B., Creaser, R.A., Gordon, G.W., Anbar, A.D., 2009. Re–Os and Mo-isotope systematics of black shales from the middle Proterozoic Velkerri and Wollogorang formations, McArthur Basin, northern Australia. Geochim. Cosmochim. Acta 73, 2534–2558. https://doi.org/10.1016/j.gca.2009.02.013.
Kendall, B., Komiya, T., Lyons, T.W., Bates, S.M., Gordon, G.W., Romaniello, S.J., Jiang, G., Creaser, R.A., Xiao, S., McFadden, K., Sawaki, Y., Tahata, M., Shu, D., Han, J., Li, Y., Chu, X., Anbar, A.D., 2015. Uranium and molybdenum isotope evidence for an episode of widespread ocean oxygenation during the late Ediacaran Period. Geochim. Cosmochim. Acta 156, 173–193. https://doi.org/10.1016/j.gca.2015.02.025.
Kendall, B., Dahl, T.W., Anbar, A.D., 2017. Good golly, why moly? The stable-isotope geochemistry of molybdenum. In: Johnson, C.M., Beard, B.L., Albarède, F. (Eds.), Rev. Mineral. Geochem, 82, pp. 683–732. https://doi.org/10.2138/rmg.2017.82.16.
King, E.K., Perakis, S.S., Pett-Ridge, J.C., 2018. Molybdenum isotope fractionation during adsorption to organic matter. Geochim. Cosmochim. Acta 222, 584–598. https://doi.org/10.1016/j.gca.2017.11.014.
Kivimägi, E., Loog, A., 1972. Main structural types of graptolitic argillites of the Toolse deposit. Proc. Acad. Sci. Est. SSR Chem. Geol. 21, 143–147.
Kivimägi, E., Teedumäe, A., 1971. Results of a complex estimation of the rocks in the phosphorite deposit of Toolse. Proc. Acad. Sci. Est. SSR Chem. Geol. 20, 243–250.
Klinkhammer, G.P., Palmer, M.R., 1991. Uranium in the oceans: where it goes and why. Geochim. Cosmochim. Acta 55, 1799–1806. https://doi.org/10.1016/0016-7037(91)90024-Y.
Kowalski, N., Dellwig, O., Beck, M., Gräwe, U., Neubert, N., Nägler, T.F., Badewien, T.H., Brumsack, H.J., van Beusekom, J.E.E., Böttcher, M.E., 2013. Pelagic molybdenum concentration anomalies and the impact of sediment resuspension on the molybdenum budget in two tidal systems of the North Sea. Geochim. Cosmochim. Acta 119, 198–211. https://doi.org/10.1016/j.gca.2013.05.046.
Li, G., Cheng, L., Zhu, J., Trenberth, K.E., Mann, M.E., Abraham, J.P., 2020. Increasing ocean stratification over the past half-century. Nat. Clim. Chang. 10, 1116–1123. https://doi.org/10.1038/s41558-020-00918-2.
Liu, J., Algeo, T.J., 2020. Beyond redox: control of trace-metal enrichment in anoxic marine facies by water-mass chemistry and sedimentation rate. Geochim. Cosmochim. Acta 287, 296–317. https://doi.org/10.1016/j.gca.2020.02.037.
Loog, A., Petersell, V., 1994. Distribution of micro-elements in Tremadoc graptolitic argillite of Estonia. Acta Comment. Univ. Tartu. 972, 57–76.
Malinovsky, D., Rodushkin, I., Baxter, D.C., Ingri, J., Öhlander, B., 2005. Molybdenum-isotope ratio measurements on geological samples by MC-ICP-MS. Int. J. Mass Spectrom. 245, 94–107.
Manabe, S., Stouffer, R.J., 1993. Century-scale effects of increased atmospheric CO_2 on the ocean–atmosphere system. Nature 364, 215–218.
McManus, J., Berelson, W.M., Severmann, S., Poulson, R.L., Hammond, D.E., Klinkhammer, G.P., Holm, C., 2006. Molybdenum and uranium geochemistry in continental-margin sediments: palaeoproxy potential. Geochim. Cosmochim. Acta 70, 4643–4662. https://doi.org/10.1016/j.gca.2006.06.1564.
Meidla, T., Ainsaar, L., Hints, O., Radzevičius, S., 2023. Ordovician of the Eastern Baltic Palaeobasin and the Tornquist Sea margin of Baltica. Geol. Soc. Lond. Spec. Publ. 532, 317–343. https://doi.org/10.1144/SP532-2022-141.
Miller, C.A., Peucker-Ehrenbrink, B., Walker, B.D., Marcantonio, F., 2011. Re-assessing the surface cycling of molybdenum and rhenium. Geochim. Cosmochim. Acta 75, 7146–7179. https://doi.org/10.1016/j.gca.2011.09.005.
Morford, J.L., Emerson, S., 1999. The geochemistry of redox-sensitive trace metals in sediments. Geochim. Cosmochim. Acta 63, 1735–1750. https://doi.org/10.1016/S0016-7037(99)00126-X.
Nägler, T.F., Siebert, C., Lüschen, H., Böttcher, M.E., 2005. Sedimentary Mo-isotope record across the Holocene fresh–brackish-water transition of the Black Sea. Chem. Geol. 219, 283–295. https://doi.org/10.1016/j.chemgeo.2005.03.006.
Nägler, T.F., Neubert, N., Böttcher, M.E., Dellwig, O., Schnetger, B., 2011. Molybdenum-isotope fractionation in pelagic euxinia: evidence from the modern Black and Baltic Seas. Chem. Geol. 289, 1–11. https://doi.org/10.1016/j.chemgeo.2011.07.001.
Nakagawa, Y., Takano, S., Firdaus, M.L., Norisuye, K., Hirata, T., Vance, D., Sohrin, Y., 2012. The molybdenum isotopic composition of the modern ocean. Geochem. J. 46, 131–141. https://doi.org/10.2343/geochemj.1.0158.
Ndiaye, M., Liiv, M., Kallaste, T., Graul, S., Hints, R., 2023a. Nitrogen and organic-carbon isotope record in Tremadocian highly metalliferous black shales from Baltica. Est. J. Earth Sci. 72, 78–81. https://doi.org/10.3176/earth.2023.25.
Ndiaye, M., Pajusaar, S., Liiv, M., Graul, S., Kallaste, T., Hints, R., 2023b. Fine-clay shuttle as a key mechanism for V hyper-enrichment in shallow-water Tremadocian black shale from Baltica. Chem. Geol. 634, 121583. https://doi.org/10.1016/j.chemgeo.2023.121583.
Nemliher, J., Puura, I., 1996. Upper Cambrian basal conglomerate of the Kallavere Formation on the Pakri Peninsula, NW Estonia. Proc. Est. Acad. Sci. Geol. 45, 1–8.
Neubert, N., Nägler, T.F., Böttcher, M.E., 2008. Sulfidity controls molybdenum-isotope fractionation into euxinic sediments: evidence from the modern Black Sea. Geology 36, 775–778. https://doi.org/10.1130/G24959A.1.
Nielsen, A.T., Schovsbo, N.H., 2015. The regressive Early–Mid-Cambrian "Hawke Bay Event" in Baltoscandia: epeirogenic uplift in concert with eustasy. Earth Sci. Rev. 151, 288–350. https://doi.org/10.1016/j.earscirev.2015.09.012.
Nielsen, A.T., Høyberget, M., Ahlberg, P., 2020. The Furongian (upper Cambrian) Alum Shale of Scandinavia: revision of zonation. Lethaia 53, 462–485. https://doi.org/10.1111/let.12370.
Noordmann, J., Weyer, S., Montoya-Pino, C., Dellwig, O., Neubert, N., Eckert, S., Paetzel, M., Böttcher, M.E., 2015. Uranium and molybdenum isotope systematics in modern euxinic basins: case studies from the Central Baltic Sea and Kyllaren Fjord. Chem. Geol. 396, 182–195. https://doi.org/10.1016/j.chemgeo.2014.12.012.
Noordmann, J., Weyer, S., Georg, R.B., Jöns, S., Sharma, M., 2016. 238U/235U isotope ratios of crustal material, rivers and products of hydrothermal alteration: new insights on the oceanic U-isotope mass balance. Isot. Environ. Health Stud. 52, 141–163. https://doi.org/10.1080/10256016.2015.1047449.
Pagani, M., Pedentchouk, N., Huber, M., Sluijs, A., Schouten, S., Brinkhuis, H., Sinninghe Damsté, J.S., Dickens, G.R., 2006. Arctic hydrology during global warming at the Palaeocene/Eocene thermal maximum. Nature 442, 671–675. https://doi.org/10.1038/nature05043.
Pajusaar, S., Hints, R., Kallaste, T., Kiipli, T., Urtson, K., 2021. Chemical-composition data of Tremadocian black-shale reference samples from Estonia. In: SARV Geosci. Data Repos. 1.0, Dataset. https://doi.org/10.23679/512.

Petersell, V., 1997. Dictyonema argillite. In: Raukas, A., Teedumäe, A. (Eds.), Geology and Mineral Resources of Estonia. Estonian Academy Publishers, Tallinn, pp. 327–331.
Pontér, S., Rodushkin, I., Engström, E., Rodushkina, K., Paulukat, C., Peinerud, E., Widerlund, A., 2021. Early diagenesis of anthropogenic uranium in lakes receiving deep groundwater from the Kiruna mine, northern Sweden. Sci. Total Environ. 793, 148441. https://doi.org/10.1016/j.scitotenv.2021.148441.
Popov, L.E., Álvaro, J.J., Holmer, L.E., Bauert, H., Ghobadi Pour, M., Dronov, A.V., Lehnert, O., Hints, O., Männik, P., Zhang, Z.F., Zhang, Z.L., 2019. Glendonite occurrences in the Tremadocian of Baltica: first Early Palaeozoic evidence of massive ikaite precipitation at temperate latitudes. Sci. Rep. 9, 43707. https://doi.org/10.1038/s41598-019-43707-4.
Poulson Brucker, R.L., McManus, J., Severmann, S., Berelson, W.M., 2009. Molybdenum behaviour during early diagenesis: insights from Mo isotopes. Geochem. Geophys. Geosyst. 10, Q06010. https://doi.org/10.1029/2008GC002180.
Pukkonen, E.M., 1989. Major and minor elements in Estonian graptolite argillite. Oil Shale 6, 11–18.
Pukkonen, E., Rammo, M., 1992. Distribution of molybdenum and uranium in the Tremadoc Graptolite Argillite (Dictyonema Shale) of North-Western Estonia. Bull. Geol. Surv. Est. 2, 3–15.
Puura, V., Vaher, R., 1997. Cover structure. In: Raukas, A., Teedumäe, A. (Eds.), Geology and Mineral Resources of Estonia. Estonian Academy Publishers, Tallinn, pp. 167–177.
Richards, C., Bourgault, D., Galbraith, P.S., Hay, A., Kelley, D.E., 2013. Measurements of shoaling internal waves and turbulence in an estuary. J. Geophys. Res. Oceans 118, 273–286. https://doi.org/10.1029/2012JC008154.
Rippeth, T.P., 2005. Mixing in seasonally stratified shelf seas: a shifting paradigm. Philos. Trans. R. Soc. A 363, 2837–2854. https://doi.org/10.1098/rsta.2005.1662.
Rudnick, R.L., Gao, S., 2003. Composition of the continental crust. In: Rudnick, R.L. (Ed.), The Crust, Treatise on Geochemistry, vol. 4. Elsevier-Pergamon, Oxford, pp. 1–64.
Schauble, E.A., 2007. Role of nuclear volume in driving equilibrium stable-isotope fractionation of mercury, thallium, and other very heavy elements. Geochim. Cosmochim. Acta 71, 2170–2189. https://doi.org/10.1016/j.gca.2007.02.004.
Scheiderich, K., Helz, G.R., Walker, R.J., 2010. Century-long record of Mo-isotopic composition in sediments of a seasonally anoxic estuary (Chesapeake Bay). Earth Planet. Sci. Lett. 289, 189–197. https://doi.org/10.1016/j.epsl.2009.11.008.
Schieber, J., 1990. Pyritic shales and microbial mats: significant factors in the genesis of stratiform Pb–Zn deposits of the Proterozoic? Mineral. Deposita 25, 7–14. https://doi.org/10.1007/BF03326378.
Schieber, J., Baird, G., 2001. On the origin and significance of pyrite spheres in Devonian black shales of North America. J. Sediment. Res. 71, 155–166. https://doi.org/10.1306/051600710155.
Scholz, F., McManus, J., Sommer, S., 2013. The manganese and iron shuttle in a modern euxinic basin and implications for molybdenum cycling at euxinic ocean margins. Chem. Geol. 355, 56–68. https://doi.org/10.1016/j.chemgeo.2013.07.006.
Scholz, F., Siebert, C., Dale, A.W., Frank, M., 2017. Intense molybdenum accumulation under a nitrogenous water column and implications for Mo-isotope palaeoredox proxies. Geochim. Cosmochim. Acta 213, 400–417. https://doi.org/10.1016/j.gca.2017.06.048.
Scholz, F., Baum, M., Siebert, C., Eroglu, S., Dale, A.W., Naumann, M., Sommer, S., 2018. Sedimentary molybdenum cycling after seawater inflow to the intermittently euxinic Gotland deep, Central Baltic Sea. Chem. Geol. 491, 27–38. https://doi.org/10.1016/j.chemgeo.2018.04.031.
Schovsbo, N.H., Nielsen, A.T., Harstad, A.O., Bruton, D.L., 2018. Stratigraphy and geochemical composition of the Cambrian Alum Shale Formation in the Porsgrunn core, Skien–Langesund district, southern Norway. Bull. Geol. Soc. Den. 66, 1–20. https://doi.org/10.37570/bgsd-2018-66-01.
Schulz, H.M., Yang, S., Panova, E., Bechtel, A., 2019. Role of Pleistocene meltwater-controlled uranium leaching in assessing irradiation-induced alteration of organic matter in Tremadocian Koporie Formation (western Russia). Geochim. Cosmochim. Acta 245, 133–153. https://doi.org/10.1016/j.gca.2018.10.029.
Scotese, C.R., 2023. Ordovician plate tectonic and palaeogeographical maps. Geol. Soc. Lond. Spec. Publ. 532, 91–109. https://doi.org/10.1144/SP532-2022-311.
Scott, C., Lyons, T.W., Bekker, A., Shen, Y., Poulton, S.W., Chu, X., Anbar, A.D., 2008. Tracing the stepwise oxygenation of the Proterozoic Ocean. Nature 452, 456–459. https://doi.org/10.1038/nature06811.
Shulga, A., Serebrennikova, O., Mozzhelina, T., 1987. VO-deoxophylloerythroetioporphyrin—the major representative of porphyrins in Dictyonema shale. Oil Shale 4, 229–232.
Siebert, C., Nägler, T.F., von Blanckenburg, F., Kramers, J.D., 2003. Molybdenum-isotope records as a potential new proxy for palaeoceanography. Earth Planet. Sci. Lett. 211, 159–171. https://doi.org/10.1016/S0012-821X(03)00189-4.
Somelar, P., Kirsimäe, K., Hints, R., Kirs, J., 2010. Illitization of early Palaeozoic K-bentonites in the Baltic Basin: decoupling of burial- and fluid-driven processes. Clay Clay Miner. 58, 388–398. https://doi.org/10.1346/ccmn.2010.0580309.
Somlyay, A., Palcsu, L., Kiss, G.I., Clarkson, M.O., Kovács, E.B., Vallner, Z., Zajzon, N., Pálfy, J., 2023. Uranium-isotope evidence for extensive seafloor anoxia after the end-Triassic mass extinction. Earth Planet. Sci. Lett. 614, 118190. https://doi.org/10.1016/j.epsl.2023.118190.
Sørensen, A.L., Nielsen, A.T., Thibault, N., Zhao, Z., Schovsbo, N.H., Dahl, T.W., 2020. Astronomically forced climate change in the late Cambrian. Earth Planet. Sci. Lett. 548, 116475. https://doi.org/10.1016/j.epsl.2020.116475.
Stirling, C.H., Andersen, M.B., Potter, E.K., Halliday, A.N., 2007. Low-temperature isotopic fractionation of uranium. Earth Planet. Sci. Lett. 264, 208–225. https://doi.org/10.1016/j.epsl.2007.09.019.
Sturesson, U., Popov, L., Holmer, L.E., Bassett, M.G., Felitsyn, S., Belyatsky, B., 2005. Neodymium-isotopic composition of Cambrian–Ordovician biogenic apatite in the Baltoscandian Basin. Geol. Mag. 142, 419–439. https://doi.org/10.1017/S0016756805000877.
Stylo, M., Neubert, N., Wang, Y., Monga, N., Romaniello, S.J., Weyer, S., Bernier-Latmani, R., 2015. Uranium isotopes fingerprint biotic reduction. Proc. Natl. Acad. Sci. USA 112, 5619–5624. https://doi.org/10.1073/pnas.1421841112.
Taylor, S.R., McLennan, S.M., 1985. The Continental Crust: Its Composition and Evolution. Blackwell, Oxford, p. 312.
Tissot, F.L.H., Dauphas, N., 2015. Uranium-isotopic compositions of the crust and ocean: age corrections, U budget and global extent of modern anoxia. Geochim. Cosmochim. Acta 167, 113–143. https://doi.org/10.1016/j.gca.2015.06.034.
Tossell, J.A., 2005. Calculating the partitioning of Mo isotopes between oxidic and sulfidic aqueous species. Geochim. Cosmochim. Acta 69, 2981–2993. https://doi.org/10.1016/j.gca.2005.01.016.
Tribovillard, N., Algeo, T.J., Lyons, T., Riboulleau, A., 2006. Trace metals as paleoredox and paleoproductivity proxies: an update. Chem. Geol. 232 (1–2), 12–32. https://doi.org/10.1016/j.chemgeo.2006.02.012.
Trotter, J.A., Williams, I.S., Barnes, C.R., Lécuyer, C., Nicoll, R.S., 2008. Did cooling oceans trigger Ordovician biodiversification? Evidence from conodont thermometry. Science 321, 550–554. https://doi.org/10.1126/science.1155814.
Vind, J., Ofili, S., Mänd, K., Soesoo, A., Kirsimäe, K., 2023. Redox-sensitive trace-metal hyper-enrichment in Tremadocian Alum Shale (Graptolite Argillite), North-Western Estonia. Chem. Geol. 640, 121746. https://doi.org/10.1016/j.chemgeo.2023.121746.
Voegelin, A.R., Nägler, T.F., Samankassou, E., Villa, I.M., 2009. Molybdenum-isotopic composition of modern and Carboniferous carbonates. Chem. Geol. 265, 488–498. https://doi.org/10.1016/j.chemgeo.2009.05.015.
Voegelin, A.R., Pettke, T., Greber, N.D., von Niederhäusern, B., Nägler, T.F., 2014. Magma differentiation fractionates Mo-isotope ratios: evidence from the Kos Plateau Tuff (Aegean Arc). Lithos 190–191, 440–448. https://doi.org/10.1016/j.lithos.2013.12.016.
Vorlicek, T.P., Kahn, M.D., Kasuya, Y., Helz, G.R., 2004. Capture of molybdenum in pyrite-forming sediments: role of ligand-induced reduction by polysulfides. Geochim. Cosmochim. Acta 68, 547–556. https://doi.org/10.1016/S0016-7037(03)00444-7.
Wang, X., Johnson, T.M., Lundstrom, C.C., 2015. Isotope fractionation during oxidation of tetravalent uranium by dissolved oxygen. Geochim. Cosmochim. Acta 150, 160–170. https://doi.org/10.1016/j.gca.2014.12.007.
Wasylenki, L.E., Rolfe, B.A., Weeks, C.L., Spiro, T.G., Anbar, A.D., 2008. Effects of temperature and ionic strength on Mo-isotope fractionation during adsorption to Mn oxides. Geochim. Cosmochim. Acta 72, 5997–6005. https://doi.org/10.1016/j.gca.2008.08.027.
Wei, W., Algeo, T.J., 2020. Elemental proxies for palaeosalinity analysis of ancient shales and mudrocks. Geochim. Cosmochim. Acta 287, 341–366. https://doi.org/10.1016/j.gca.2019.06.034.
Weyer, S., Anbar, A.D., Gerdes, A., Gordon, G.W., Algeo, T.J., Boyle, E.A., 2008. Natural fractionation of 238U/235U. Geochim. Cosmochim. Acta 72, 345–359. https://doi.org/10.1016/j.gca.2007.11.012.
Wheat, C.G., Mottl, M.J., Rudnicki, M., 2002. Trace-element and REE composition of a low-temperature ridge-flank hydrothermal spring. Geochim. Cosmochim. Acta 66, 3693–3705. https://doi.org/10.1016/S0016-7037(02)00894-3.
Wilde, P., Lyons, T.W., Quinby-Hunt, M.S., 2004. Organic-carbon proxies in black shales: molybdenum. Chem. Geol. 206, 167–176. https://doi.org/10.1016/j.chemgeo.2003.12.005.
Wilkin, R.T., Barnes, H.L., 1997. Formation processes of framboidal pyrite. Geochim. Cosmochim. Acta 61, 323–339. https://doi.org/10.1016/S0016-7037(96)00320-1.
Xu, L., Lehmann, B., Mao, J., Nägler, T.F., Neubert, N., Böttcher, M.E., Escher, P., 2012. Mo-isotope and trace-element patterns of Lower Cambrian black shales in South China: multi-proxy constraints on the palaeoenvironment. Chem. Geol. 318–319, 45–59. https://doi.org/10.1016/j.chemgeo.2012.05.016.
Xu, L., Lehmann, B., Weyer, S., Wen, H., Mao, J., Neubert, N., Jian, W., 2024. Inverse Mo- versus U-isotope correlation of Early Cambrian highly metalliferous black shales in South China indicates synsedimentary metal enrichment from a near-modern ocean. Mineral. Deposita 59, 155–167. https://doi.org/10.1007/s00126-023-01201-y.
Yamaguchi, R., Suga, T., 2019. Trend and variability in global upper-ocean stratification since the 1960s. J. Geophys. Res. Oceans 124, 8933–8948. https://doi.org/10.1029/2019JC015439.
Yang, S., Lu, X., Chen, X., Zheng, W., Owens, J.D., Young, S.A., Kendall, B., 2023. U- and Mo-isotope evidence for globally extensive marine euxinia during the Devonian-Carboniferous Hangenberg Crisis. Geochim. Cosmochim. Acta 352, 133–156. https://doi.org/10.1016/j.gca.2023.04.027.
Zaback, D.A., Pratt, L.M., Hayes, J.M., 1993. Transport and reduction of sulphate and immobilisation of sulphide in marine black shales. Geology 21, 141–144. https://doi.org/10.1130/0091-7613(1993)021<0141:TAROSA>2.3.CO;2.
Zhang, Y., Wang, Z., Yang, X., Huang, L., Li, Y., Qin, L., 2022. Petrological and Ni–Mo-isotopic evidence for the genesis of Ni- and Mo-sulfide-enriched early Cambrian black shale from Southwest China. Chem. Geol. 598, 120812. https://doi.org/10.1016/j.chemgeo.2022.120812.
Zhao, Z., Thibault, N.R., Dahl, T.W., Schovsbo, N.H., Sørensen, A.L., Rasmussen, C.M.Ø., Nielsen, A.T., 2022. Synchronising rock clocks in the late Cambrian. Nat. Commun. 13, 1990. https://doi.org/10.1038/s41467-022-29651-4.
Zhao, Z., Pang, X., Zou, C., Dickson, A.J., Basu, A., Guo, Z., Pan, S., Nielsen, A.T., Schovsbo, N.H., Jing, Z., Dahl, T.W., 2023. Dynamic oceanic redox conditions across

the late Cambrian SPICE event constrained by molybdenum and uranium isotopes. Earth Planet. Sci. Lett. 604, 118013. https://doi.org/10.1016/j.epsl.2023.118013.

Curriculum vitae

Personal data

Name:	Mawo Ndiaye
Date of birth:	02/01/1995
Place of birth:	Gouye Mbeuth
Citizenship:	Senegalese

Contact data

E-mail:	Mawo123466@gmail.com
Phone:	+37258527534

Education

2021−2025	Tallinn University of Technology (TalTech), Tallinn, Estonia, doctoral studies (speciality: Earth Sciences) University of
2018−2020	Poitiers, Poitiers, France, M.Sc. in Earth and Planetary Sciences
2017−2018	
	University of Reunion Island, France, B.Sc. in Earth and Environmental Sciences
2015−2017	
	University of Chouaîb Doukkali, El Jadida, Marocco, Earth sciences/Biology

Language competence

French	
Wolof	Native
English	Native
Italian	Fluent
Arabe	Average
Estonian	Basic
	Basic

Professional employment

Apr 2021−Dec 2025	Tallinn University of Technology, Tallinn, Estonia: early-stage researcher
Feb 2020−Sep 2020	BRGM, Orléans, France: research tntern, clay-organic interactions
Apr 2019−Aug 2019	Orano, Limoges, France: research intern, uranium metallurgy
Feb 2019−Apr 2019	
	IC2PM, Poitiers, France: research intern, North Sea reservoir analysis

External studies

2021–2022	Technical University of Denmark (DTU), Copenhagen, Denmark, Coursework in density functional theory

Courses, Conferences and Seminars

Graul, Sophie; Ndiaye, Mawo; Kallaste, Toivo; Monchal, Vincent; Joosu, Lauri; Moilanen, Marko; Hints, Rutt; (2025). CRM potential of EU sedimentary basins: Insights on Estonian phosphorites and black shales. EGU 2025. Vienna: European Geosciences Union. DOI: 10.5194/egusphere-egu25-16358.

Graul, Sophie; Monchal, Vincent; Rateau, Rémi; Joosu, Lauri; Moilanen, Marko; Ndiaye, Mawo; Hints, Rutt (2024). LA-ICP-MS imaging technique application on Estonian sedimentary phosphorites: Revealing REE enrichment stages and advanced ore characterisation. LA-ICP-MS imaging technique application on Estonian sedimentary phosphorites: Revealing REE enrichment stages and advanced ore characterisation: EGU General Assembly 2024. Vienna: Copernicus Publications. DOI: 10.5194/egusphere-egu24-7319.

Graul,Sophie; Monchal, Vincent; Rateau, Rémi; Joosu, Lauri; Moilanen, Marko; Ndiaye, Mawo; Hints, Rutt (2024). REE potential in sedimentary apatite: Delve deeper with microanalytics. 4th European Mineralogical Conference. Dublin: Trinity College Dublin, 275.

Ndiaye, Mawo; Kallaste, Toivo; Graul, Sophie; Hints, Rutt (2024). Exploring Critical Element Enrichment Pathways in Black Shales: A Case Study of Türisalu Formation in Estonia. 4th European Mineralogical Conference. Dublin: Trinity College Dublin, 251.

Graul, Sophie; Joosu, Lauri; Ndiaye, Mawo; Hints Rutt; (2024). REE resources of Estonian phosphorites. CRM for a suistanable future. Tallinn: EuroGeoSurveys. DOI: 10.13140/RG.2.2.18959.39840.

Ndiaye,Mawo; Hints, Rutt; Graul, Sophie; Schulz, Hans-Martin; (2024). Geochemical Processes in Estonian Graptolite Argillite: Insights into Vanadium Concentration Mechanisms. CRM for a suistanable future. Tallinn: EuroGeoSurveys. DOI: 10.13140/RG.2.2.28186.86728.

Graul, Sophie; Joosu, Lauri; Hints, Rutt; Ndiaye, Mawo; Monchal, Vincent; Moilanen, Marko; (2024). REE enrichment in shelly phosphorites. CRM for sustainable future. Tallinn: EuroGeoSurveys. DOI: 10.13140/RG.2.2.32381.17128.

Ndiaye, Mawo; Graul, Sophie; Kallaste, Toivo; Hints, Rutt (2023). The Enrichment Process of Vanadium in Lower Ordovician Vanadiferous Black Shales from Estonia: Investigating Critical Metal Resources in Europe. Goldschmidt 2023. Lyon: European Association of Geochemistry. DOI: 10.7185/gold2023.14076.

Hints, Rutt; Graul, Sophie; Kallaste, Toivo; Pajusaar, Siim (2022). Trace element signatures in Early Ordovician phosphorites and black shales from the Baltic Palaeobasin: sulfidic facies control of the P cycle. Second Annual Meeting of IGCP 735. October 19-20, 2022. Rocks and the Rise of Ordovician Life. Abstract Book. Marrakech: Hassan II Academy Press, 36.

List of publications

Ndiaye, M., et al. (2025). Trace-metal hyper-enrichment in Tremadocian black shales of the Baltic Palaeobasin linked to transgression and ultra-slow sedimentation rates. Chemical Geology (In Review).

Ndiaye, M., et al. (2023). Fine clay shuttle as a key mechanism for V hyper-enrichment in shallow water Tremadocian black shale from Baltica. Chemical Geology, 634, 121583. DOI: 10.1016/j.chemgeo.2023.121583 (Cited by 30 articles).

Ndiaye, M., et al. (2023). Nitrogen and organic carbon isotope record in Tremadocian highly metalliferous black shales from Baltica. Estonian Journal of Earth Sciences, 72(1), 78–81. DOI: 10.3176/earth.2023.25

Graul, S., et al. (2023). REE+Y distribution in Tremadocian shelly phosphorites (Toolse, Estonia): Multi-stage enrichment in shallow marine sediments during early diagenesis. Journal of Geochemical Exploration, 72(1), 78–81. DOI: 10.1016/j.gexplo.2023.107311

Graul, S., et al. (2023). Early diagenetic transformation stages revealed by micro-analytical studies of shelly phosphorites, Rakvere region. Estonian Journal of Earth Sciences, 72(1), 34–37. DOI: 10.3176/earth.2023.12

Elulookirjeldus

Isikuandmed

Nimi:	Mawo Ndiaye
Sünniaeg:	02/01/1995
Sünnikoht:	Gouye Mbeuth
Kodakondsus**:**	Senegalese

Kontaktandmed

E-post:	Mawo123466@gmail.com
Telefon:	+37258527534

Hariduskäik

2021−2025	Tallinna Tehnikaülikool – doktorantuur (eriala: maateadustes)
2018−2020	Poitiers' Ülikool, Poitiers, Prantsusmaa, magistrikraad maa- ja planetaarteadustes
2017−2018	Réunion Island Ülikool, Prantsusmaa, bakalaureusekraad maa- ja keskkonnateadustes
2015−2017	Chouaîb Doukkali Ülikool, El Jadida, Maroko, Maateadused/Bioloogia

Keelteoskus

Prantsuse keel	Emakeel
Volofi keel	Emakeel
Inglise keel	Sujuv
Itaalia keel	Keskmine
Araabia keel	Põhitase
Eesti keel	Põhitase

Teenistuskäik

Apr 2021−Dets 2025	Tallinna Tehnikaülikool, nooremteadur
Veeb 2020−Sept 2020	BRGM, Orléans, Prantsusmaa, teaduspraktikant, savi ja orgaanilise aine vastastikmõjud
Apr 2019−Aug 2019	Orano, Limoges, Prantsusmaa, teaduspraktikant, uraani metallurgia
Veeb 2019−Apr 2019	IC2PM, Poitiers, Prantsusmaa, teaduspraktikant, Põhjamere veehoidla analüüs

Välisõpingud

2021–2022	Taani Tehnikaülikool (DTU), Kopenhaagen, Taani, tihedusfunktsionaalteooria kursused

Konverentsid ja seminarid

Graul, Sophie; Ndiaye, Mawo; Kallaste, Toivo; Monchal, Vincent; Joosu, Lauri; Moilanen, Marko; Hints, Rutt; (2025). CRM potential of EU sedimentary basins: Insights on Estonian phosphorites and black shales. EGU 2025. Viin: Euroopa Geoteaduste Liit. DOI: 10.5194/egusphere-egu25-16358.

Graul, Sophie; Monchal, Vincent; Rateau, Rémi; Joosu, Lauri; Moilanen, Marko; Ndiaye, Mawo; Hints, Rutt (2024). LA-ICP-MS imaging technique application on Estonian sedimentary phosphorites: Revealing REE enrichment stages and advanced ore characterisation. LA-ICP-MS imaging technique application on Estonian sedimentary phosphorites: Revealing REE enrichment stages and advanced ore characterisation: EGU General Assembly 2024. Viin: Copernicuse väljaanded. DOI: 10.5194/egusphere-egu24-7319.

Graul,Sophie; Monchal, Vincent; Rateau, Rémi; Joosu, Lauri; Moilanen, Marko; Ndiaye, Mawo; Hints, Rutt (2024). REE potential in sedimentary apatite: Delve deeper with microanalytics. 4th European Mineralogical Conference. Dublin: Trinity kolledž Dublinis, 275.

Ndiaye, Mawo; Kallaste, Toivo; Graul, Sophie; Hints, Rutt (2024). Exploring Critical Element Enrichment Pathways in Black Shales: A Case Study of Türisalu Formation in Estonia. 4th European Mineralogical Conference. Dublin: Trinity College Dublin, 251.

Graul, Sophie; Joosu, Lauri; Ndiaye, Mawo; Hints Rutt; (2024). REE resources of Estonian phosphorites. CRM for a suistanable future. Tallinn: EuroGeoSurveys. DOI: 10.13140/RG.2.2.18959.39840.

Ndiaye,Mawo; Hints, Rutt; Graul, Sophie; Schulz, Hans-Martin; (2024). Geochemical Processes in Estonian Graptolite Argillite: Insights into Vanadium Concentration Mechanisms. CRM for a suistanable future. Tallinn: EuroGeoSurveys. DOI: 10.13140/RG.2.2.28186.86728.

Graul, Sophie; Joosu, Lauri; Hints, Rutt; Ndiaye, Mawo; Monchal, Vincent; Moilanen, Marko; (2024). REE enrichment in shelly phosphorites. CRM for sustainable future. Tallinn: EuroGeoSurveys. DOI: 10.13140/RG.2.2.32381.17128.

Ndiaye, Mawo; Graul, Sophie; Kallaste, Toivo; Hints, Rutt (2023). The Enrichment Process of Vanadium in Lower Ordovician Vanadiferous Black Shales from Estonia: Investigating Critical Metal Resources in Europe. Goldschmidt 2023. Lyon: Euroopa Geokeemia Assotsiatsioon. DOI: 10.7185/gold2023.14076.

Hints, Rutt; Graul, Sophie; Kallaste, Toivo; Pajusaar, Siim (2022). Trace element signatures in Early Ordovician phosphorites and black shales from the Baltic Palaeobasin: sulfidic facies control of the P cycle. Second Annual Meeting of IGCP 735. October 19-20, 2022. Rocks and the Rise of Ordovician Life. Abstract Book. Marrakech: Hassan II Akadeemia. Press, 36.

Publikatsioonid

Ndiaye, M., et al. (2025). Trace-metal hyper-enrichment in Tremadocian black shales of the Baltic Palaeobasin linked to transgression and ultra-slow sedimentation rates. Chemical Geology (In Review).

Ndiaye, M., et al. (2023). Fine clay shuttle as a key mechanism for V hyper-enrichment in shallow water Tremadocian black shale from Baltica. Chemical Geology, 634, 121583. DOI: 10.1016/j.chemgeo.2023.121583 (Cited by 30 articles).

Ndiaye, M., et al. (2023). Nitrogen and organic carbon isotope record in Tremadocian highly metalliferous black shales from Baltica. Estonian Journal of Earth Sciences, 72(1), 78–81. DOI: 10.3176/earth.2023.25

Graul, S., et al. (2023). REE+Y distribution in Tremadocian shelly phosphorites (Toolse, Estonia): Multi-stage enrichment in shallow marine sediments during early diagenesis. Journal of Geochemical Exploration, 72(1), 78–81. DOI: 10.1016/j.gexplo.2023.107311

Graul, S., et al. (2023). Early diagenetic transformation stages revealed by micro-analytical studies of shelly phosphorites, Rakvere region. Estonian Journal of Earth Sciences, 72(1), 34–37. DOI: 10.3176/earth.2023.12

ISSN 2585-6901 (PDF)
ISBN 978-9916-80-448-3 (PDF)